III International Conference and School
"Synthesis, Structure, and Properties of High-Entropy Materials"
October 11-15, 2021

№

Tomsk Polytechnic University

E-mail *boi5@list.ru*

THERMAL STABILITY OF Ti-O-N FILMS

Boytsova E.L.
Tomsk Polytechnic University, Lenina 2, Tomsk, 634050, Russia.

Abstrakt

The thermal stability of Ti-O and Ti-O-N coatings was studied by heating at 1300 ° C using differential thermal analysis (DTA) and scanning electron microscopy (SEM).

Goal and tasks

- The aim is to study the thermal stability of thin Ti-O and Ti-O-N films
- The tasks are to investigate the thermal stability of Ti-O and Ti-O-N samples to the melting temperature of the substrate (Si)
- The object of the study is samples of Ti-O and Ti-O-N films deposited by the method of reactive magnetron sputtering onto plates of Si (10 × 10 × 1 mm) [1]

Doping with nitrogen atoms is the most accessible and rational way to improve the performance of TiO2:

+ Significant change in the refractive index
+ Increase in hardness, increase in electrical conductivity
+ Increase in elastic modulus.

Nitrogen atoms, as a rule, are built into the structure TiO2 either at the oxygen position or in the interstice of the crystal lattice. [2]

To determine the chemical bonds present in Ti-O and Ti-O-N coatings, the IR method was used. The IR spectrum was obtained on a device by the industrial system of Fourier transform IR spectroscopy (FTIR) ReactIR 45P GP, "Shimadzu", Japan.
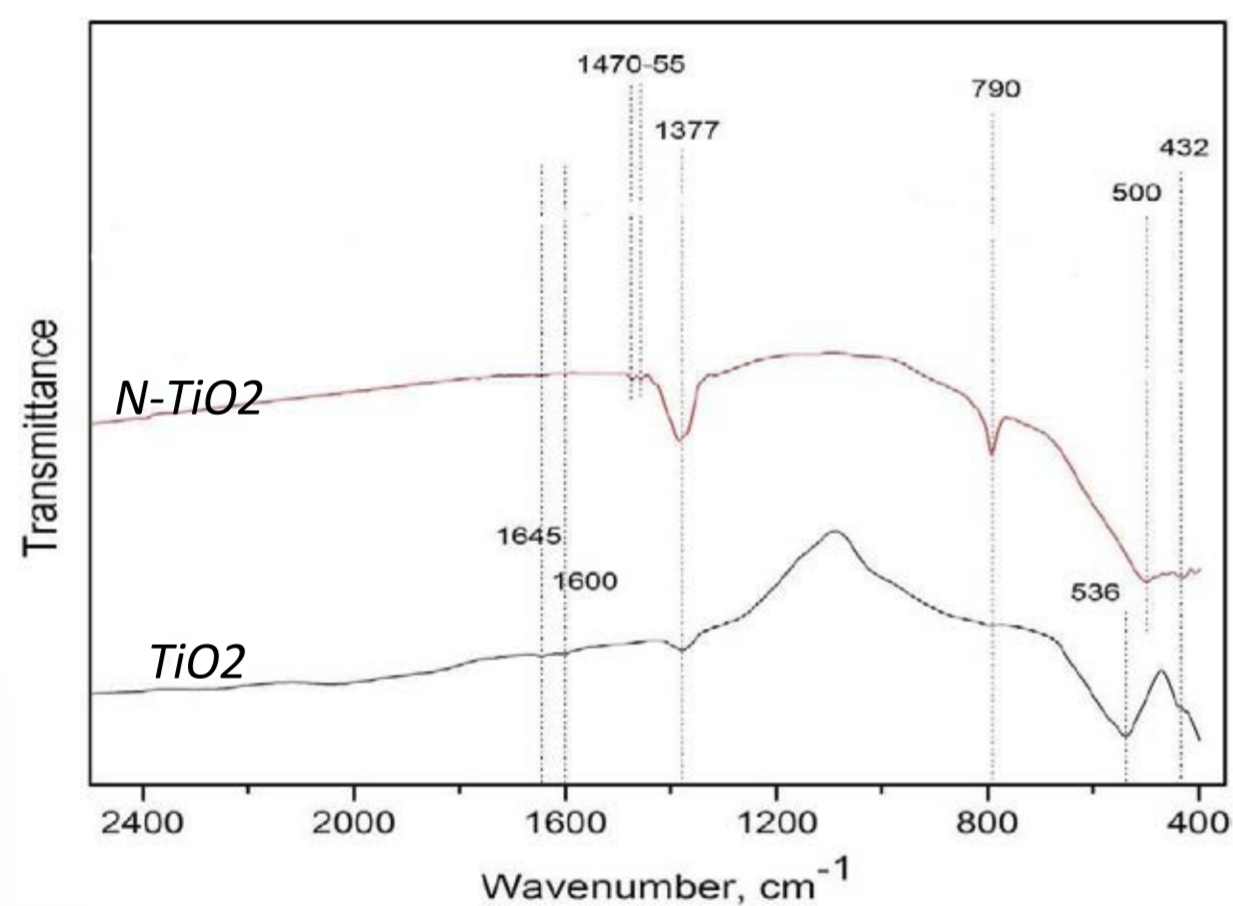
fig.1 FTIR spectra of TiO2 and N-TiO2 thin films with different N2 - O2.

The FTIR spectra of TiO2 and N-TiO2 films with different nitrogen concentration are shown. The bands located in range of 430–600 cm−1 correspond to the vibrations of Ti - O and Ti − O - Ti stretching modes. The peak at 790 cm−1 appeared in N-TiO2 spectra can be assigned to the vibration of Ti - O or N − Ti - O formation bonds. The strong peak at around 1377 cm−1 is due to the lattice vibrations of titanium oxide.[4]

The character of the morphology and the relief of the surface is shown in fig.3. It was found that when annealed at 1300 ° C, the films show no apparent integrity problems and have good adhesion to the substrate.

- 3a – Photomicrograph of a coated sample.
- 3b –High resolution photomicrograph.
- 3d–Sample calcined at 1300 ° C. The coating is homogeneous, multilayered.
- 3c –On the coating after annealing, a break in the film formed due to local overheating is visible. Noticeable inclusions - substrate fragments formed during sample preparation.
The coating thickness is less than 50 nm, Ti: O: Si = 20: 75: 5

Scope of coatings:

- Microelectronic industry
- Nuclear Engineering
- Tool production
- Medicine

Conditions

Substrate – silicon
Cathode – Ti
Mixture of gases - O2 and N2
The pressure in the chamber is 0.1 Pa
Power - 1kW
Current strength - 3A [3]

Experimental data

The Ti-O and Ti-O-N coatings were studied by differential thermal analysis (DTA) in the temperature range 20-1300 ° C at a heating rate of 10 ° C / min in an argon flow on an SDT Q600 thermal analyzer (TG, DTA, DSC) , TA Instruments (USA).

Experimentally obtained thermogravimetric curves (TG) of Ti-O and Ti-O-N coatings show a constant mass, and even a small mass gain (less than 0.2% of the total mass, within the permissible error).
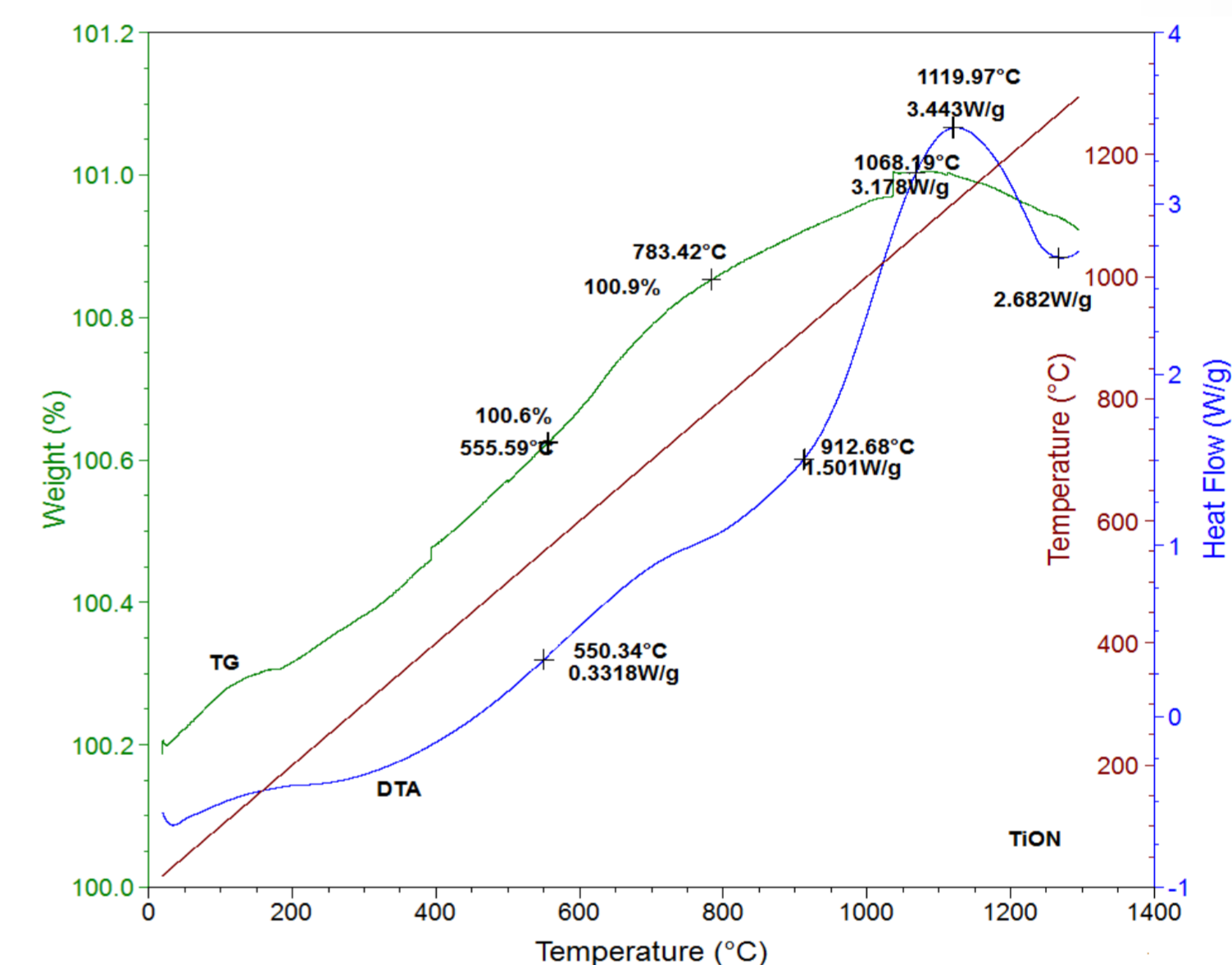
fig.2 DTA data for samples with Ti-O-N, (thermogravimetric curve (TG), differential thermal curve (DTA)).

- Microscopy, surface properties were examined using a Tescan Vega3 SBU scanning electron microscope, with an EMF attachment, (Czech Republic).

3a *3b* *3c* *3d*

fig.3 SEM images of surface morphology of samples with Ti-O-N, max resolution - 40,000 times.

Conclusions

Thus, when studying the properties of coatings by DTA found that titanium oxide and oxynitride coatings are thermally stable in a wide temperature range, high corrosion properties suggest, and are promising for practical application.
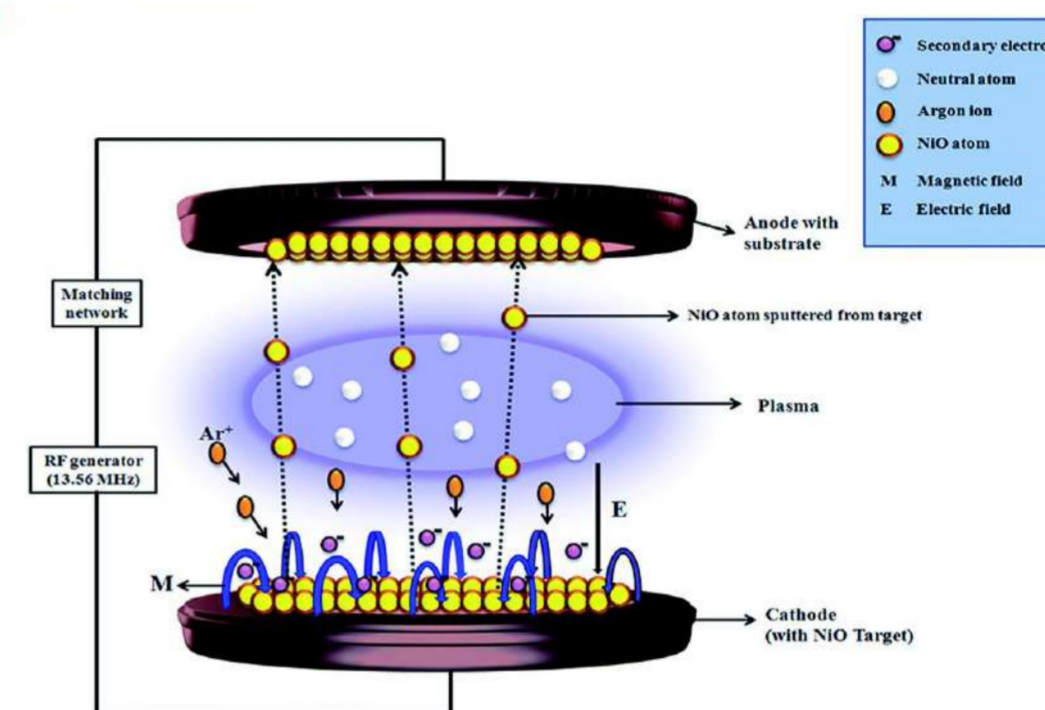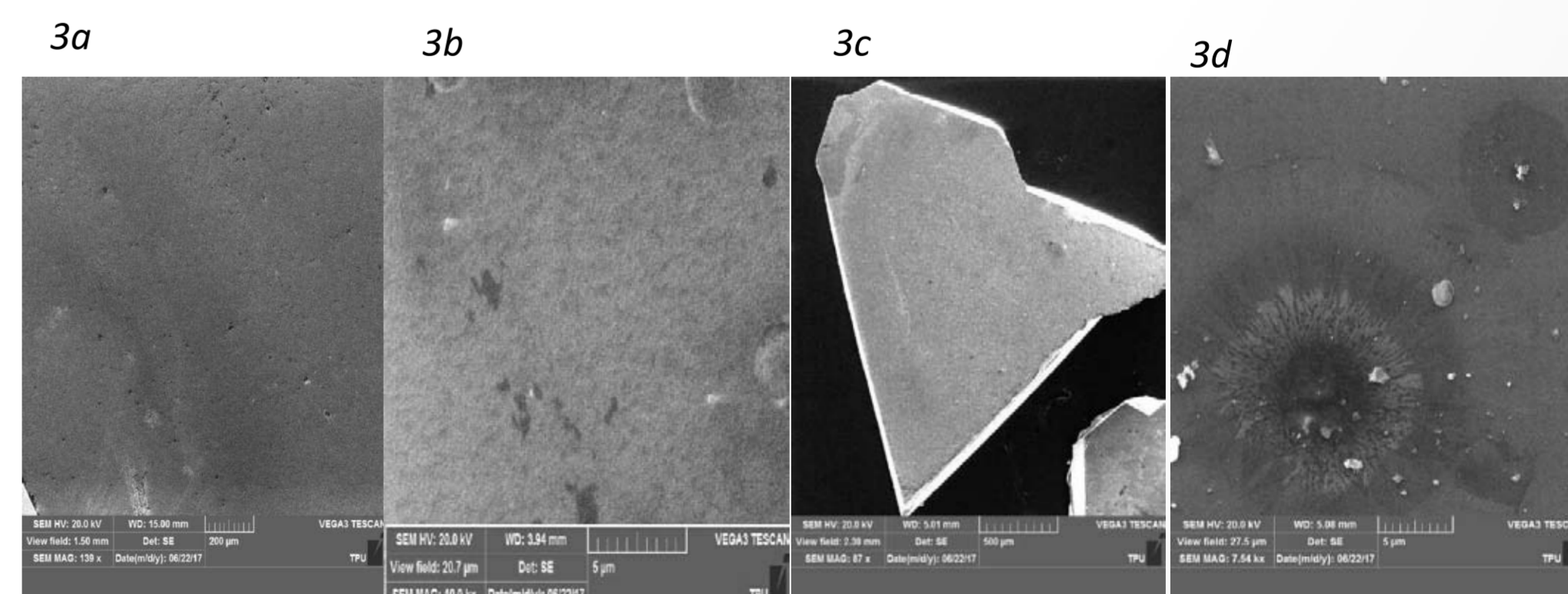
Bibliography
[1] Investigating Thin Ti–O–N Films Deposited via Reactive Magnetron Sputtering / E.L. Boytsova, L.A. Leonova // Bulletin of the Russian Academy of Sciences: Physics. – 2018. – Vol. 82 – № 9. – p. 1143–1147.[
[2] The study of the properties of titanium dioxide films formed by various methods / TW Molodechkina., AV Vasiukov, AV Bor, MO Molodechkin // New materials and technologies in mechanical engineering: materials of the 7th Int. scientific and engineering. Internet Conf. Bryansk – 2007
[3] Leonova L.A., Boytsova E.L., Pustovalova A.A. The study of titanium oxynitride coatings solubility deposited by reactive magnetron sputtering// IOP Conference Series: Materials Science and Engineering. 2016. Vol. 135 (1) [012026, 5 p.]
[4] Pustovalova, A.A. Formation and structural features of nitrogen-doped titanium dioxide thin films grown by reactive magnetron sputtering / A. Pustovalova, **E. Boytsova**, D. Aubakirova, M. Bruns, S. Tverdokhlebov, V. Pichugin // Applied Surface Science. – 2020. – Vol. 534. doi.org/10.1016/j.apsusc.2020.147572.

III International Conference and School
"Synthesis, Structure, and Properties of High-Entropy Materials"
October 11-15, 2021

№ 2

vinnikda@susu.ru

SYNTHESIS AND STUDY OF HIGH-ENTROPY OXIDE PHASES WITH THE MAGNETOPLUMBITE STRUCTURE

Vinnik D. A., Zaitseva O. V., Gudkova S. A., Zhivulin V. E., Zherebtsov D. A., Myasnikova A. A., Starikov A. Yu., Trofimov E. A.

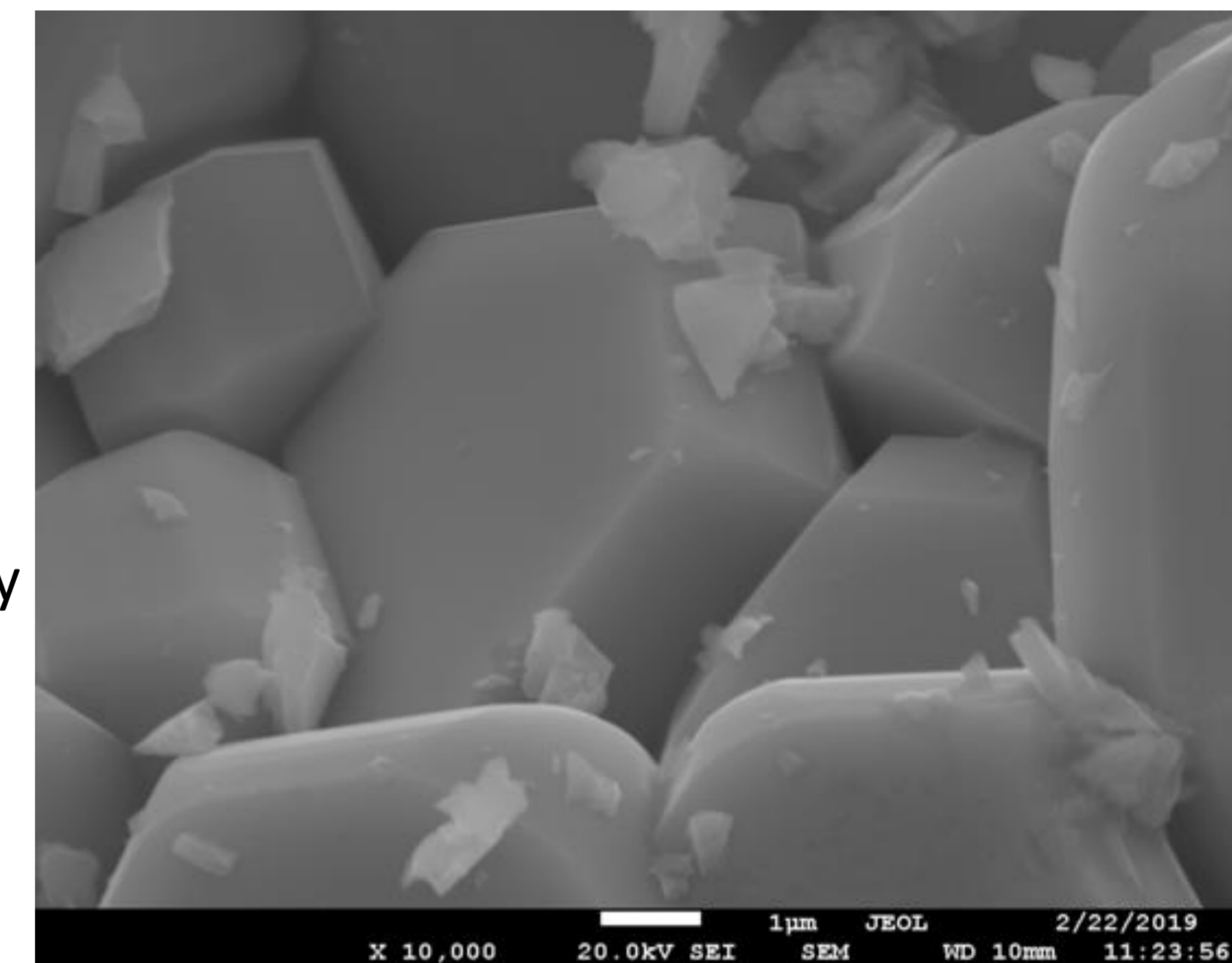*South Ural State University, Chelyabinsk, Russian Federation*

In the course of the research, the following tasks were solving:

- obtaining samples of a new class of high-entropy oxide phases - high-entropy phases with a magnetoplumbite structure;

- investigation of the composition and structure, as well as the properties of the obtained samples;

- analysis of the obtained experimental data in order to formulate the general laws governing the formation of high-entropy phases with a magnetoplumbite structure.

The main result of the investigation was the discovery (for the first time in the world) of a special class of high-entropy oxide compounds - high-entropy phases with a magnetoplumbite structure. The fact of the possibility of obtaining such compounds has been indisputably proven. A number of elements that can participate in the formation of compounds with such a structure have been determined; for a number of other elements, the impossibility of their inclusion in the composition of high-entropy phases with a magnetoplumbite structure in significant amounts has been shown.

The main results of the research also include the following:

1. Synthesized samples of high-entropy oxide phases with a magnetoplumbite structure. Data on temperature and concentration ranges of stability of phases of this kind.

2. A successfully implemented technique for the synthesis of high-entropy oxide phases with a magnetoplumbite structure by means of solid-phase synthesis. Data on the stable modes of obtaining samples, including the composition of the batch, as well as the temperature conditions of the process, ensuring the production of single-phase samples suitable for studying their physical characteristics.

3. A thermodynamic model has been developed for high-entropy oxide phases with a magnetoplumbite structure with a set of model parameters that make it possible to describe the dependence of the thermodynamic functions of such phases on their composition and temperature. The results of modeling the synthesis of high-entropy oxide phases with a magnetoplumbite structure from precursors have been obtained and compared with experimental data.

4. A lot of data have been obtained on the structure and composition of experimental samples. These data were obtained by methods of X-ray fluorescence spectroscopy, scanning electron microscopy, as well as methods of X-ray phase analysis.

5. Obtained data on the magnetic and microwave characteristics of experimental samples. Results of the analysis of the dependence of the magnetic and microwave characteristics on the crystal structure and composition of the samples. Wide possibilities of fine control of these characteristics (in particular, the Curie temperature, resonance frequency, etc.) by changing the composition of the phases under study have been found.

6. The analysis of the results obtained made it possible to formulate recommendations on the use of crystal phases obtained in the process of research for the manufacture of electronic components.

III International Conference and School
"Synthesis, Structure, and Properties of High-Entropy Materials"
October 11-15, 2021

№3

INCREASED EROSION RESISTANCE OF UFG TITANIUM ALLOYS WITH PROTECTIVE ION-PLASMA COATING

Valiev R.R., Savina Ya.N.

rovaliev@gmail.com

Introduction

As is known, parts made of titanium alloys used in a gas turbine engine during operation are subjected to high dynamic loads and erosive surface wear, which leads to a decrease in performance and reliability. In this regard, at the same time with an increase in the mechanical properties of the material, it is necessary to protect the surface with special protective coatings. In this paper, a combined approach to improving the operational reliability of materials subject to erosive wear is considered. This approach combines an increase in the specific strength due to the refinement of the grain microstructure in the bulk of the metal, using the methods of severe plastic deformation (SPD), and surface protection by deposition of an ion-plasma coating.
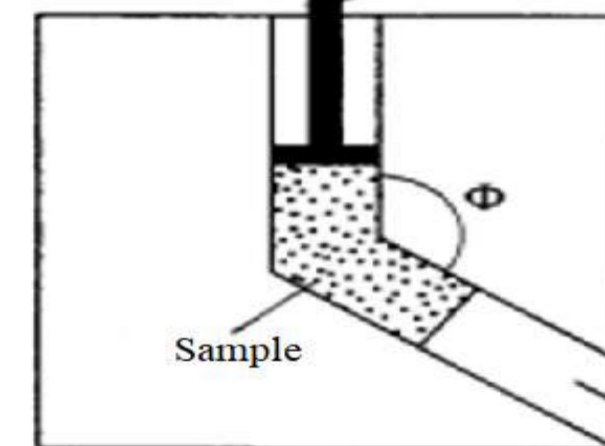
Materials

Structural titanium alloys VT6 and VT8M-1 were used as materials for the research.

VT6 (Ti-6Al-4V)	Ti	Al	V	Fe	Zr	O	C	Si	N	H	Other
	86,45 - 90,9	5,3-6,8	3,5-5,3	0,6	0,3	0,2	0,1	0,1	0,05	0,0015	0,3

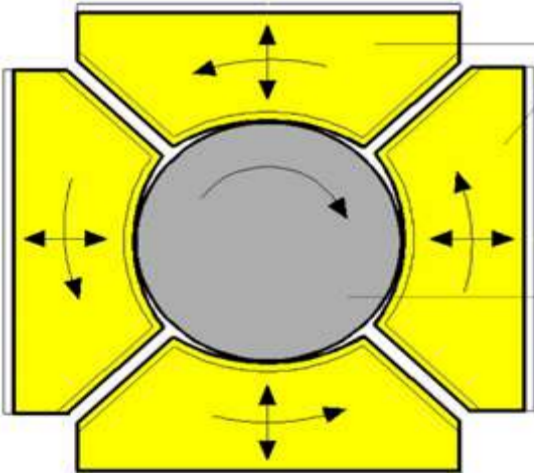| VT8M-1 (Ti-6Al-4Mo-1.5Zr)	Ti	Al	Mo	Sn	Zr	Si	Fe	C	O	N	H	Other
	85,78 - 91	5,0 -5,8	3,0-4,3	0,3-1,5	0,3– 1,5	0,1– 0,22	<0,3	<0,1	<0,15	0,03	<0,015	0,3

SPD

Equal-channel angular pressing (ECAP)

Ultrafine-grained structure of Ti-6Al-4V alloy was obtained by equal channel angular pressing (ECAP)
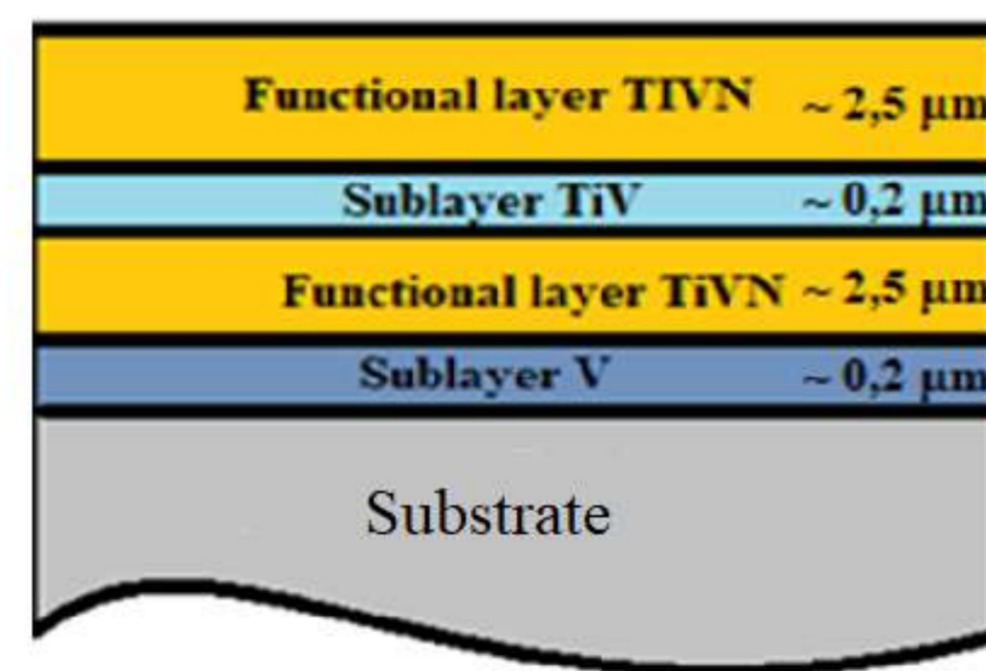- angle ψ = 120° at the temperature of 650 °C
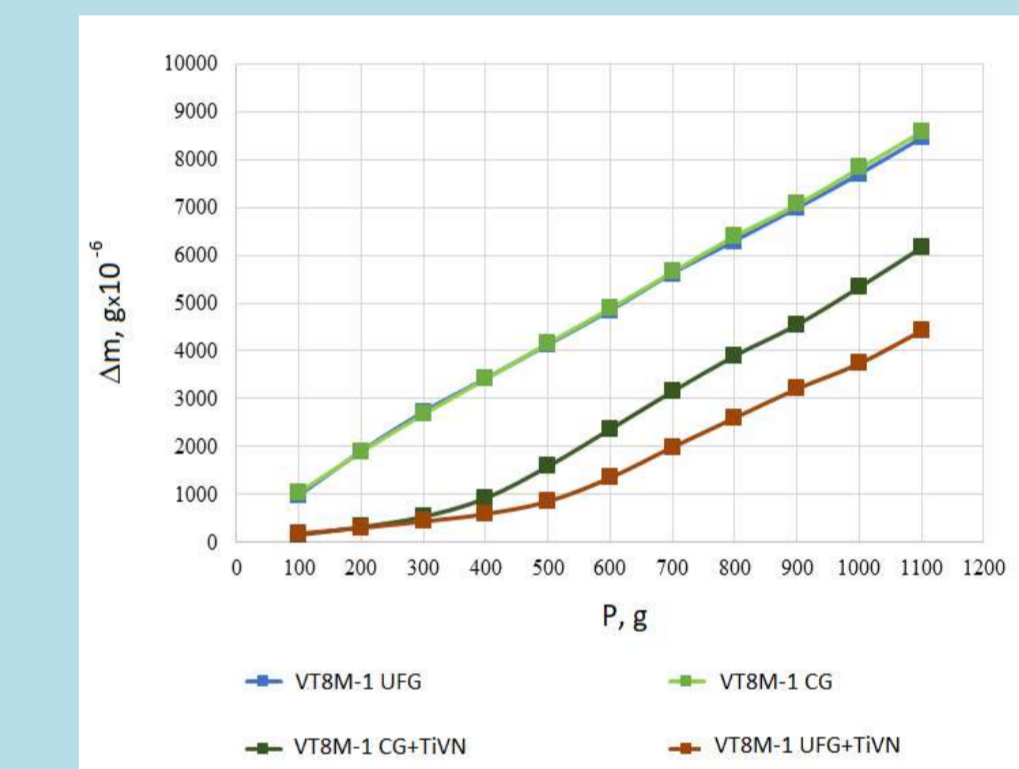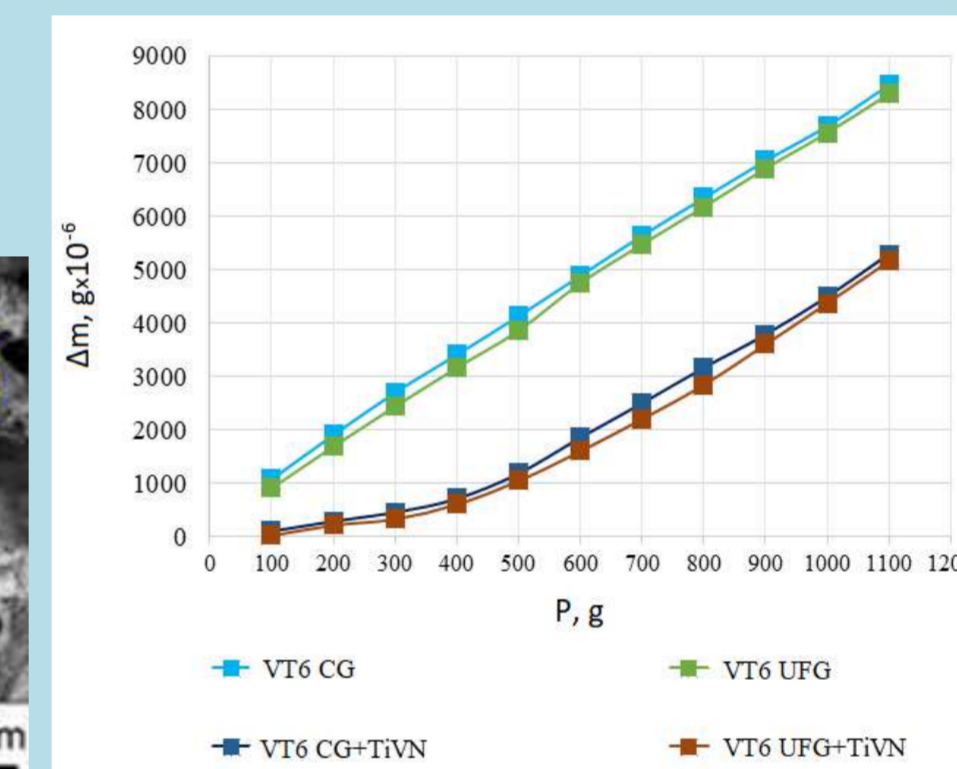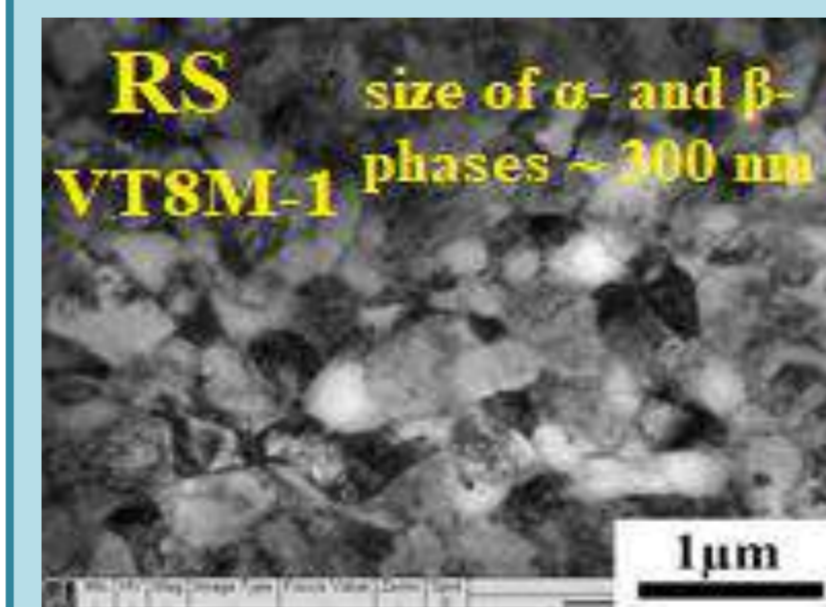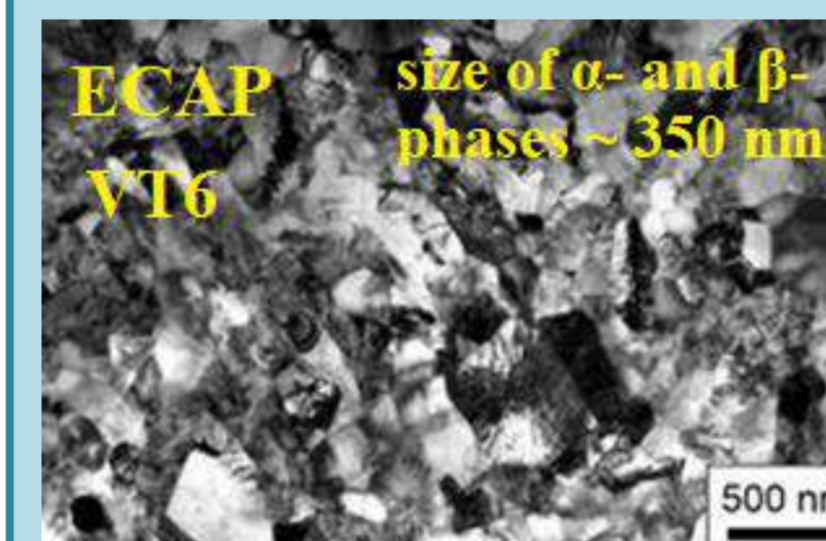- route Bc
- number of passes - 6

Rotary swaging (RS)

Ultrafine-grained structure of Ti-6Al-4Mo-1.5Zr alloy was obtained by rotary swaging (RS)

TiVN ion plasma coating architecture

Functional layer TIVN	~ 2,5 µm
Sublayer TiV	~ 0,2 µm
Functional layer TiVN	~ 2,5 µm
Sublayer V	~ 0,2 µm
Substrate	

The deposition of a protective coating was carried out by the ion-plasma method on a special vacuum installation in a nitrogen atmosphere using two metal cathodes – commercially pure titanium and vanadium.

Research methods

Installation for erosion testing

electrocorundum particles (Al_2O_3) used for erosion testing

Erosive wear tests

Performed according to the method of comparative tests. Al_2O_3 with a particle size of d = 40 - 50 µm was used as an abrasive material, 11 test cycles were carried out, the time of one cycle was t = 65 s, the rotational speed of the disk was n = 8600 rpm, the consumption of the abrasive per cycle was P = 100 g, angle of attack 65 °.

Experimental results

ECAP VT6 — size of α– and β– phases ~ 350 nm — 500 nm

RS VT8M-1 — size of α– and β– phases ~ 300 nm — 1µm

Legend: VT6 CG, VT6 UFG, VT6 CG+TiVN, VT6 UFG+TiVN; VT8M-1 UFG, VT8M-1 CG, VT8M-1 CG+TiVN, VT8M-1 UFG+TiVN
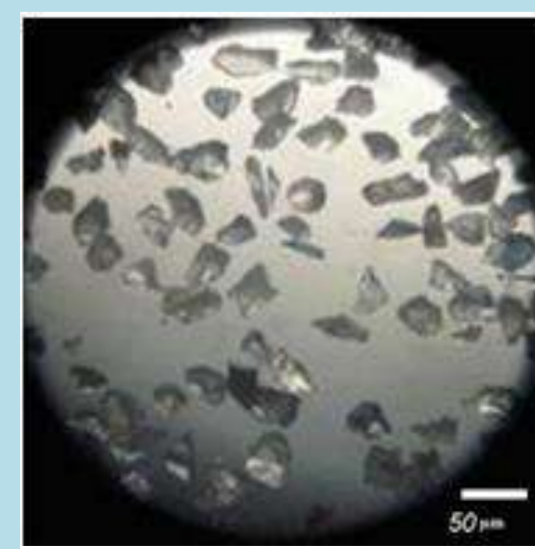
Dependence of the mass carry-over of samples of titanium alloys VT6 and VT8M-1 in the CG and UFG state, coated and uncoated at an angle of attack of 65 °

Sample	HV	Adhesive strength, H	Relative erosion resistance
VT6 CG	325.1±5.0	-	1
VT6 CG+TiVN coating	795.6±6.0	6.90±0.30	1.62
VT6 UFG	387.5±5.0	-	1.50
VT6 UFG+TiVN coating	925.7±4.0	14.20±0.15	2.00
VT8M-1 CG	331,4±5,0	-	1
VT8M-1 CG+TiVN coating	798,6±7,0	7,69± 0,17	1.45
VT8M-1 UFG	360,5±6,0	-	1.32
VT8M-1 UFG+TiVN coating	914,4±5,0	18,1±0.13	2.00

Conclusions

According to the results of the tests carried out, the following was established:

1) The deposition of an ion-plasma protective TiVN coating on the surface of titanium alloys VT6 and VT8M-1 in the coarse-grained (CG) and ultrafine-grained (UFG) state significantly reduces the mass carryover during erosion tests.

2) The erosion resistance of an alloy with an UFG structure and coating increases by 2 times in comparison with an uncoated CG alloy.

Thus, using a approach that combines the refinement of the grain structure in the bulk of the material and the deposition of an ion-plasma coating on its surface, it was possible to increase a whole range of properties - adhesive strength, mechanical properties* and erosion resistance.

*R.R. Valiev, Y.M. Modina, K.S. Selivanov, I.P. Semenova, E.D. Khafizova, R.Z. Valiev, Ya.N. Savina, Enhanced service properties of a protective coating on a titanium alloy with an ultrafine-grained structure, Materials Letters, Vol. 305, 2021, 130781 (https://doi.org/10.1016/j.matlet.2021.130781).

**III International Conference and School
"Synthesis, Structure, and Properties of High-Entropy Materials"
October 11-15, 2021**

№4

НИУ БелГУ
BELGOROD STATE
UNIVERSITY (BSU)

zherebtsov@bsu.edu.ru

Zherebtsov S.V., Ozerov M.S., Shaysultanov D.G., Stepanov N.D.

DEVELOPMENT OF CO-CR ALLOYS FOR MEDICAL APPLICATION

The aim: Development and obtaining of a Co-Cr-based dental alloy for removable / fixed dentures

Technical requirements

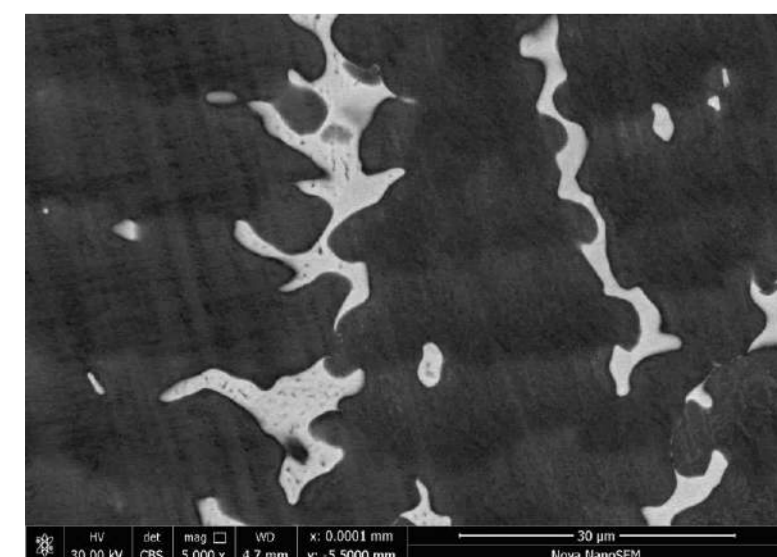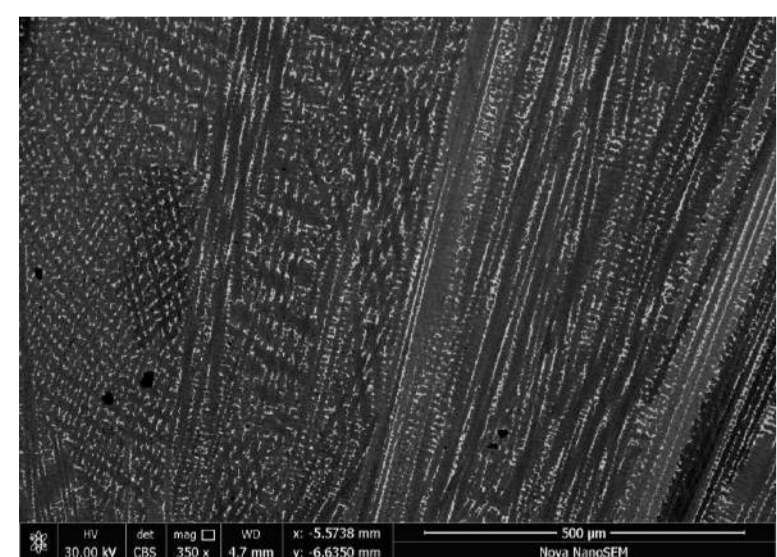| Requirements	Values
Yield strength (σ_{02}), MPa, not less	700
Tensile strength (σ_B), MPa, not less	925
Tensile elongation (δ), %, not less	10
Young's modulus, (E), GPa	108-220
Vickers hardness (HV), not less	300
Corrosion resistance (metal ion yield) mg/cm^2, not more	200
Fluidity, mm, not below average	350-340

Method of obtaining

Vacuum arc remelting
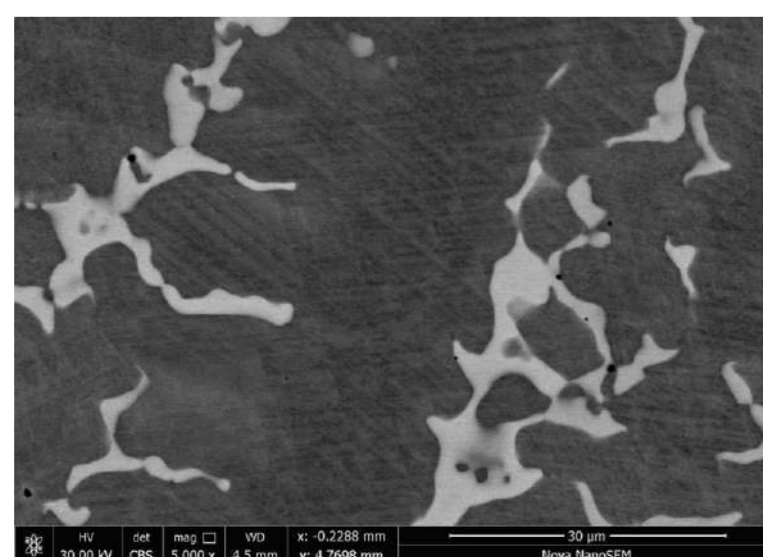
Mechanical processing
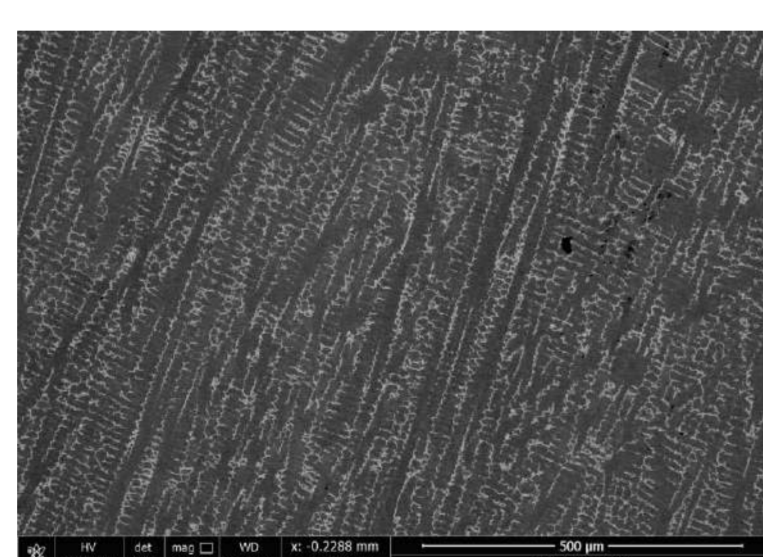
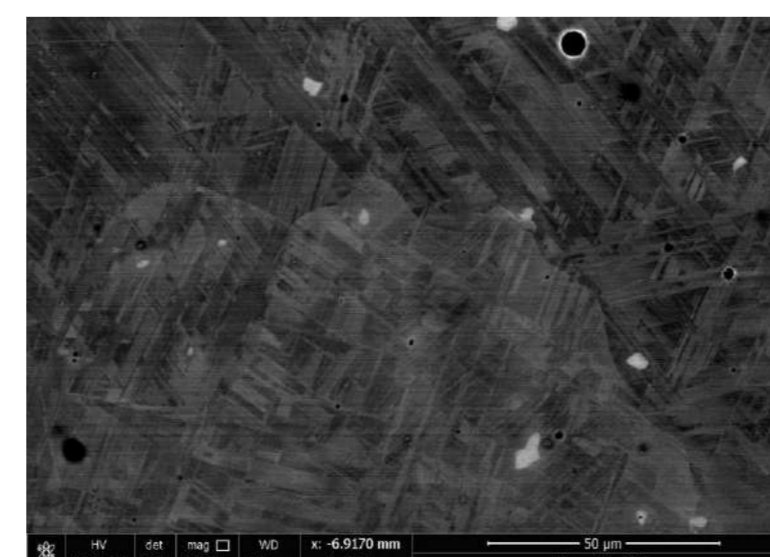Buehler Arc Melter 200
(Германия)
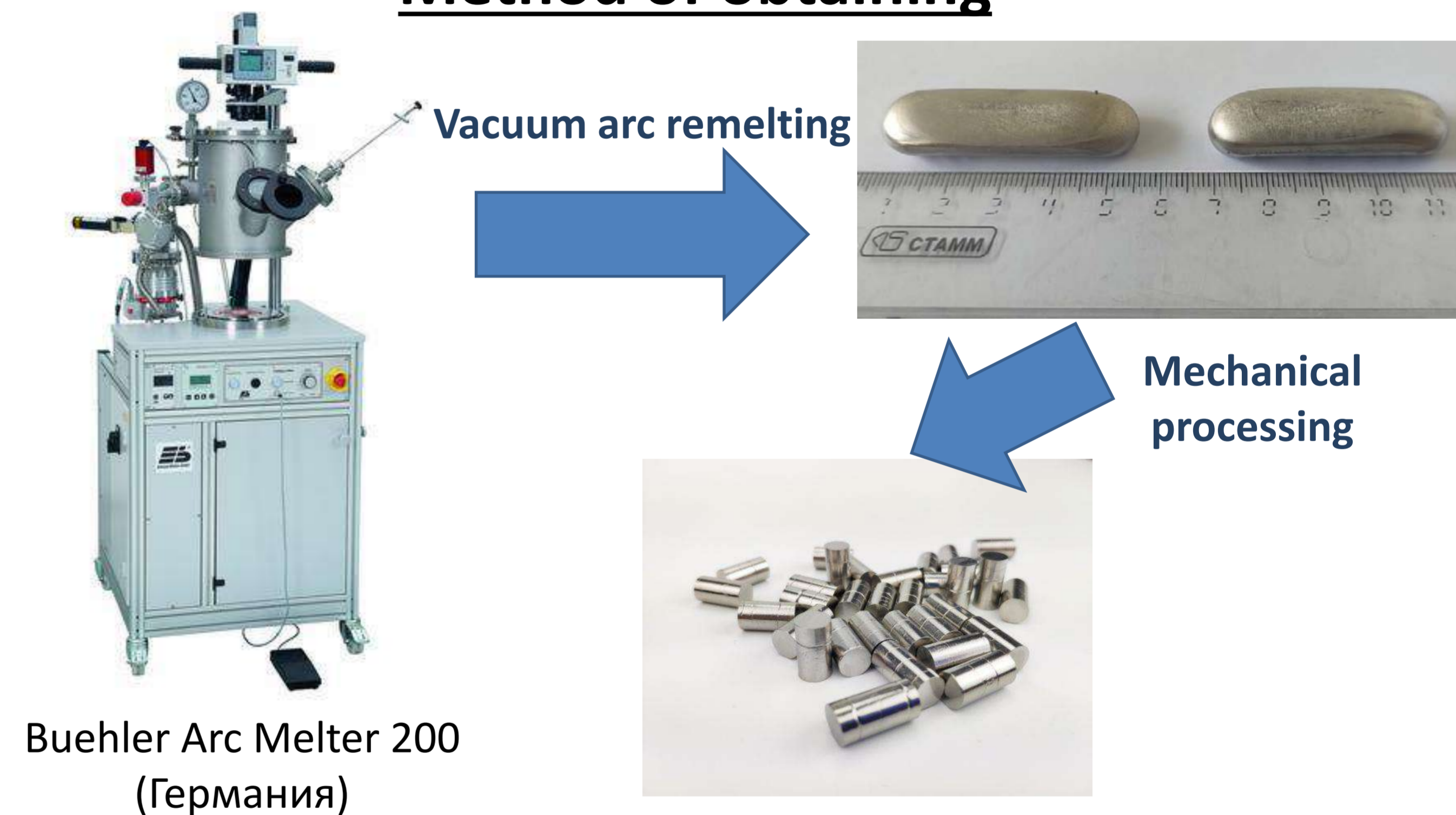
Microstructure

Heraenium
59Co25Cr10W4Mo1Si0.8Mn0.2C

60Co30Cr5W5Mo

65Co30Cr5Mo

Results

Engineering stress, MPa

- 59Co25Cr10W4Mo1Si0.8Mn0.2C
- 60Co30Cr5W5Mo
- 65Co30Cr5Mo
- 64Co30Cr5Mo1.0Si
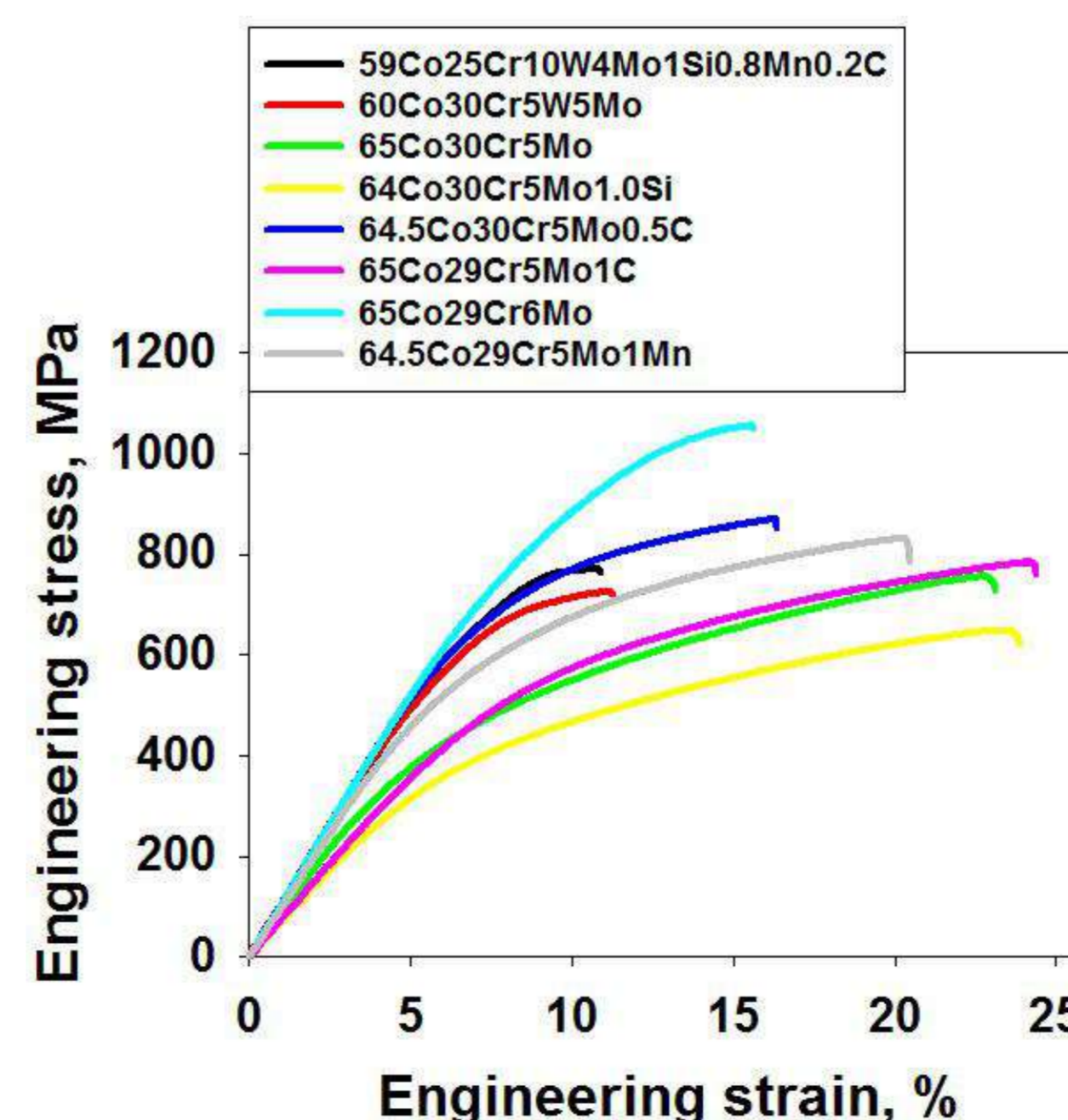- 64.5Co30Cr5Mo0.5C
- 65Co29Cr5Mo1C
- 65Co29Cr6Mo
- 64.5Co29Cr5Mo1Mn

Engineering strain, %
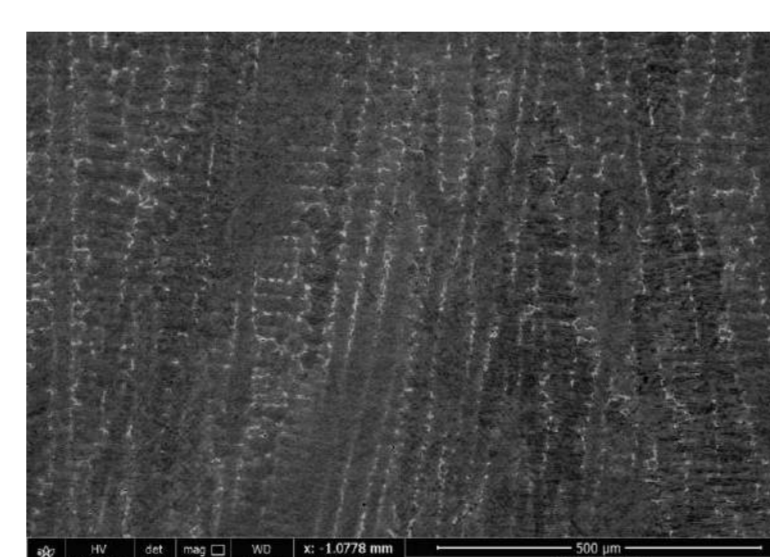
Mechanical properties

Alloys	Tensile strength, MPa	Yield strength, MPa	δ,%
Heraenium 59Co25Cr10W4Mo1Si0.8Mn0.2C	770	595	3
60Co30Cr5W5Mo	726	460	4
65Co30Cr5Mo	756	310	11
64Co30Cr5Mo1.0Si	648	300	11.4
64.5Co30Cr5Mo0.5C	869	560	6
65Co29Cr5Mo1C	784	390	11
65Co29Cr6Mo	1055	660	3.6
64.5Co29Cr5Mo1Mn	832	445	9

E-mail: vekro@ihte.uran.ru

FORMATION MECHANISM OF CRYSTALLINE SOLID SOLUTIONS UO₂ - ThO₂ AND UO₂ - ThO₂ - ZrO₂ IN MOLTEN SALTS. INFLUENCE OF CURRENT ON THEIR COMPOSITION.

KROTOV V.E.

IHTE Ural Branch of RAS, Ekaterinburg, Russia

The solid solutions UO_2 - ThO_2 and UO_2 - ThO_2 - ZrO_2 are nuclear fuel [1]. They were obtained only in the powder form. **The purpose of the present work is to test the possibility of synthesizing the crystalline forms of these systems.** The study was performed at 750 ° C in the molten equimolar mixture of NaCl-KCl containing UO_2Cl_2, $ThCl_4$ and $ZrCl_4$. The crystalline solid solutions were obtained as a result of the during simultaneous implementation of two processes at the cathode: the reaction of electrochemical reduction of UO_2^{2+} ions to crystalline uranium dioxide UO_2 (1), and the chemical reaction between UO_2 and thorium (zirconium) cations present in the molten electrolyte (2). The process can be represented in a simplified manner using the following equations:

$$UO_2^{2+}(melt) + 2e^- = UO_2(s) \tag{1}$$

$$UO_{2\,(s)} + xMe^{4+}_{(melt)} = xMeO_2(1-x)UO_{2(s)} + xU^{4+}_{(melt)} \tag{2}$$
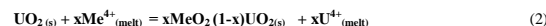
The proposed method is of undoubted scientific interest for another reason. In the literature, electrochemical reactions are known accompanied by previous or subsequent chemical reactions. However, there no information with the exception of our works [2-4] about the electrochemical reactions, when simultaneously with them on the cathode chemical reactions occurs.

The UO₂–ThO₂ and UO₂–ZrO₂ systems

The ThO_2 and ZrO_2 content in cathode deposits decreases with a increase in the electrolysis current (Fig. 1), which is explained by an increase in the rate of the electrochemical reaction (1) while maintaining a constant rate of the chemical reaction (2).
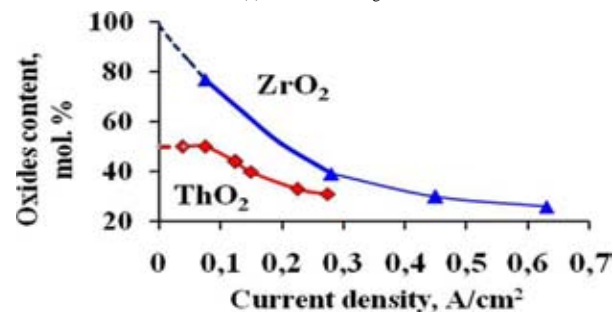

Figure 1. Effect of the electrolysis current density on the ThO_2 and ZrO_2 content in the UO_2–$Th(Zr)O_2$ cathode deposits at 1023 K. The melts composition, mol.%: (NaCl-KCl)–UO_2Cl_2(3)–$ThCl_4$(3,5) and (NaCl–KCl)–UO_2Cl_2(3)–$ZrCl_4$(1,4)

The ZrO_2 concentration in the cathode deposit reached 98 mol. % [3]. The ThO_2 content in the oxide phase was less than the ZrO_2 concentration, which is caused by the difference in the values of equilibrium constants for the exchange reactions of $ThCl_4$ and $ZrCl_4$ with uranium dioxide (2). For example, their values at 1023 K are 3 and 170 respectively. At an electrolysis current density of less than 0.08 A / cm², the quantitative composition of the UO_2 – ThO_2 oxide phase remains unchanged, and the concentrations of uranium and thorium dioxides in the cathode deposit were practically the same and equal to 50 mol%. The results are consistent with the literature data [5], where the maximum concentration of ThO_2 in powdered uranium dioxide according to reaction (2) was 49 mol.%. As in our studies, only half of the uranium dioxide was replaced by thorium dioxide. The UO_2–ThO_2 cathode deposits are single-phase cubic solid solution. The parameter of its crystal lattice increases linearly with an increase in the content of thorium dioxide.

The UO₂–ThO₂–ZrO₂ system

The three-phase oxide system consisted of two binary cubic solid solutions and contained mol. %: UO_2 (38-71) - ThO_2 (6-16) - ZrO_2 (23-46). The crystal lattice parameter of one phase was (5,476 – 5,492) and the other - (5,460 – 5,484) Å. The dependence in the composition of the cathode deposits UO_2 - ThO_2 - ZrO_2 on the electrolysis current density is shown in Fig. 2

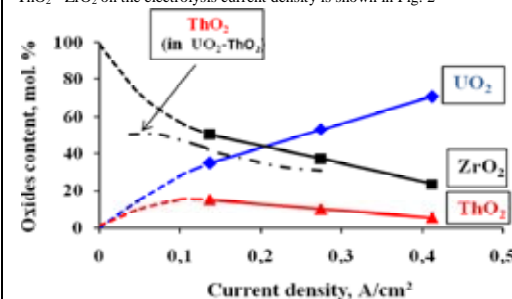Figure 2. Influence of the electrolysis current density on the U, Th and Zr oxides content in the UO_2–ThO_2–ZrO_2 cathode deposits at 750 °C. The melt composition, mol.%: (NaCl-KCl)–UO_2Cl_2 (4.7) –$ThCl_4$ (1.2) –$ZrCl_4$ (0.3)

The concentrations of UO_2 and ZrO_2 change in the same way as in the two-component The content of ZrO_2 decreases continuously whereas the concentration of UO_2 steadily increases with the increasing current density. However, the concentration dependence of ThO_2 has a different form. With values of current density above 0.1 A / cm² the concentration of thorium dioxide increases as in binary system, but at lower its values on the contrary, it decreases. In this range of current densities, the cathode deposit contains more than 60 mol. % ZrO_2, and, accordingly, a large amount of U^{4+} ions appeared in the salt melt. They shift to the left the equilibrium of the exchange reaction (2) between UO_2 and Th^{4+} ions, because its equilibrium constant is about 60 times less than with Zr^{4+} ions.

Conclusions. The crystalline solid solutions UO_2 - ThO_2 and UO_2 - ThO_2 - ZrO_2 were obtained for the first time. The mechanism of their formation has been developed. It was shown the effect of electrolysis current density on composition of solid solutions.

References
1. A. G. Samoylov, A. I. Kashtanov, and V. S. Volkov, The Dispersion Fuel Elements of Nuclear Reactors (Atomizdat, Moscow) p. 343 (1965).
2. V.Ye. Krotov, Regularities of cathode deposit formation during simultaneous reduction and exchange reactions. The mechanism of UO_2–ZrO_2 cathode deposit formation, Electrochim. Acta 115 (2014) 28-30
3. V.Ye. Krotov, Ye.S. Filatov, Regularities of cathode deposit formation during simultaneous reduction and exchange reactions. Influence of the electrolysis conditions on the concentration of components in the UO_2 - ZrO_2 cathode deposit, Electrochim. Acta 116 (2014) 484-489
4. V. Krotov, Ye. Filatov, Anomalous influence of electrochemically inert $ZrCl_4$ on UO_2 current efficiency during electrolysis in (NaCl-KCl)ₑqᵤᵢₘ -UO_2Cl_2-$ZrCl_4$ melt, Electrochim. Acta 145C (2014) 254-258
5. P. Chiotti, M.C. Jha, M.J. Tschetter, Reaction of thorium and $ThCl_4$ with UO_2 and $(Th,U)O_2$ in fused chloride salts. J. Less-Common Metals. 42 (1975) 141-161

III International Conference and School
"Synthesis, Structure, and Properties of High-Entropy Materials"
October 11-15, 2021

№6

rusfive@mail.ru

DENSITY AND ELECTRICAL RESISTIVITY
OF Al-Ni-Co-R GLASS-FORMING ALLOYS

Rusanov B.A.[1], Sidorov V.E.[1], Moroz A.I.[1], Svec P.Sr.[2], Janickovic D.[2]

[1]Ural State Pedagogical University, Ekaterinburg, Russia

[2]Institute of Physics Slovak Academy of Sciences, Bratislava, Slovakia

Aluminum-based amorphous alloys, especially Al-Ni-R and Al-Co-R compositions, have unique mechanical and corrosion properties. In this work we investigated density and electrical resistivity of Al-Ni-Co-R alloys in crystalline and liquid states.

The alloys of $Al_{86}Ni_6Co_2R_6$ (R = Nd, Sm, Gd, Tb, Yb) compositions were prepared by remelting of pure initial components in arc-melting furnace in argon atmosphere. Density of the alloys in crystalline and liquid states was measured by the absolute variant of gamma-absorption method on an automated experimental set-up in helium atmosphere. Electrical resistivity was investigated by contactless method in rotating magnetic field.
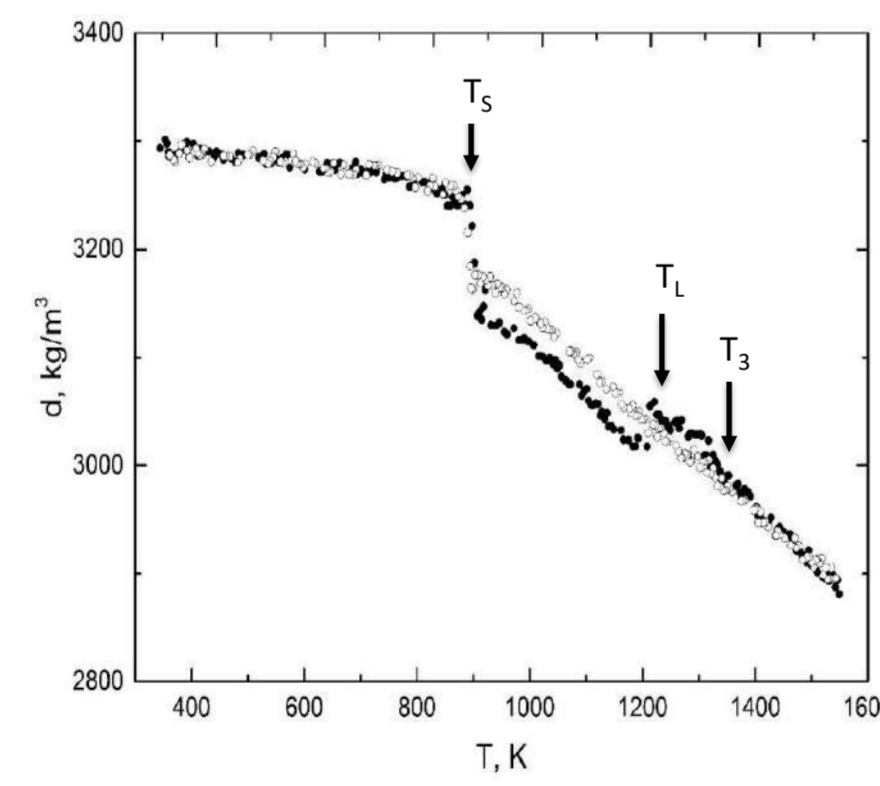

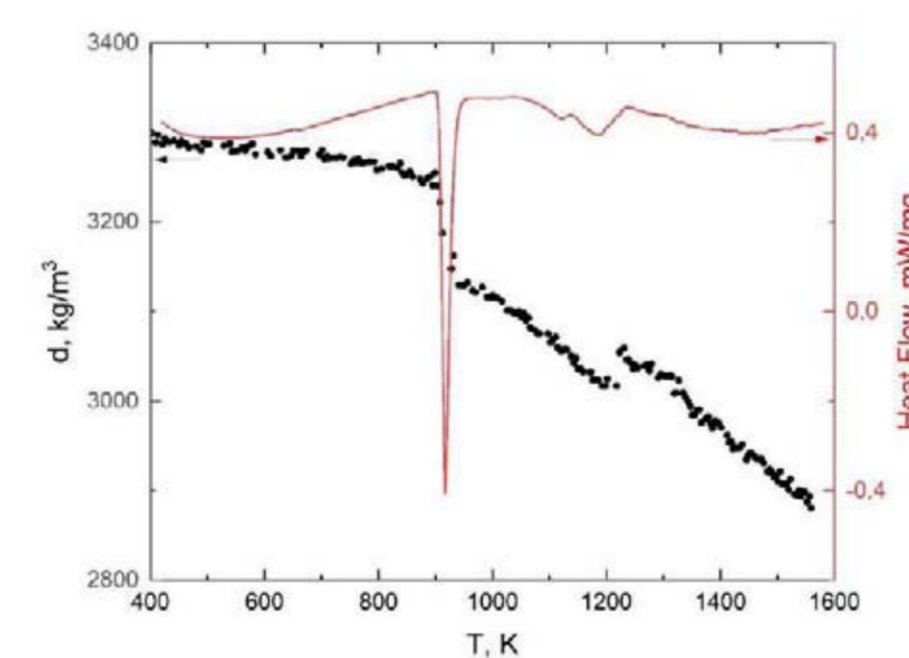Experimental installation for density measurements

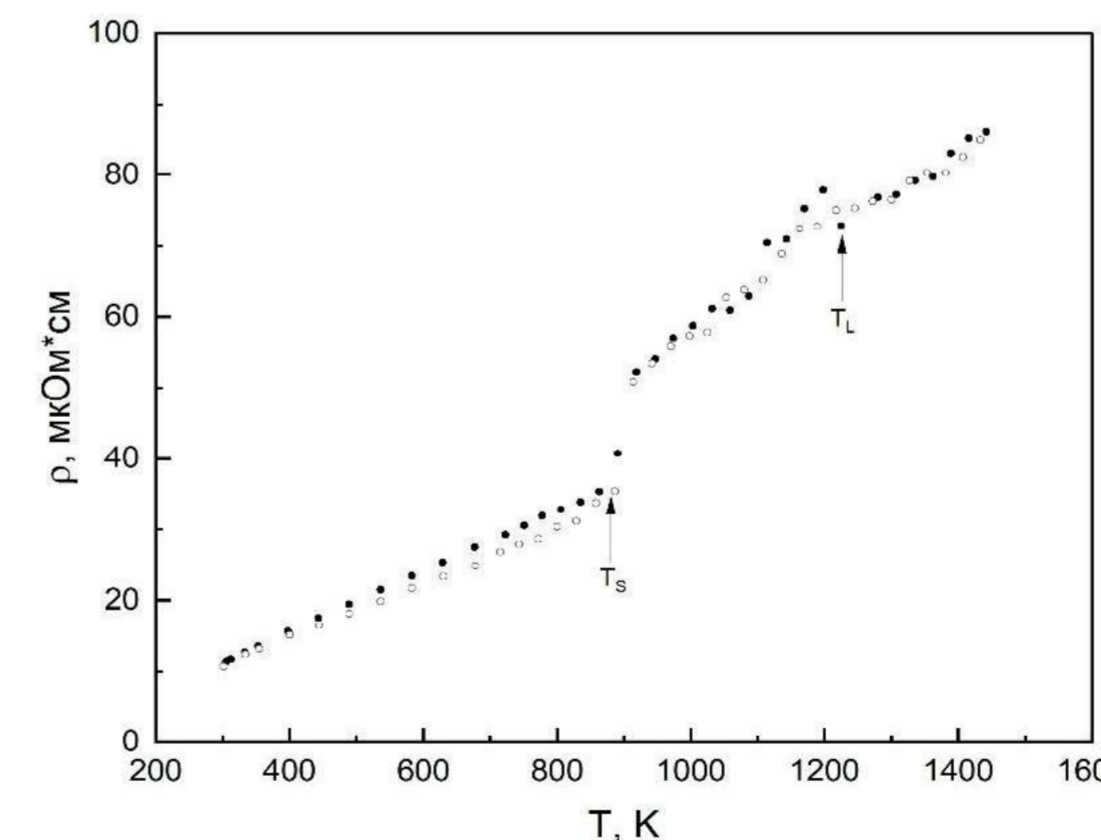Experimental installation for electrical resistivity measurements
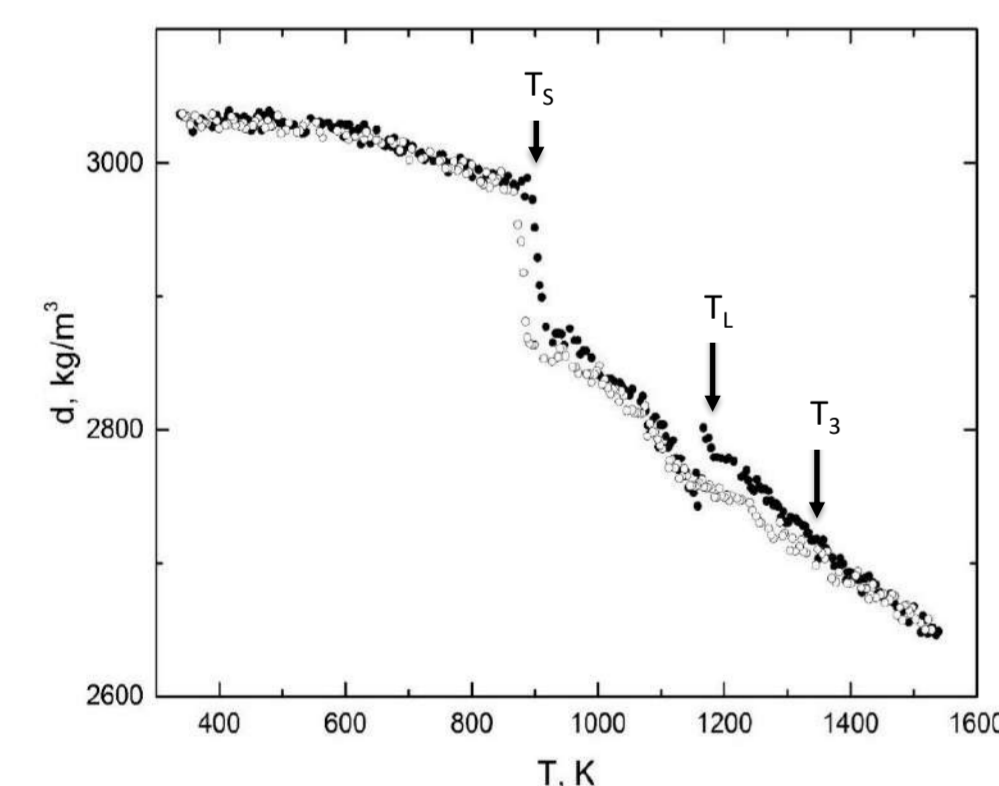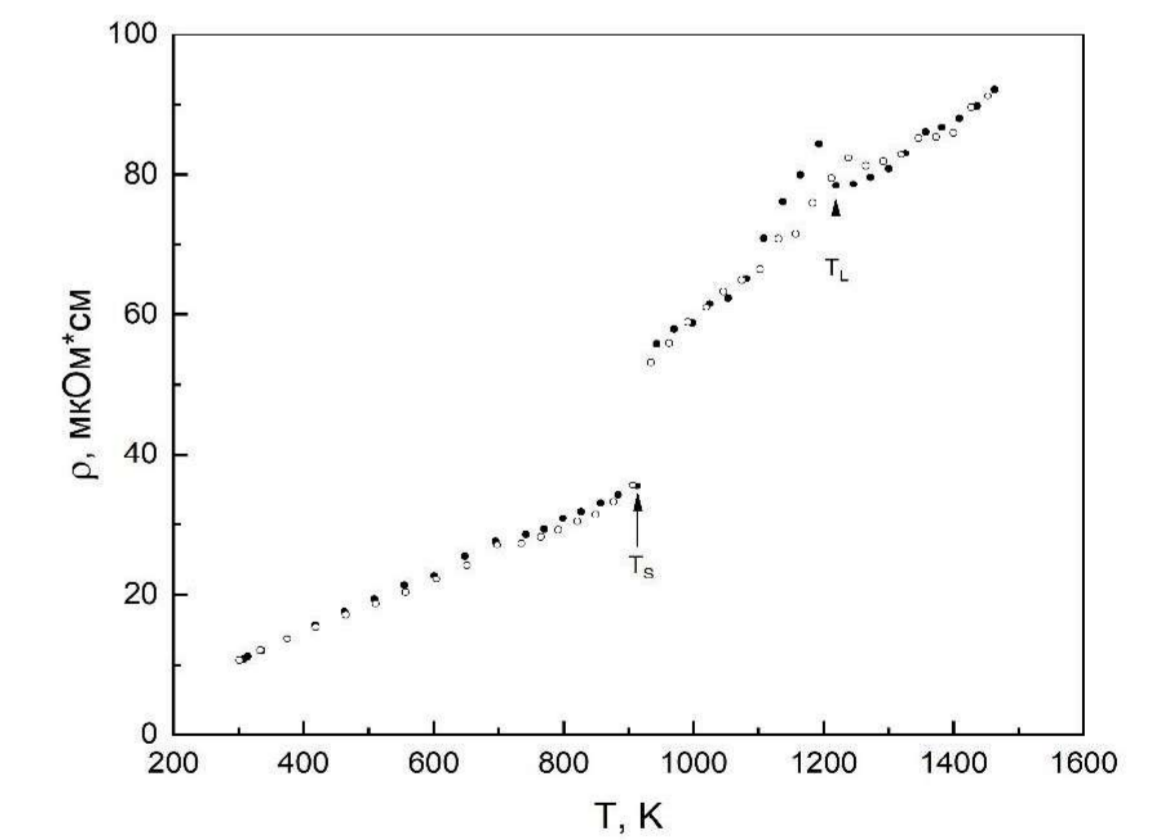

$Al_{86}Ni_4Co_4Yb_6$

$Al_{86}Ni_4Co_4Gd_6$

Density and DTA curves for $Al_{86}Ni_4Co_4Gd_6$ alloy

$Al_{86}Ni_4Co_4Gd_6$

$Al_{86}Ni_4Co_4Tb_6$

It was found that all the compositions have a wide two-phase zone (transition from solid to liquid state) and specific behavior of properties (density and electrical resistivity) at liquidus temperature (T ~ 950 K). Hysteresis of density at T < 1300 K (i.e. incoincidence of heating and cooling curves) was found for all the alloys. This can indicate the fact that the alloys remain microheterogeneous after melting and some structural transformations connected with medium range order take place at near 1350 K.

III International Conference and School
"Synthesis, Structure, and Properties of High-Entropy Materials"
October 11-15, 2021

№ 7

Ural Federal University
named after the first President
of Russia B.N.Yeltsin

THE FREQUENCE DISPERSION FEATURES OF THE DIELECTRIC CHARACTERISTICS OF HAFNIUM DISULFIDE INTERCALED WITH SILVER ATOMS

V.G.Pleshchev
Institute of Natural Sciences and Mathematics, Ural Federal University, Ekaterinburg, Russia
v.g.pleshchev@urfu.ru

INTRODUCTION and MOTIVATION

The feature of the crystal structure of transition (T) metal dichalcogenides TX_2 (X = S, Se, Te) compounds is the presence of tri-layer X–T–X units with weak van der Waals (vdW) bonds between them. The insertion of various atoms or structural fragments into vdW gaps may lead to significant changes in physical properties of these compounds. Hafnium diselenide has a wider vdW gap in comparison with TiSe2; therefore, a weaker interaction of intercalated atoms with adjacent layers can be expected in M_xHfSe_2. A considerable mobility of Ag ions was revealed in transition metal dichalcogenides intercalated with silver, in particular, in AgxTiSe2 [2] , as well in some silver-containing Ag-Hf-S phases]. Redistribution of mobile ions in an electric field leads to polarization processes and forms a dielectric response to an external field. The dielectric characteristics of such silver-containing intercalated compounds have practically not been studied before, and this work is devoted to their study.

EXPERIMENTAL DETAILS

SYNTHESIS: Initial hafnium disulfide and intercalated Ag_xHfS_2 (x = 0.10, 0.2) , polycrystalline samples were synthesized using the method of solid state reactions in evacuated quartz cells followed by multistage homogenization, Structure and phase purity of the samples were examined at room temperature using powder X-ray diffraction on a Bruker D8 Advance diffractometer ($Cu_{K\alpha}$ radiation). For Rietveld refinements of the crystal structure, the FULLPROF program was used .

ELECTRICAL MEASUREMENTS: The impedance measurements were carried out at alternating current at various temperatures in the range of linear frequencies (f) 1 Hz - 5 MHz using the universal frequency response analyzer Solartron 1260A. with an excitation signal amplitude of 200 mV. The impedance data were used to determine the values of the imaginary and real components of the complex permittivity and electrical module.
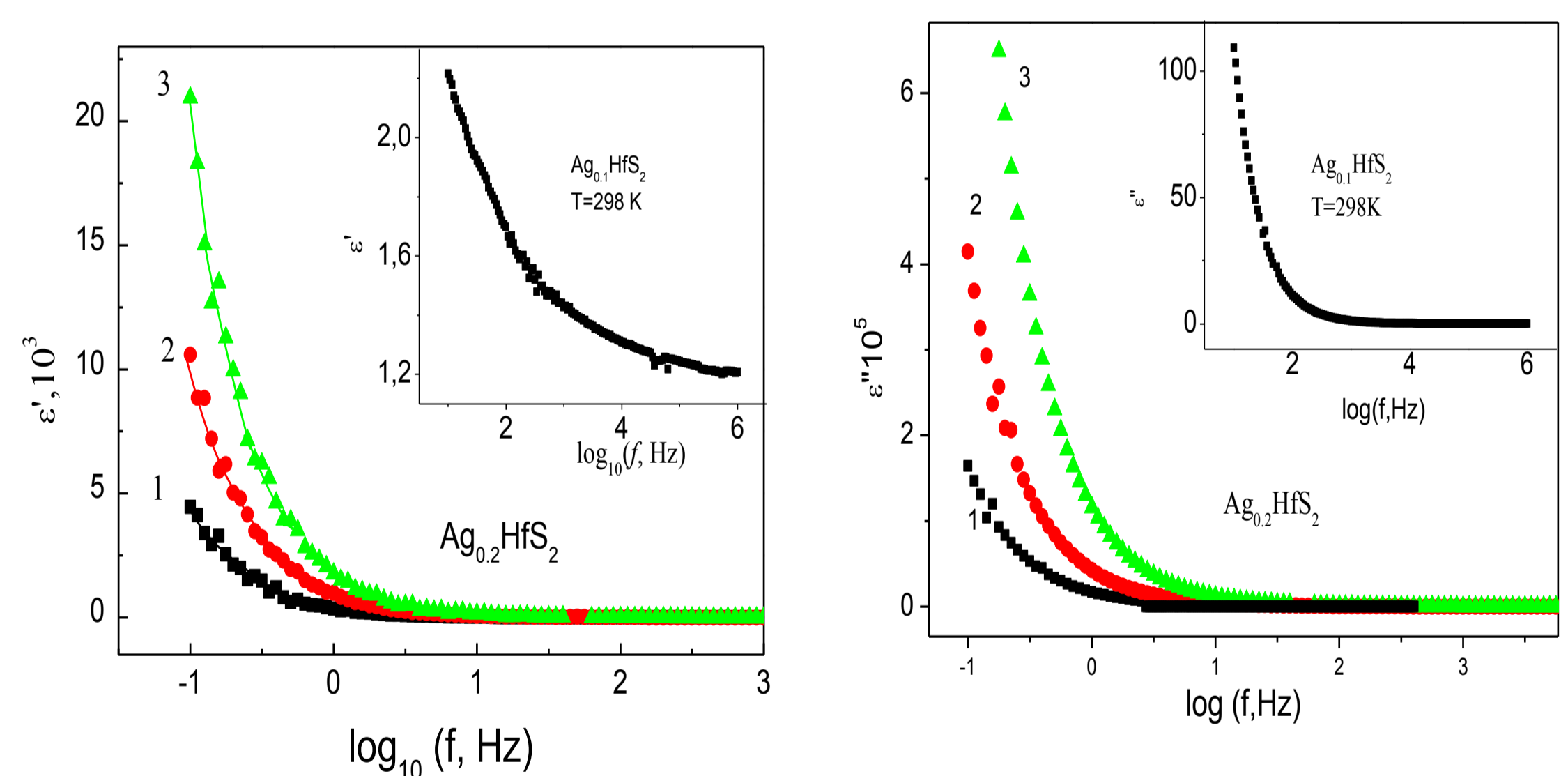

Fig.1, 2. Frequency dependences of the real and imaginary components of relative dielectric permeability of intercalated Ag_xHfS_2 samples. T=275K(1),298K(2), 330K(3)
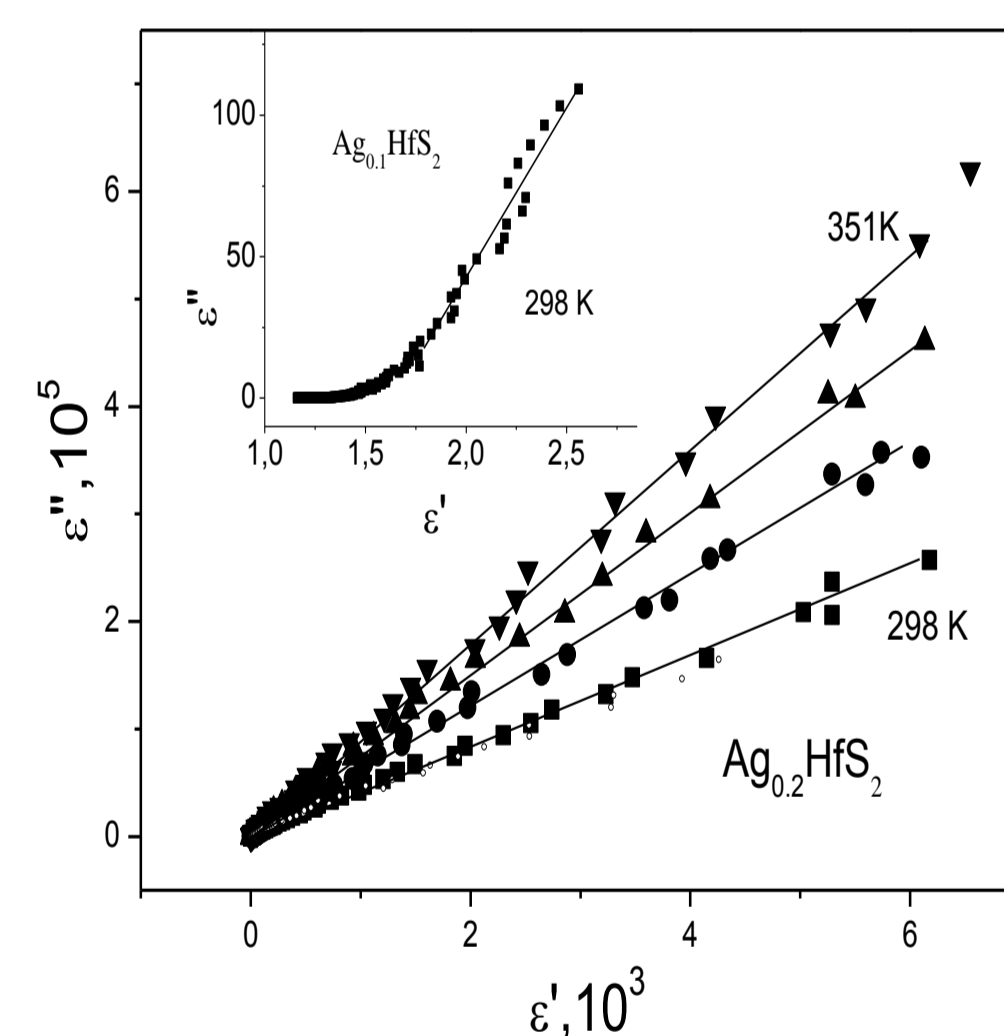
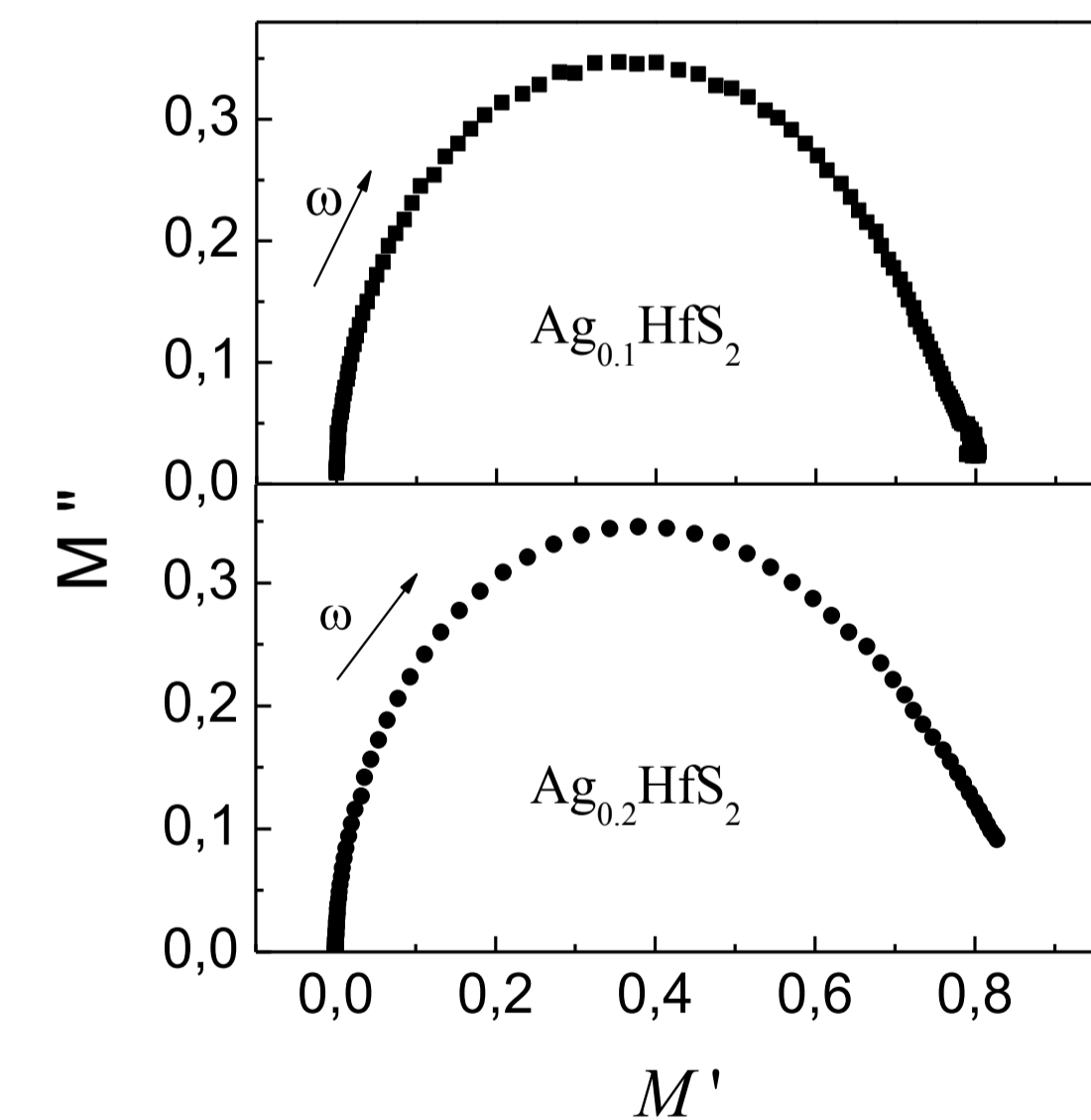Fig3. Linear dielectric permeability dispersion of AgxHfS2
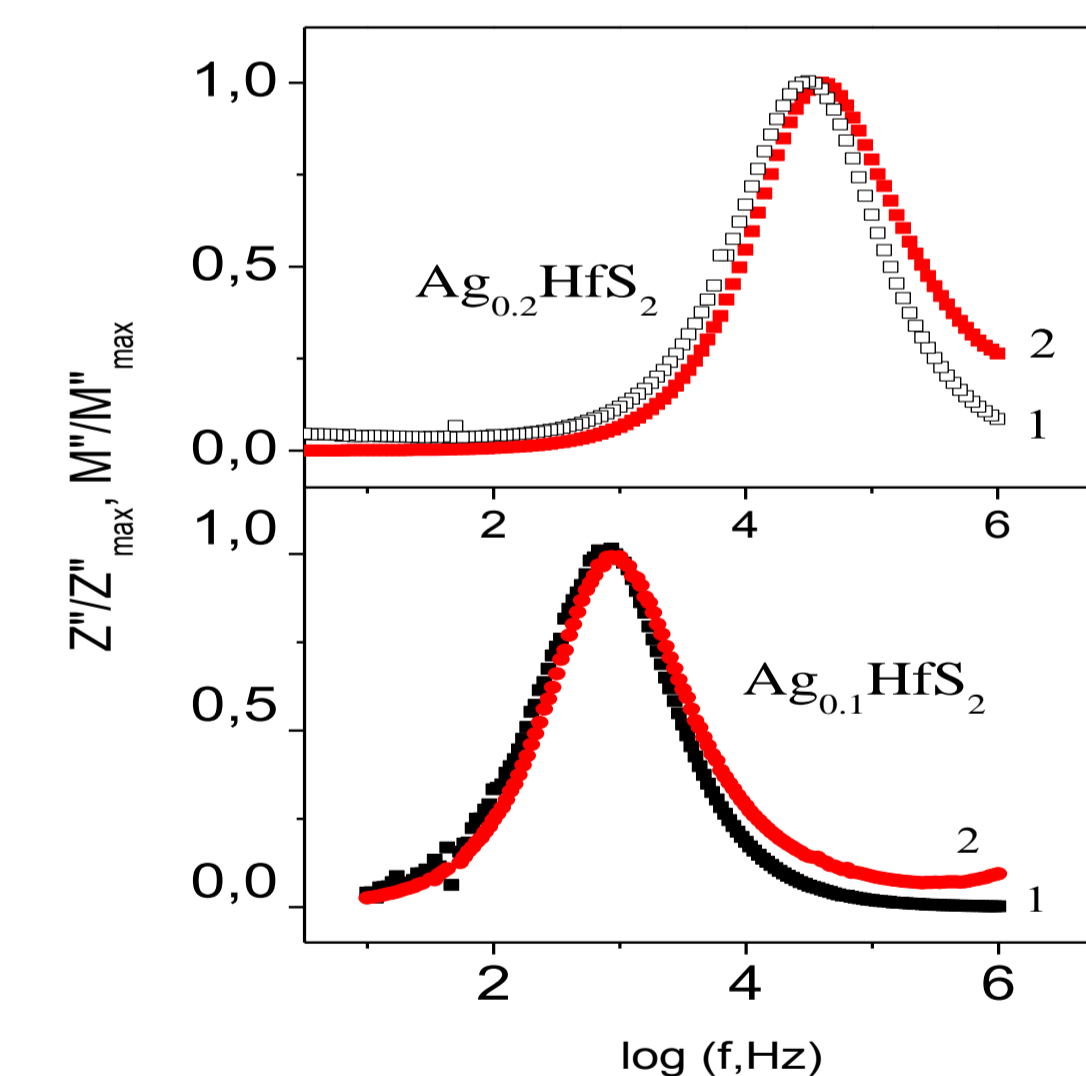
Fig4. Electrical module spectra of AgxHfS2

Fig.5 Frequency dependences of the relative values of imaginary components impedance(1) and electrical module (2)

RESULTS AND CONCLUSIONS

Investigation of dielectric characteristics of hafnium disulfide intercalated with silver atoms were carried out for the first time. Dielectric properties were analyzed in terms of dielectric constant (Fig. 1-3) and in terms of dielectric modulus (fig.4,5). It is shown that the modular formalism in this case is more informative for the quantitative determination of the relaxation characteristics of these materials. The data in Fig. 5 demonstrate that the relaxation times during charge transfer practically coincide with the times of dielectric relaxation. This may indicate that the kinetics of polarization processes is mainly determined by the kinetics of charge transfer. Kelaxation times decrease with an increase in the content of silver atoms in compounds.

III International Conference and School
"Synthesis, Structure, and Properties of High-Entropy Materials"
October 11-15, 2021

№ 8

skachkov@ihim.uran.ru

Skachkov V. M.
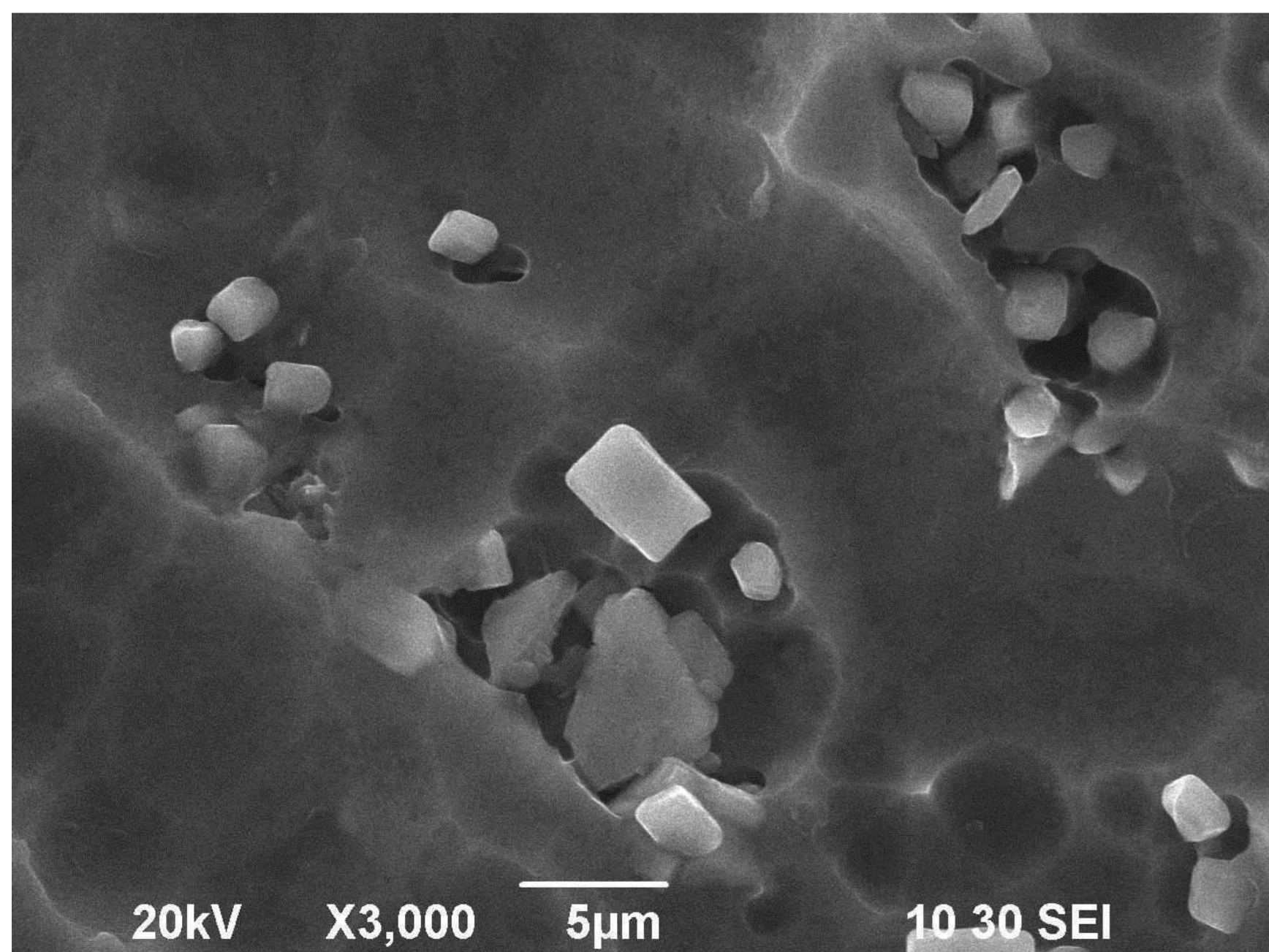ISSC UB RAS, Ekaterinburg, Russia

COMPOSITE MATERIAL ALUMINUM-TITANIUM

The appearance of a working centrifuge
ОС-6МУХЛ4.2

Microstructure of the boundary of the aluminum matrix and the Al-Ti bottom sediment (x28,6)

20kV　X3,000　5μm　10 30 SEI

During prolonged exposure , Al interacts with Ti to form the intermetallic compound Al₃Ti

The laboratory of chemistry of heterogeneous processes has developed and patented [1] a method for producing high-strength composite materials Al (Al-alloy) - Ti with an increased content of fine titanium (standard powder, crushed titanium sponge, etc.), cemented with an aluminum matrix. Such a material is suitable for use as modified deformable and cast aluminum composite alloys, and is a titanium metal powder distributed in an aluminum matrix or an alloy based on it. The method of obtaining such material includes several sequential operations: 1) melting of aluminum or aluminum alloy at a temperature of $780\pm20^{o}C$; 2) introduction of titanium metal powder into the melt by injection with an inert gas; 3) temperature recovery within 5-10 minutes to $780\pm20^{o}C$; 4) centrifugation of the liquid melt at a rotation speed of 1000-3000 rpm for 10-12 minutes before solidification; 5) separation of the bottom sediment along the outer boundary (the sediment is darker) after crystallization and cooling. The results of measuring the microhardness of the obtained materials are presented in the table.

Table – Microhardness of samples

№	Composite alloy	Initial alloy, microhardness, HV, GPa.	After centrifugation, the bottom sediment	
			The content of Ti, wt.%	Microhardness, HV, GPa.
1	01421-Ti	1,33	3,2	1,71
2	01570-Ti	1,03	6,4	2,60
3	Al-Ti	0,39	14,8	2,10

It follows from the table that the method developed in the laboratory produces high-strength composite materials Al (Al-alloy) - Ti based on titanium metal powders in an aluminum matrix or an alloy based on it.

1. Patent RU No. 2,742,874 C1 Method for obtaining a composite material based on aluminum or its alloy alloyed with titanium / Skachkov V. M., Pasechnik L. A., Bibanaeva S. A., Yatsenko S. P., Sabirzyanov N. A. Publ.: 11.02.2021 Byul. No. 5. (Application: 2020126589, 10.08.2020)
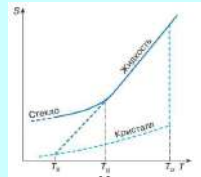
ldson@yandex.ru

**III International Conference and School
"Synthesis, Structure, and Properties of High-Entropy Materials"
October 11-15, 2021**

9

Non-Hibbs Thermodynamics of Glassy Systems

L.D.Son, IMET UB RAS, Ekaterinburg, Russia Support: RSF 21-13-002-02

Phenomenological Adam – Hibbs theory

Kauzman paradox: Stretched KWW relaxation:

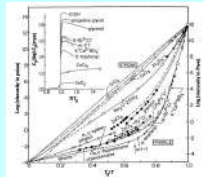$$g = g_0 \exp\left[-\left(\frac{t}{\tau}\right)^{\beta}\right]$$

$$0 < \beta < 1$$

$$\beta \Leftrightarrow \frac{B(T)}{T - T_k} \neq \frac{A}{T}$$

$$S_c = k\frac{N}{Z}\ln\omega$$

$$S_c(T) = \int_{T_k}^{T} \frac{C(T)}{T} dT = A(T)(T - T_k)$$

$$E = \alpha Z = \frac{TB(T)}{T - T_k} \qquad B(T) = \alpha\frac{Nk\ln\omega}{TA(T)}$$

$$\tau \sim \exp\left[\frac{E}{T}\right] = \exp\left[\frac{B(T)}{T - T_k}\right]$$

Dynamical theory by W.Gotze.

Mode coupling scheme:

One cannot provide self consistency without generalized function, so that delta-function in spectra and memory occur:

$$\ddot{\Phi}(t) + \nu\dot{\Phi} + \Omega^2\Phi + \Omega^2\int_0^t m(t-t')\dot{\Phi}(t')dt' = 0$$

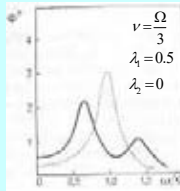$$\Phi(0) = 1, \quad \dot{\Phi}(0) = 0 \qquad m(t) = \lambda_1\Phi(t) + \lambda_2\Phi^2(t)$$

$$\Phi(z) = i\int_0^\infty e^{izt}\Phi(t)dt \qquad \Phi(z) = \frac{1}{\pi}\int_{-\infty}^\infty \frac{\Phi''(\omega)}{\omega - z}d\omega \qquad \Phi''(\omega) = \frac{1}{2}\int_{-\infty}^\infty e^{i\omega t}\Phi(t)dt$$

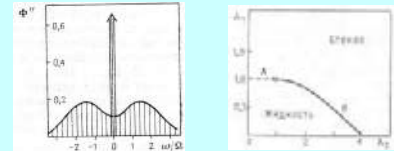$$\Phi(z) = -\frac{1}{z + \Omega^2 K(z)}$$

$$K(z) = -\frac{1}{z + M(z)}$$

$$M(z) = i\nu + \Omega^2 m(z)$$

$$\Phi_0(z) = -\frac{z + i\nu}{z(z + i\nu) - \Omega^2}$$

$$\nu = \frac{\Omega}{3} \quad \lambda_1 = 0.5 \quad \lambda_2 = 0$$

$$\Phi''(\omega = 0) = \frac{M''(\omega = 0)}{\Omega^2}$$

$$\frac{M''(\omega = 0)}{\Omega^2} = \frac{\nu}{\Omega^2} + \lambda_1\Phi''(\omega = 0) + \frac{\lambda_2}{\pi}\int\Phi''^2(\varepsilon)d\varepsilon$$

Thermodynamics transformation to a non-Hibbs probability distribution

$$Z = \int D\mathbf{X}D\mathbf{V}\exp\left(-\frac{H\ \mathbf{X},\mathbf{V}}{T}\right) = \int D\mathbf{V}\exp\left(-\frac{F\ \mathbf{V}}{T}\right) \qquad F\{\mathbf{V}\} = -T\ln\left(\int D\mathbf{X}\exp\left(-\frac{H\ \mathbf{X},\mathbf{V}}{T}\right)\right)$$

$$\frac{d\mathbf{V}}{dt} = \hat{\Gamma}\frac{\delta F}{\delta\mathbf{V}} + \theta \qquad \langle\theta(\mathbf{r},t)\theta(\mathbf{r}',t')\rangle = T\hat{\Gamma}\delta(\mathbf{r}-\mathbf{r}')\delta(t-t')$$

$$\frac{\partial P}{\partial t} = \int d^3\mathbf{r}\frac{\delta}{\delta\mathbf{V}}\hat{\Gamma}\left(T\frac{\delta P}{\delta\mathbf{V}} + \frac{\delta F}{\delta\mathbf{V}}P\right) \qquad P\{\mathbf{V}\} = A\exp\left(-\frac{F\ \mathbf{V}}{T}\right)$$

$$\mathbf{V} \Rightarrow \mathbf{Y}$$

$$F\{\mathbf{Y}\} \Leftrightarrow F\{\mathbf{Y}, \langle\mathbf{Y}\rangle\}$$

$$\langle\mathbf{Y}\rangle = \frac{\int D\mathbf{Y}\left(\mathbf{Y}\exp\left[-\frac{F\ \mathbf{Y},\langle\mathbf{Y}\rangle}{T}\right]\right)}{\int D\mathbf{Y}\left(\exp\left[-\frac{F\ \mathbf{Y},\langle\mathbf{Y}\rangle}{T}\right]\right)}$$

Resume:

- Theory looks like a "neural network" with "teaching" feedback. For example, general pair interaction theory:

$$\sigma_r^i = \begin{cases} 1, i - \text{номер состояния в } r \\ 0, \text{если нет} \end{cases} \qquad \omega_{rr'}^{ik} = \langle\sigma_r^i\sigma_{r'}^k\rangle$$

$$\omega_{rr'}^{ik} = \frac{\exp\left(\frac{1}{T}\sum_{r'j}M_{rr'}^{ij}\omega_{r'r}^{jk}\right)}{\sum_i\exp\left(\frac{1}{T}\sum_{r'j}M_{rr'}^{ij}\omega_{r'r}^{jk}\right)} \qquad M_{rr'}^{ij} \Leftarrow \left(\omega_{rr'}^{ij}\right)$$

$$r \Leftrightarrow (r_1, r_2, \ldots, r_m) \qquad \omega_{rr'}^{ij} = \omega^{ij}(x)$$

-Theory leads to a non-Hibbs solution of the Fokker-Plank equation.

-The shape of the order parameter allows to distinguish it from the Hibbs one

Some examples of theoretical scheme applications

Model with strong interaction. Tanaka H. A simple physical model of liquid – glass transition: intrinsic fluctuating interactions and random fields hidden in glass-forming liquids // J. Phys.: Condens. Matter. 1998. Vol. 10, № 14. P. 207–214. 128
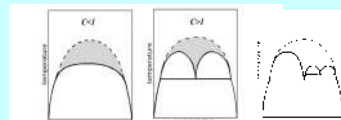
$$F\{\varphi\} = \frac{1}{2}\varphi\hat{A}\varphi + \frac{g}{4}\varphi^4 + \ldots$$

$$F = \frac{1}{2}\varphi\left(\hat{A} + \hat{\Sigma}\right)\varphi, \quad \langle\varphi\varphi\rangle = \left(\hat{A} + \hat{\Sigma}\right)^{-1} \quad \hat{\Sigma} = \hat{\Sigma}\{\langle\varphi\varphi\rangle\}$$

Lattice gas model with dynamic limitations accounted. L.Son. Dynamics of a lattice gas JETP Letters, 2014, Vol. 99, No. 12, pp. 689–94

$$\beta(r) = x(r) - \frac{1}{2}$$
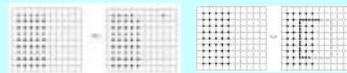
$$\frac{T}{J}x = \frac{e^{\beta}}{1 + e^{\beta}} + C\frac{e^{\beta}(1 - e^{\beta})}{(1 + e^{\beta})^3}, \quad C = C(\beta,\ldots)$$

Model with two order parameters. Tanaka H. Two-order-parameter description of liquids. I. A general model of glass transition covering its strong to fragile limit// J. Chem. Phys.. 1999. Vol. 111, № 7. P. 3163–3174.

$$Z = \int D\varphi D\psi\exp\left(-\frac{F\ \varphi,\psi}{T}\right)$$

$$\langle\psi\rangle = \frac{\int D\psi\psi\exp\left(-\frac{F\{\varphi\},\psi}{T}\right)}{\int D\psi\exp\left(-\frac{F\{\langle\varphi\rangle,\psi\}}{T}\right)} \qquad \langle\varphi\rangle = \frac{\int D\varphi\varphi\exp\left(-\frac{F\ \varphi,\langle\psi\rangle}{T}\right)}{\int D\varphi\exp\left(-\frac{F\{\varphi,\langle\psi\rangle\}}{T}\right)}$$

Model with some restrictions imposed may be presented as a model with two order parameters

$$Z = \int D\varphi\exp\left(-\frac{F\{\varphi\}}{T}\right) \qquad G(\varphi) = 0$$

$$Z = \int D\varphi D\psi\exp\left(\frac{1}{T}\left[F\{\varphi\} + iT\int dr\,\psi\,G(\varphi)\right]\right)$$

Breakthrough: Theory of spin glass

$$\ln Z = \lim_{n \to 0}\frac{Z^n - 1}{n} \qquad f(J_{ik}) = \frac{1}{\sqrt{2\pi}I}\exp\left(-\frac{J_{ik}^2}{I}\right)$$

$$Z^n = \prod_i\sum_{\mu=1}^n\exp\left(-\sum_{i<k}J_{ik}s_{i\mu}s_{k\mu}\right)$$

$$\langle s_\mu s_\nu\rangle = \frac{\sum_{\{s_\mu\}}s_\mu s_\nu\exp\left(\sum_{\mu\nu}Q_{\mu\nu}s_\mu s_\nu\right)}{\sum_{\{s_\mu\}}\exp\left(\sum_{\mu\nu}Q_{\mu\nu}s_\mu s_\nu\right)} \qquad Q_{\mu\nu} = \frac{2I}{T^2}\langle s_\mu s_\nu\rangle$$

$$\langle s_\mu s_\nu\rangle = q_{\mu\nu} = (1-q)\delta_{\mu\nu} + q\Lambda_{\mu\nu}$$

M.Goldstein   P.Anderson   G.Parisi

$$\nu \Leftrightarrow (\nu_1, \nu_2, \ldots, \nu_k) \qquad \nu_1 = \overline{1, j_1}, \nu_2 = \overline{1, j_2}, \ldots$$

$$q_{\mu\nu} = \begin{cases} q_0, \quad \mu_0 \neq \nu_0 \\ q_1, \quad \mu_0 = \nu_0, \mu_1 \neq \nu_1 \\ \ldots \\ q_k, \quad \mu_0 = \nu_0, \mu_1 = \nu_1, \ldots, \mu_k \neq \nu_k \end{cases}$$

$$q_{\mu\nu} = 1, \quad \mu_0 = \nu_0, \mu_1 = \nu_1, \ldots, \mu_k = \nu_k \qquad q(x), 0 < x < 1$$

III International Conference and School
"Synthesis, Structure, and Properties of High-Entropy Materials"
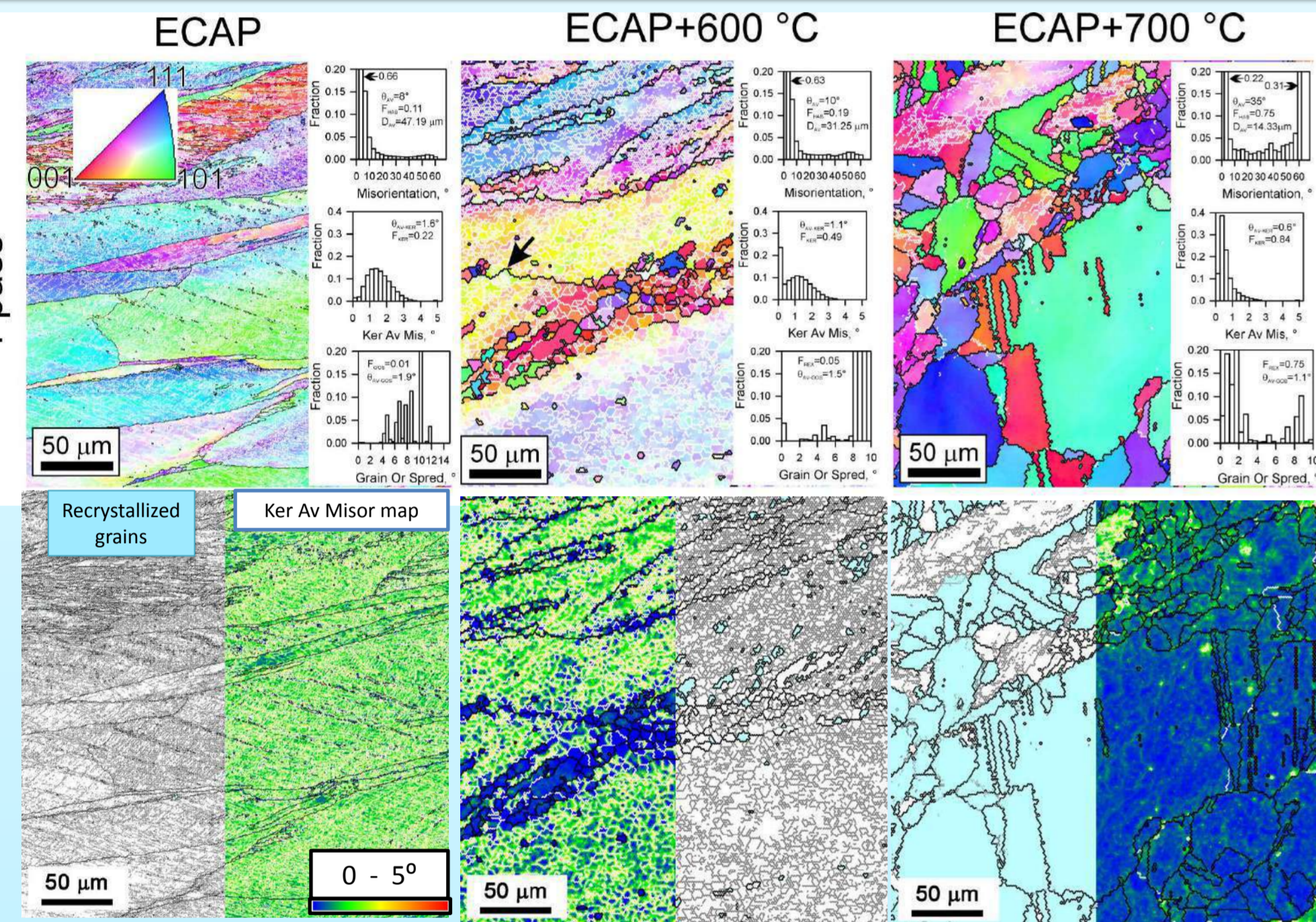## October 11-15, 2021

№12

EFFECT OF TREATMENT ON THERMAL STABILITY OF CU-CR-ZR ALLOY

Bodyakova A.I.[1,2], Pilipenko A.G.[1], Lugovskaya A.S.[1], Lamzina N.A.[1], Botchanov D.S.[1], Belyakov A.N.[1], Kaibyshev R.O.[1]

[1]Belgorod State University, Pobeda str. 85, Belgorod, 308015, Russia
[2]National University of Science & Technology (MISIS), Leninsky pr. 4, Moscow, 119049, Russia

bodyakova-ai@yandex.ru

Abstract

The thermal stability of gradient microstructures in a Cu – 0.096%Cr – 0.07%Zr (wt.%) alloy subjected to equal channel angular pressing (ECAP) at 400ºC was studied. The microstructure after intense plastic straining and aging at 300-500 °C was almost the same. Aging at 600 °C led to the development of a partially recrystallized microstructure. After aging at 700 °C, the fully recrystallized microstructure evolved. An increase in ECAP passes from 1 to 12 decreased the recrystallization temperature from 664 °C to 617 °C. The effect of deformation microstructures and particle precipitation on the recrystallization development is discussed.
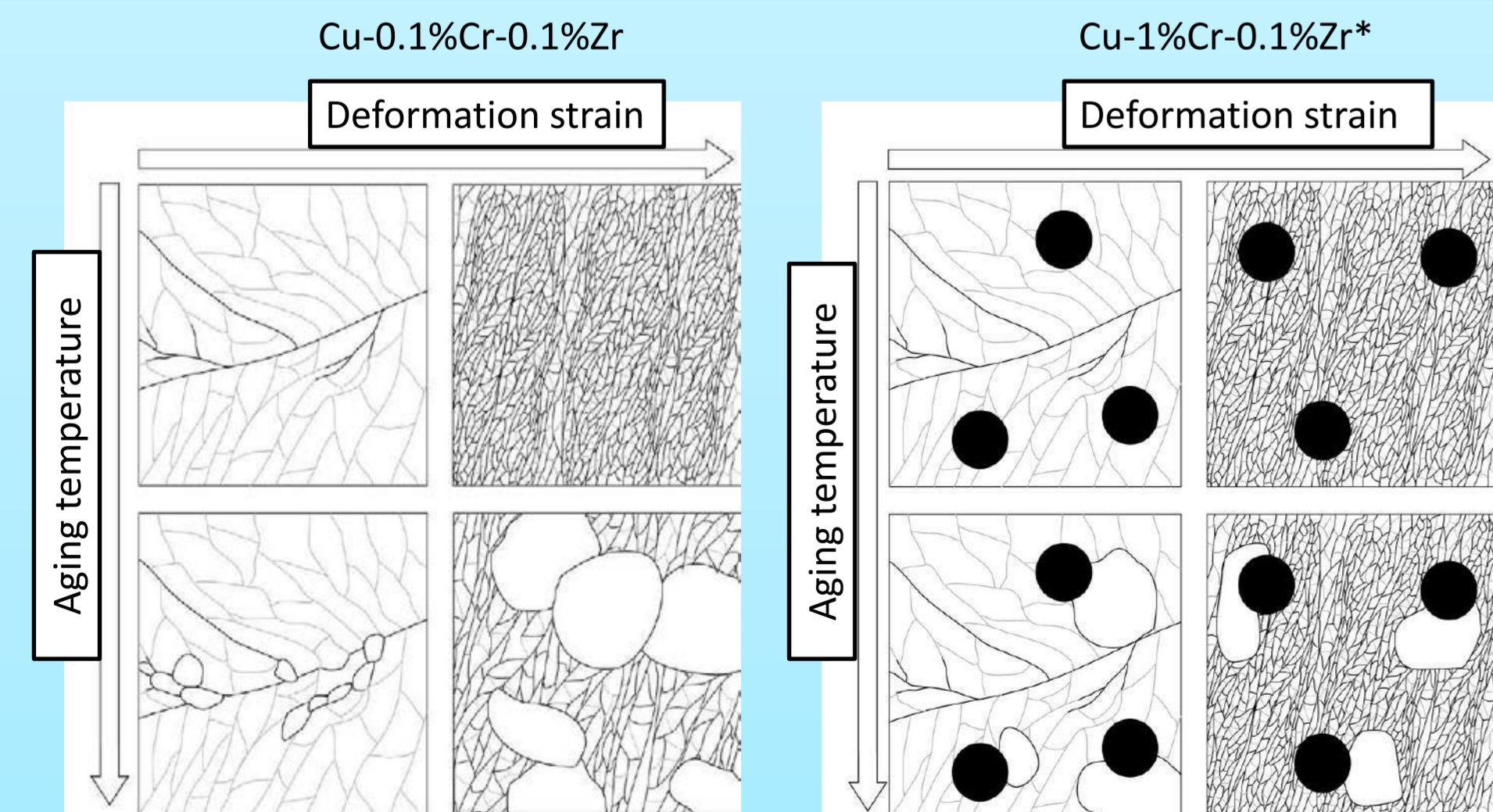
Microstructure evolution

Mechanism of microstructure evolution

Trec.	1 pass	4 passes	12 passes
Cu-0.1%Cr-0.1%Zr	664 °C	623 °C	617 °C
Cu-1%Cr-0.1%Zr*	811 °C	727 °C	561 °C

* Abib K. et al. //Materials Characterization. – 2016. – T. 118. – C. 527-534.

Materials and experimental procedure

The Cu – 0.10%Cr – 0.07%Zr (wt.%) alloy subjected to ECAP followed by aging was examined. The starting material with an initial grain size of about 150 µm was solution treated at 920 °C for 1 hour, followed by water quenching. Then, the samples were subjected to 1, 4, or 12 ECAP passes with B$_C$ route at 400 °C. The ECAP samples were aged at 300-700 °C for 1 hour with subsequent water quenching. Microstructure characterization was performed by a Nova NanoSem 450 FEI scanning electron microscope equipped with an electron backscattering diffraction (EBSD) analyzer. The mean grain size, the fraction of high angle boundaries (HAB), Kernel average misorientation (KAM), Grain orientation spread (GOS), average boundary misorientation, a recovery fraction calculated as a fraction of crystallites with KAM<1°, a recrystallized fraction calculated as a fraction of grain with GOS<3° and grain tolerance angle >15° were estimated using orientation image microscopy, OIM Analysis 6, software. The Vickers hardness test was carried out on WOLPERT 420 MVD device with a load of 50 g with 10 s dwell time. Electrical conductivity was measured by the eddy current method with Constanta K-6 equipment.

Conclusions

1. The gradient microstructure of the low-alloyed Cu-0.1%Cr-0.1%Zr alloy after ECAP is characterized by significant thermal stability. The recrystallization temperature exceeded 610 °C.

2. The recrystallization temperature decreases from 664 °C to 617 °C with an increase in ECAP passes from 1 to 12. This change result from different mechanisms of microstructure evolution, namely, discontinuous static recrystallization in the samples after 1 ECAP pass and continuous static recrystallization in UFG microstructure developed after 12 ECAP passes.

3. A decrease in recrystallization temperature with an increase in pre-strain depends on Cr content and comprises $\Delta T=4°C$ per ECAP pass for the present alloy as compared to $\Delta T=16°C$ per ECAP pass for the Cu-1%Cr-0.1%Zr alloy due to effect of particle stimulated nucleation in Cu alloys with large alloying extent and large volume fraction of primary Cr-particles.
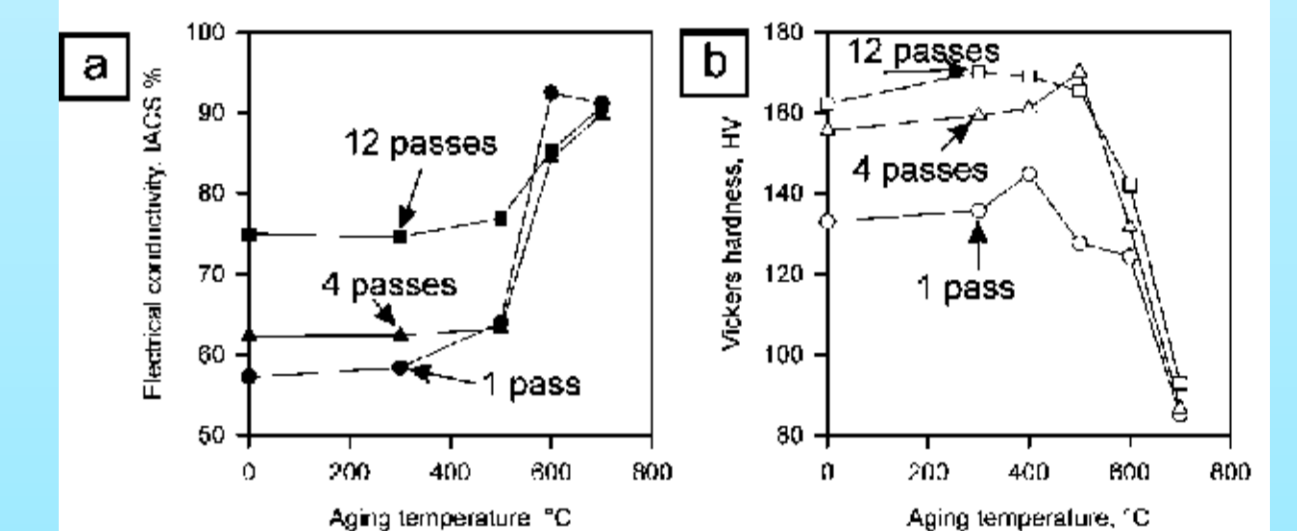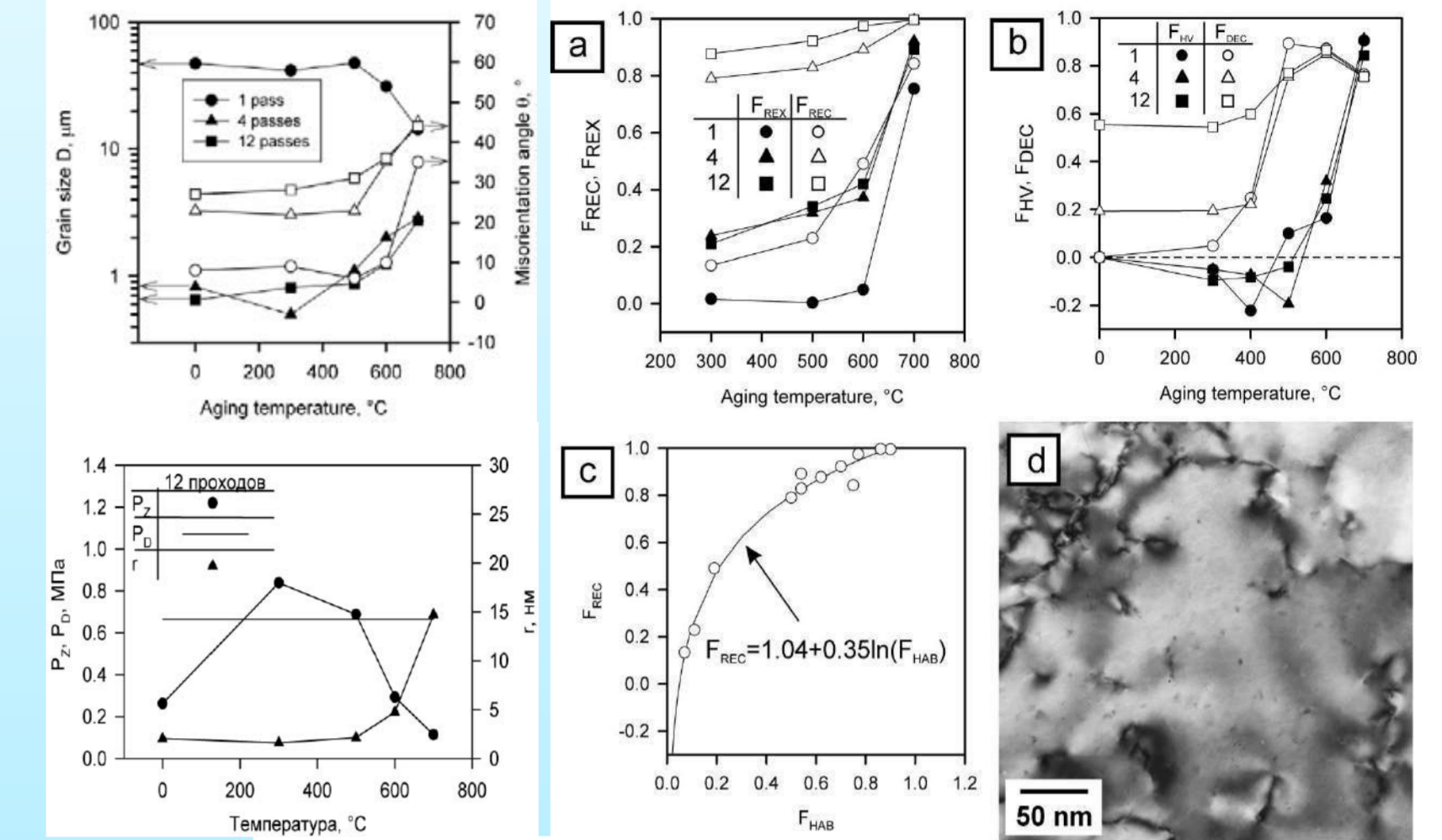
Results

An increase in the hardness resulted from the decomposition of solid solution and particle strengthening, as illustrated in Figure 3. Depletion of Cr and Zr from solid solution and a decrease in the lattice dislocation density were facilitated by ECAP strain. The fraction of solid solution decomposition can be estimated as:
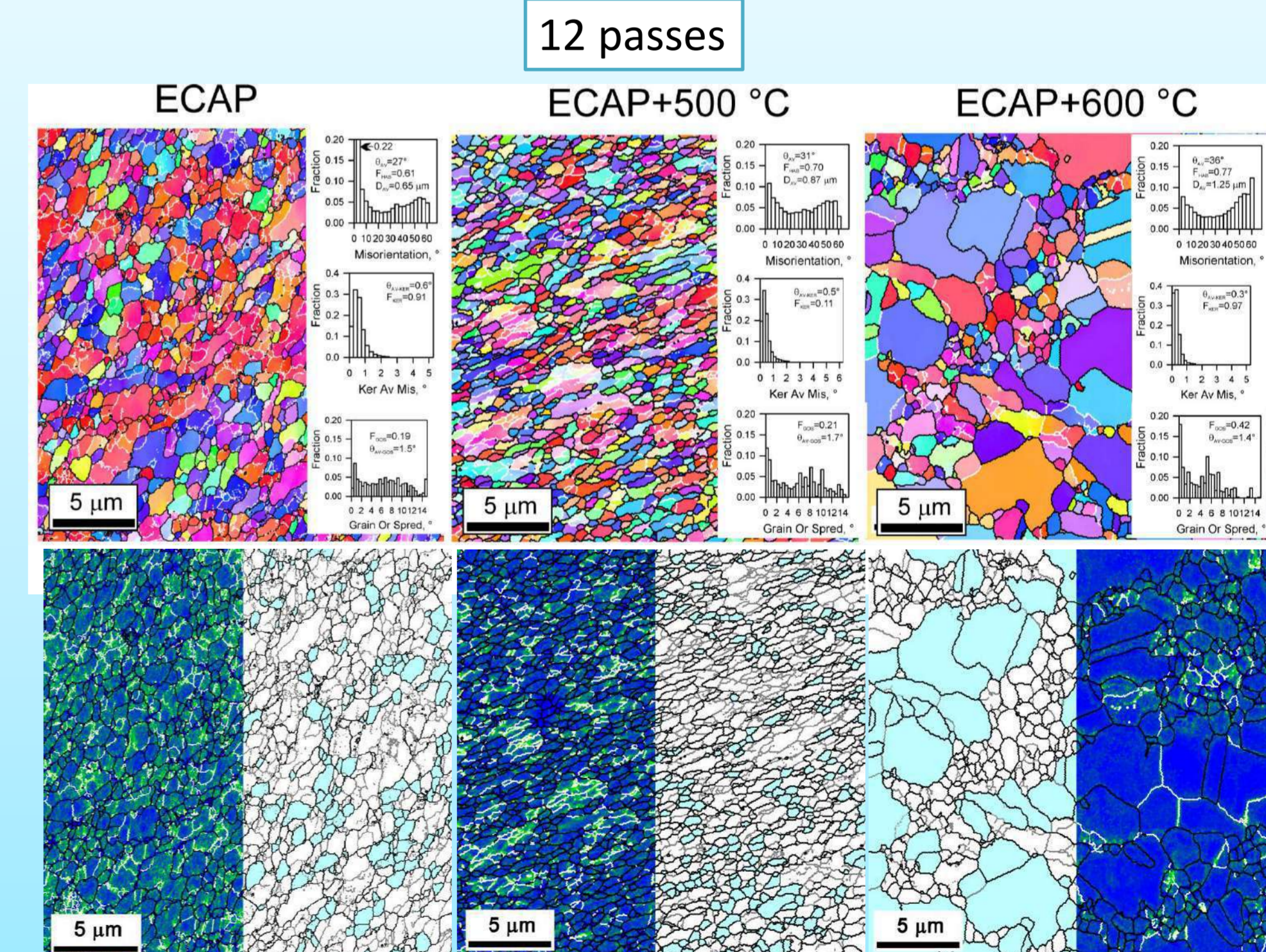
$$F_{dec} = \frac{\Omega_{ST} - \Omega_i}{\Omega_{ST} - \Omega_{ECAP}}$$

where Ω_{ST} is electrical resistivity after solution treatment, Ω_i is current electrical resistivity, Ω_{ECAP} is electrical resistivity after ECAP.

The fraction of softening was calculated by of hardness measurement

$$F_{HV} = \frac{HV_{ECAP} - HV_i}{HV_{ECAP} - HV_{ST}}$$

where HV_{ST} is Vickers hardness after solution treatment, HV_i is current Vickers hardness, HV_{ECAP} is Vickers hardness after ECAP. Cr-particles play a role of obstacles for dislocation glide/rearrangement and boundary migration, preventing recovery and recrystallization.

12 passes

III International Conference and School
"Synthesis, Structure, and Properties of High-Entropy Materials"
October 11-15, 2021

№ 13

Behavior of the Portevin-Le Chatelier bands in austenitic steel
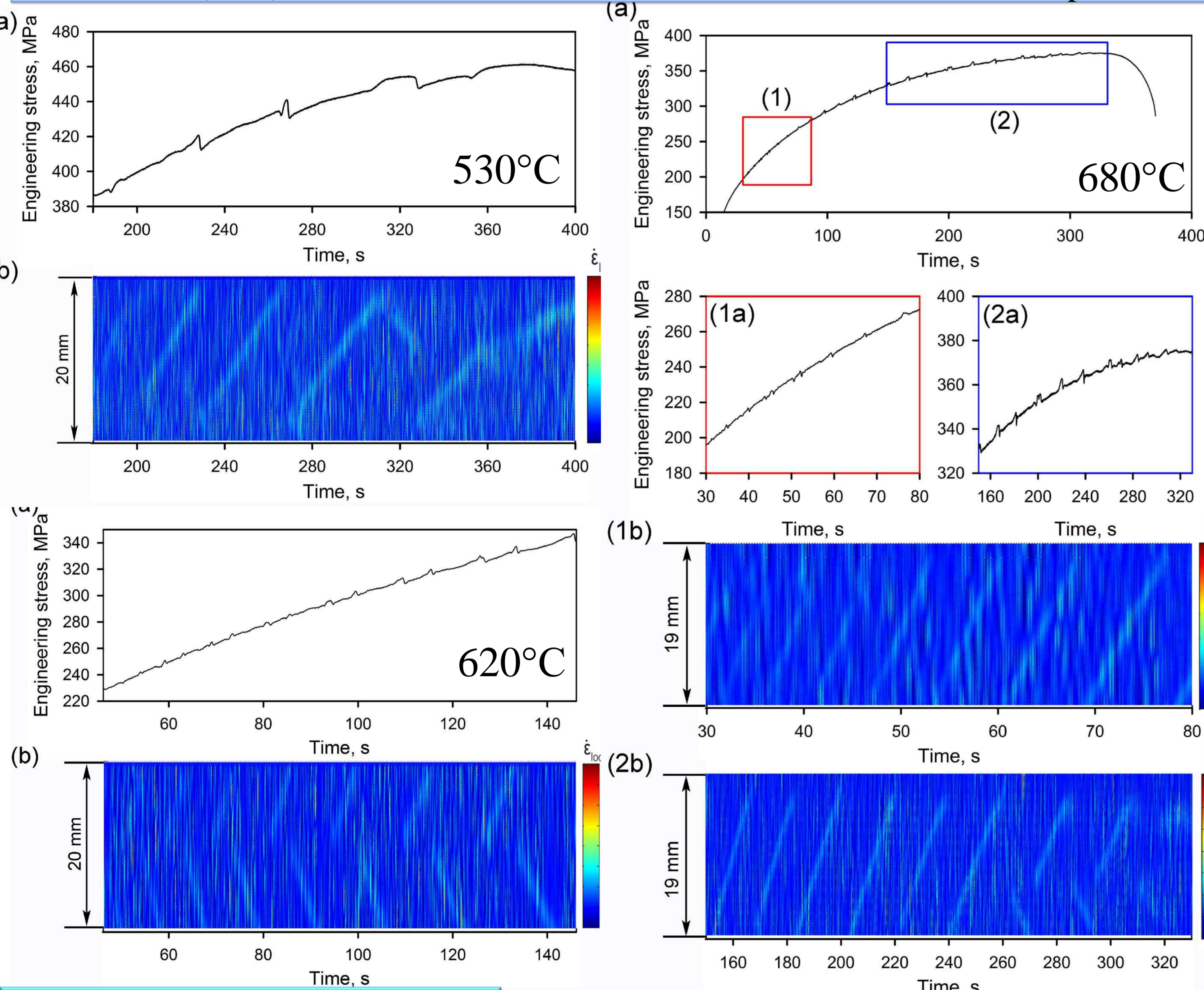
Yu. Borisova, D. Yuzbekova, A. Mogucheva

There are several methods for recording deformation bands, but recently the most widely used method is digital image correlation (DIC), which displays the distribution of strain and local strain rate on the sample surface. It should be noted that almost all studies on the behavior of the Portevin-Le Chatelier (PLC) bands in metallic materials were carried out at room temperature, since it is difficult to obtain images at elevated temperatures.

Material: Austenitic steel Fe–18Cr–8Ni–2.8Cu (wt.%) (annealed at 1150°C for 1h and then quenched in water). Tensile tests were performed at strain rate of 10^{-3} s^{-1} and temperatures 530-680°C. The PLC bands were observed using the digital image correlation (DIC) method. The calculations were performed using the Vic-2D correlation program (Vic-2D system).

The austenitic steel demonstrates the PLC effect in the temperature interval from 530°C to 680°C at a strain rate of 1×10^{-3} s^{-1}. In the entire temperature range of the existence of the PLC effect, the propagation of deformation bands occurs in a continuous manner.

An increase in the stress drops frequency and a corresponding decrease in the distance continuously propagated by the bands is observed up to a temperature of 590°C. Whereas, at temperatures above 620°C, an increase in the distance continuously propagated by the band is established, despite the increase in the frequency of stress drops.

The velocity of the PLC bands shows the continuous increase with increasing test temperature. Such kinetics of the PLC bands is explained by the influence of temperature on the aging time required for pinning of arrested dislocations by solute atoms.

borisovayuliya94@mail.ru

III International Conference and School
"Synthesis, Structure, and Properties of High-Entropy Materials"
October 11–15, 2021

14

Экспериментальное изучение единичных треков, полученных из смеси порошков Ti и Al при варьируемых параметрах процесса селективного лазерного плавления

adolbachev1@gmail.com

А.П. Долбачев, Н.А. Белов, Т.К. Акопян   Национальный исследовательский технологический университет «МИСиС», г. Москва, Россия

Введение: интерметаллиды на основе γ-TiAl считаются перспективными материалами для замены никелевых суперсплавов благодаря низкой плотности, высоким показателям удельной прочности и жесткости, а также сопротивления ползучести и стойкости к окислению при повышенных температурах. Однако изготовление сплавов на основе γ-TiAl по-прежнему затруднено из-за их низкой пластичности при комнатной температуре и плохой горячей деформируемости. Кроме того, длительный цикл обработки и высокие инвестиционные затраты также являются решающими ограничениями при использовании большинства традиционных методов обработки. Селективная лазерная плавка (СЛП), активно развивающаяся в последние годы, является перспективной технологией аддитивного производства TiAl, которая позволяет изготавливать плотные металлические изделия со свободной геометрией непосредственно из CAD-моделей без какой-либо помощи инструментов и форм. Кроме того, СЛП позволяет значительно сократить время изготовления и капитальные вложения. Однако, несмотря на достаточно большое количество работ в этой области, исследование двойных сплавов Ti–Al полученных при СЛП не проводилось.

Цель: исследование единичных треков из сплава на основе алюминидов титана, полученного с использованием технологий послойного лазерного спекания порошков при варьируемых параметрах процесса

Материал: смесь порошков сферического Ti и Al в стехиометрическом соотношении 1 : 1.

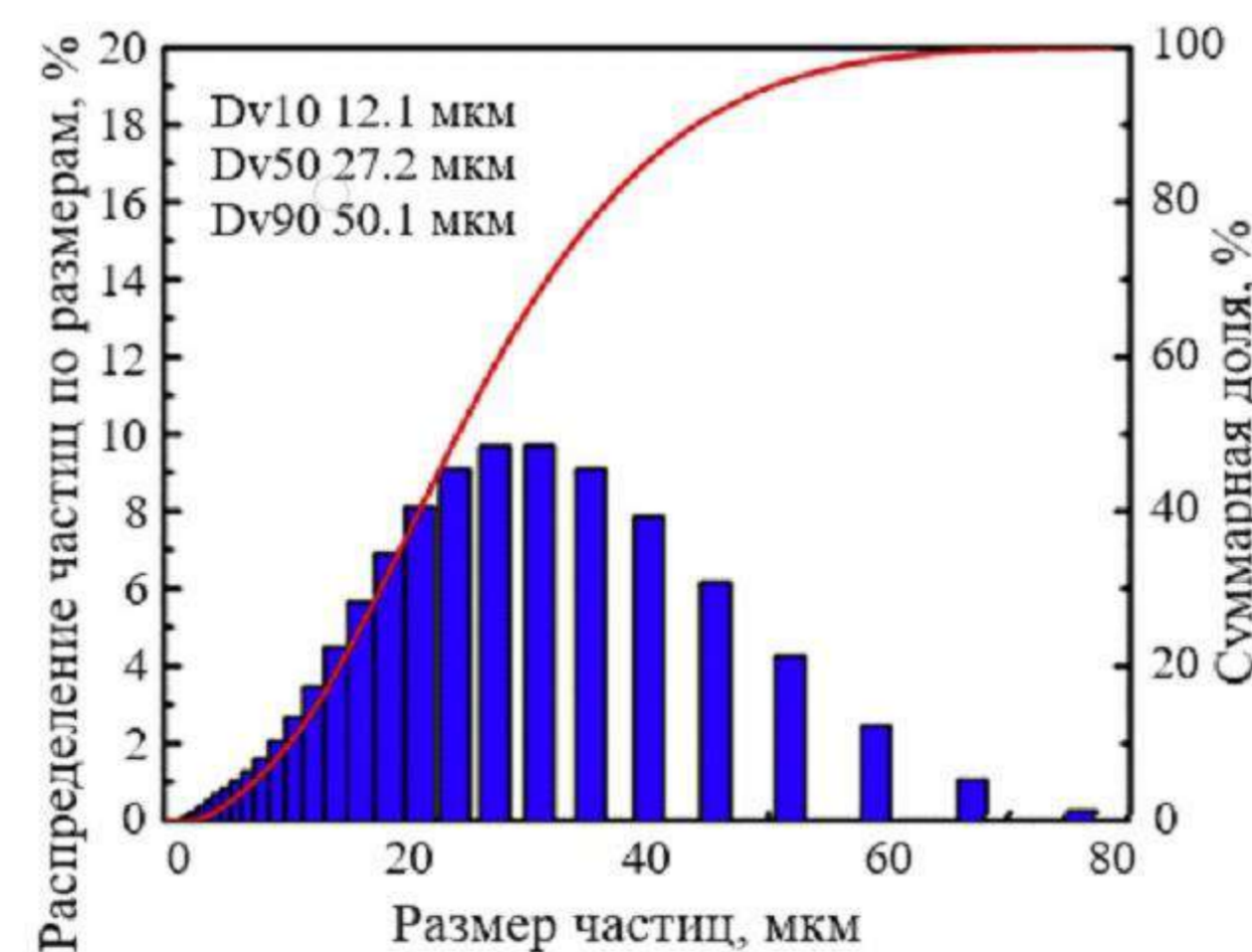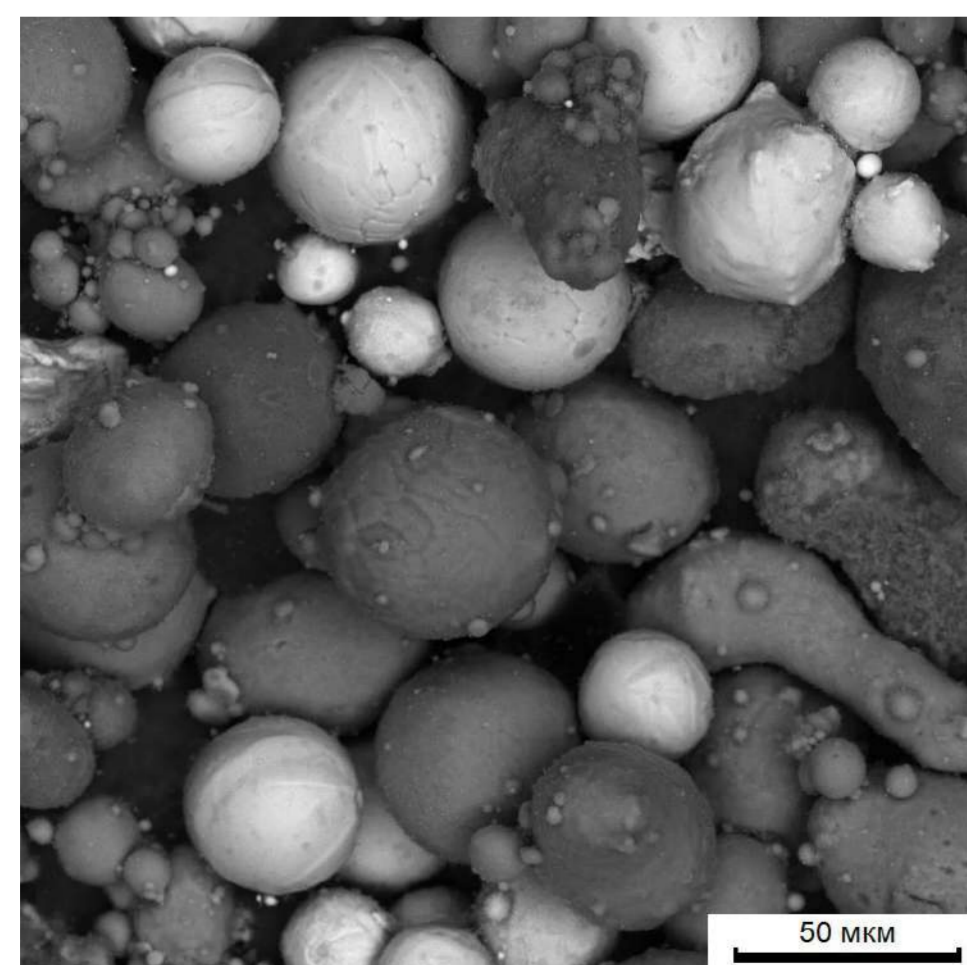### Методика эксперимента

Рис. 1. Морфология смеси порошков Ti + Al (**а**) и распределение частиц по размеру (**б**)

На машине SLM 280 HL из смеси порошков Ti + Al в стехиометрическом соотношении 1 : 1 было получено по 3 единичных трека длиной 100 мм за один проход лазера для каждого состояния. Для предотвращения воздействия кислорода рабочая камера была заполнена аргоном (99,9 %). Для каждого отдельного трека мощность лазера составляла 200 Вт в сочетании со скоростью сканирования (v_c) от 300 до 900 мм/с с шагом 300 мм/с. Толщина слоя поддерживалась постоянной δ = 50 мкм.
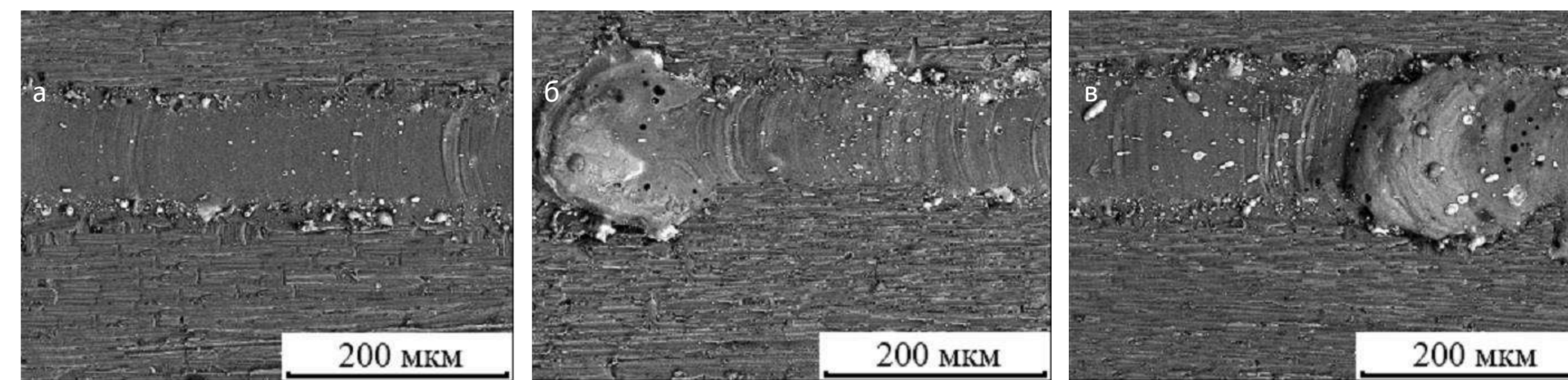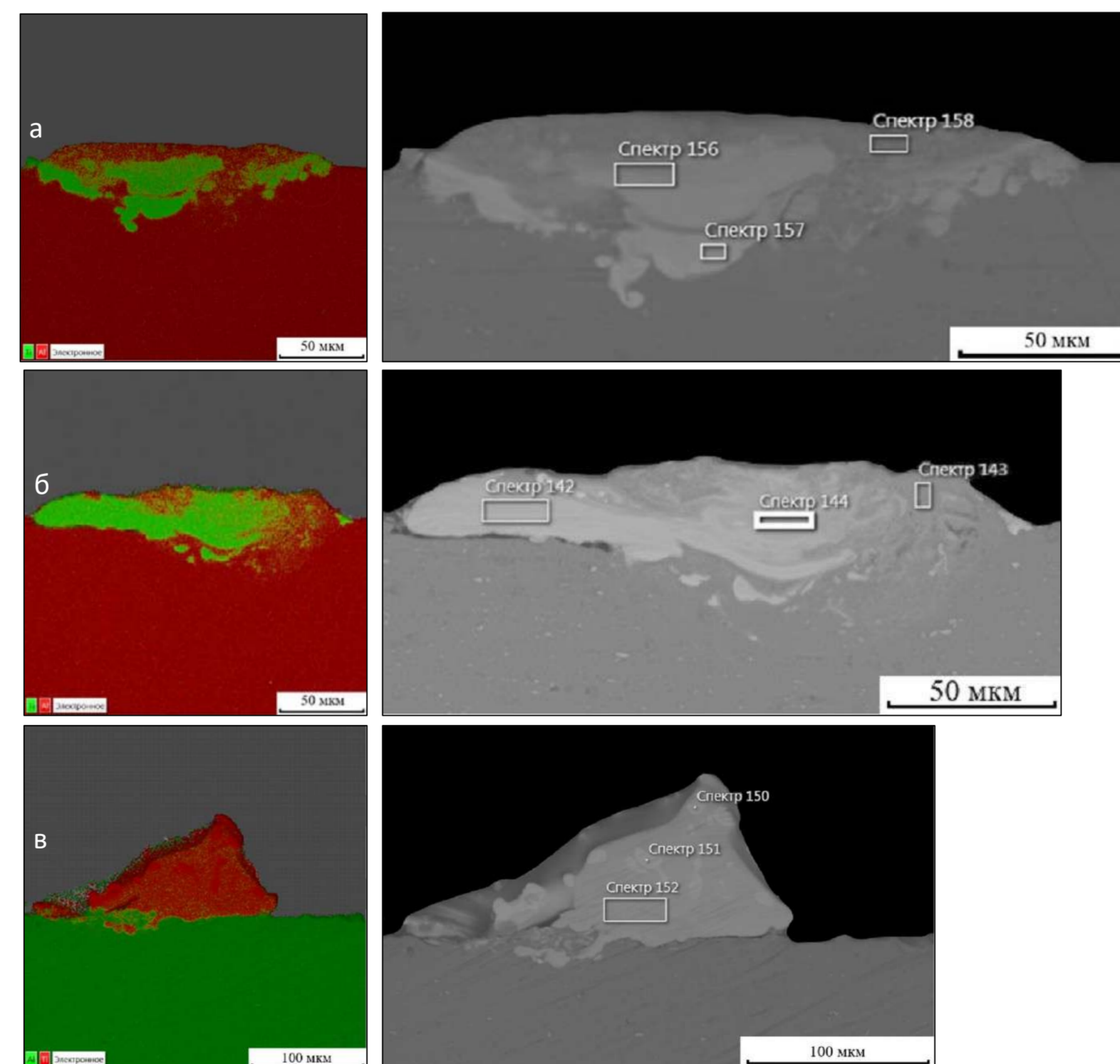

Рис. 2. Морфология поверхности единичных треков в поперечном сечении при различных скоростях сканирования лазера, мм/с: 300 (**а**), 600 (**б**) и 900 (**в**) (СЭМ)

№ спектра На рис. 3	Хим. состав, ат.%		Сумма
	Ti	Al	
156	35,41	64,59	100
157	62,05	37,95	100
158	4,57	95,43	100
142	49,76	50,24	100
143	8,89	91,11	100
144	36,1	63,9	100
150	99,63	0,37	100
151	99,45	0,55	100
152	62	38	100

Рис. 3. Результаты микрорентгеноспектрального анализа единичных треков при различных скоростях сканирования лазера, мм/с: 300 (**а**), 600 (**б**) и 900 (**в**)

Выводы:

1. Увеличение скорости сканирования приводит к искажению дорожки трека и формированию «шариков» на поверхности из-за значительной конвекции Марангони и нестабильности капиллярной жидкости в расплавленной ванне. Отмечено, что поры, образовавшиеся на поверхности трека, в основном сконцентрированы именно в шариках.

2. Повышение скорости сканирования оказывает влияние на морфологию трека: в частности, уменьшаются смачиваемость подложки и глубина ванны трека. При v_c = 900 мм/с проплавления подложки практически не наблюдалось.

3. Из анализа карт распределения элементов поперечного сечения получившегося трека при скоростях сканирования 300 и 600 мм/с видно, что перемешивание бассейна в процессе плавления происходит неравномерно. При v_c = 900 мм/с распределение элементов Ti и Al было равномерным по всей площади, однако четко различимы области, где не произошло расплавления частиц порошка титана при контакте с лазером.

III International Conference and School
"Synthesis, Structure, and Properties of High-Entropy Materials"
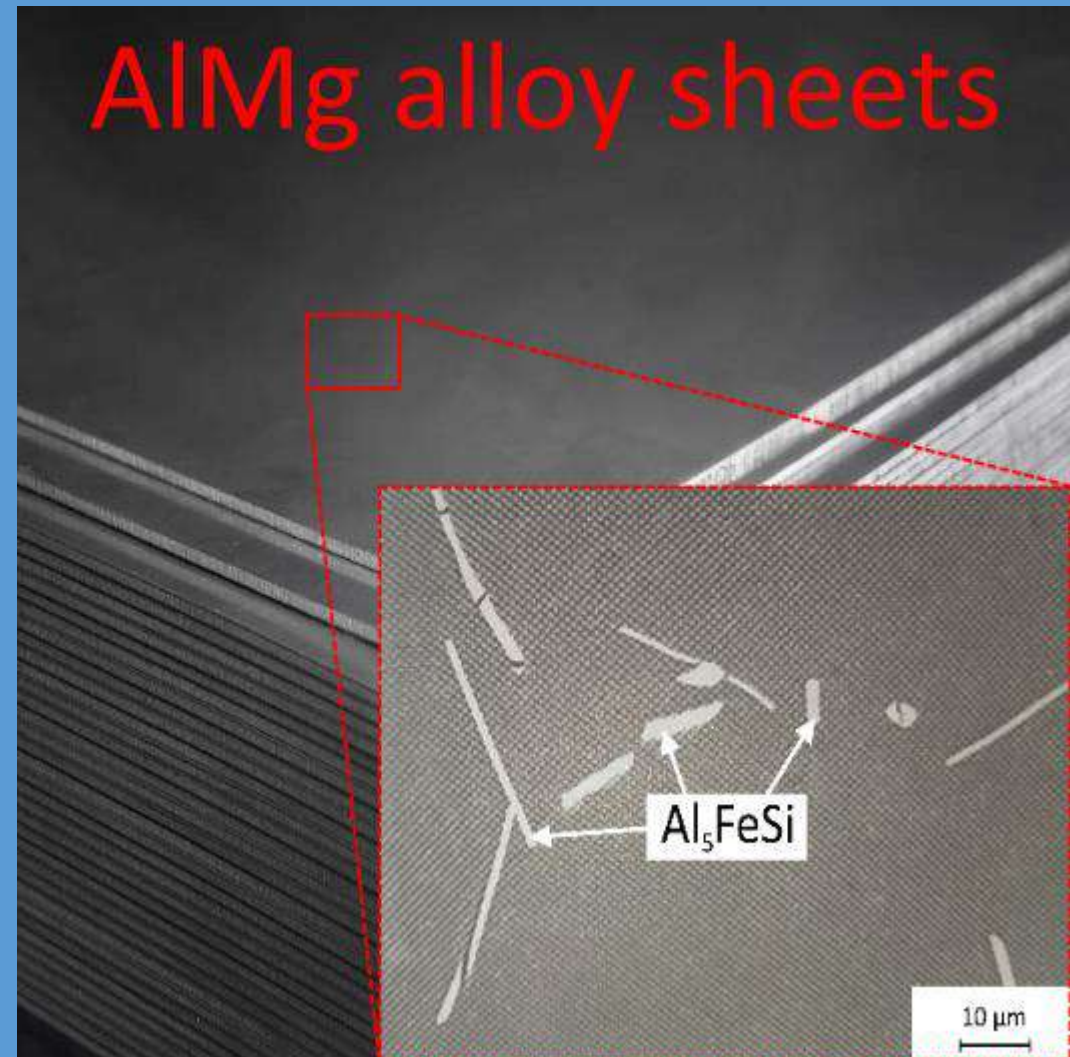## October 11–15, 2021

16

v.doroshenko@mail.ru

A possibility of obtaining corrosion-resistant deformed semifinished products from an alloy based on the Al-Ca-Mg system

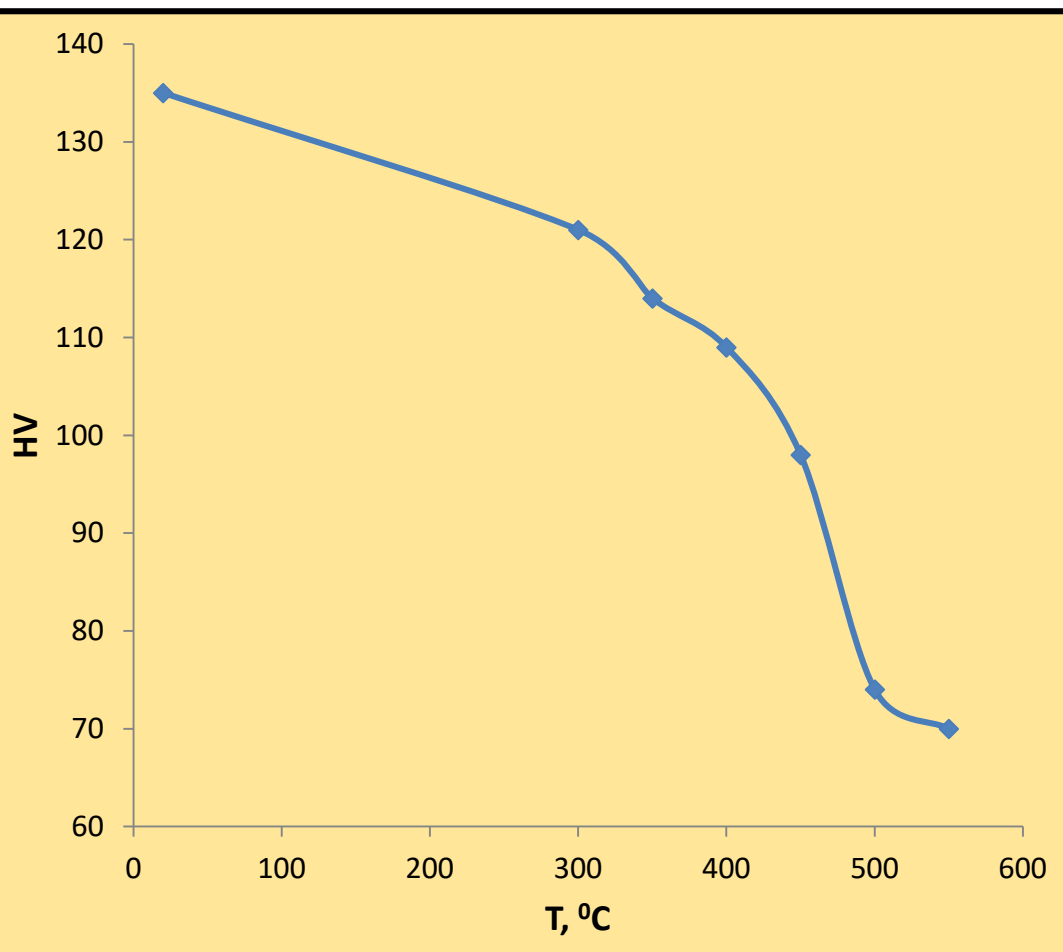Doroshenko V.V., Naumova E.A., Barykin M.A., NUST "MISiS", Moscow, Russia

(a)

AlMg alloy sheets

Al_5FeSi

10 µm

Possible Fe-containing phases in Al-1%Mg-0,5%Si-0,2%Fe alloy

To reduce the effect of iron, magnals contains up to 0.5% manganese, with which iron forms a compound of skeletal morphology.

The graph of the change in hardness during annealing

Aluminum-magnesium alloys are widely known as wrought materials. Their main advantages are: a good combination of *strength* and *ductility*, high *weldability* and low *density*. At the same time, there are technological difficulties in obtaining products. An important role is played by the **Fe** impurity, which forms phases of crystallization origin *(a)*. Although, according to GOST 4784-97, 0.5-0.7 mass.% is allowed in the composition. iron, in products for critical products it is limited to hundredths (0.01% for alloy 1541sc). This constrains the use of pure raw materials, which increases the cost of production, and also does not correspond to the global trend for the use of secondary raw materials. New alloys doped with calcium can cope with this task (reducing the cost of production while maintaining the level of physical and mechanical properties). Studies of the last 3 years have shown that calcium effectively binds Fe into a terna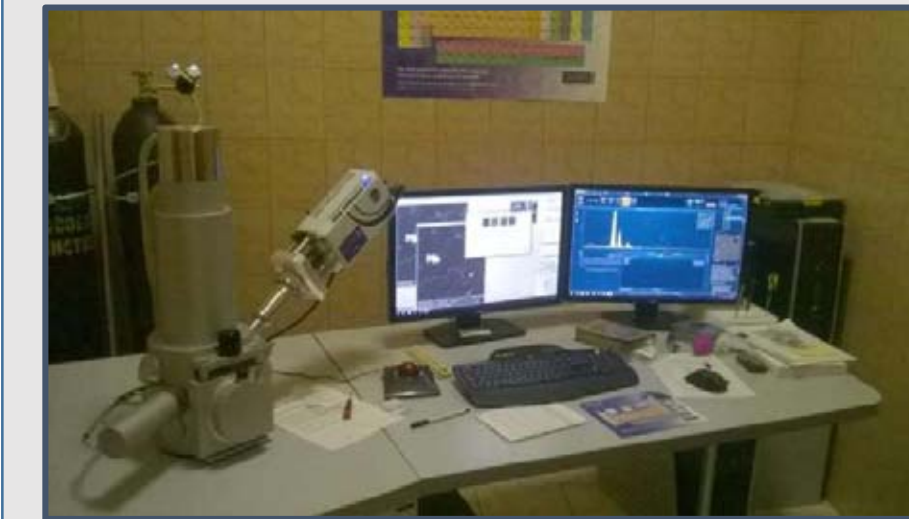ry compound of compact morphology *(b)*, which is part of a multicomponent eutectic. In addition, despite the high proportion of the second phases (more than 20% vol.), high-quality deformed semifinished products can be obtained from alloys with calcium *(c)*.

The composition Al – 2.5% Mg – 1% Mn – 0.4% Fe was chosen as the base one; with an average (for AMg2-type alloys) concentration of magnesium and close to the limiting (for magnals) concentration of manganese. The latter element, during crystallization, is capable of entering into the composition (Al) and, upon heating, to form secondary precipitates of the Al_6Mn phase. This makes it possible to increase the strength properties of sheets in the annealed state. Zirconium and scandium are necessary for strengthening due to the formation of $L1_2$ nanoparticles during heterogenization annealing of castings and ingots. The optimal combination of the hardening effect and the economy of alloying can be realized at ~ 0.1% Sc and 0.2-0.25% Zr. Thus, the composition of the experimental alloy was substantiated: Al – 2.5Ca – 2.5% Mg – 1% Mn – 0.4% Fe – 0.1% Sc – 0.2% Zr (hereinafter Al2.5Ca2.5Mg).

Due to the low ductility in the cold rolled state (less than 0.5%), it was necessary to justify the annealing regime. The first step was to determine the thermal stability of the cold-worked state. For this, the influence of the annealing temperature on the hardness and microstructure of cold-rolled sheets was studied. As you can see from the graph of the change in hardness, as the temperature rises, there is a gradual decrease in hardness. At the same time, the unrecrystallized structure is retained up to 400 °C, which is due to the high volume fraction of secondary aluminides, both $Al_3(Zr,Sc)$ and Al_6Mn.

(b) Metallographic studies of the effect of calcium on iron

СЭМ (TESCAN VEGA 3) MPCA (Oxford/Aztec)

$(Al) + Al_4Ca + Al_{10}CaFe_2 + Al_2CaSi_2$

$Al_{10}CaFe_2$
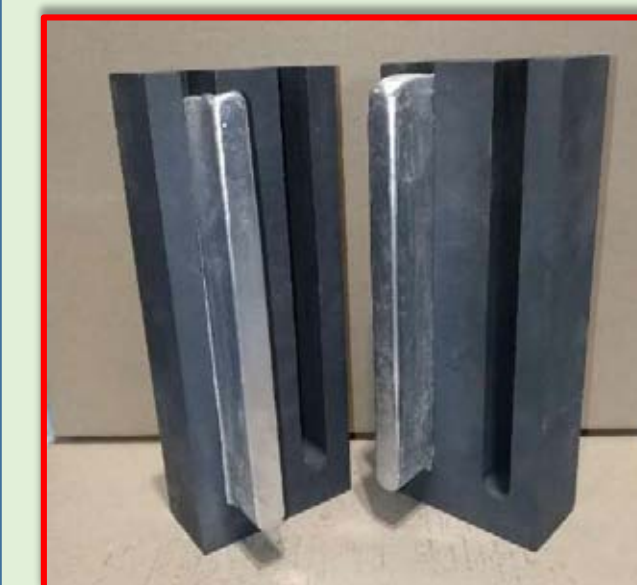
50 µm

100 µm

SEM of Al-6%Ca-1%Si-1%Fe
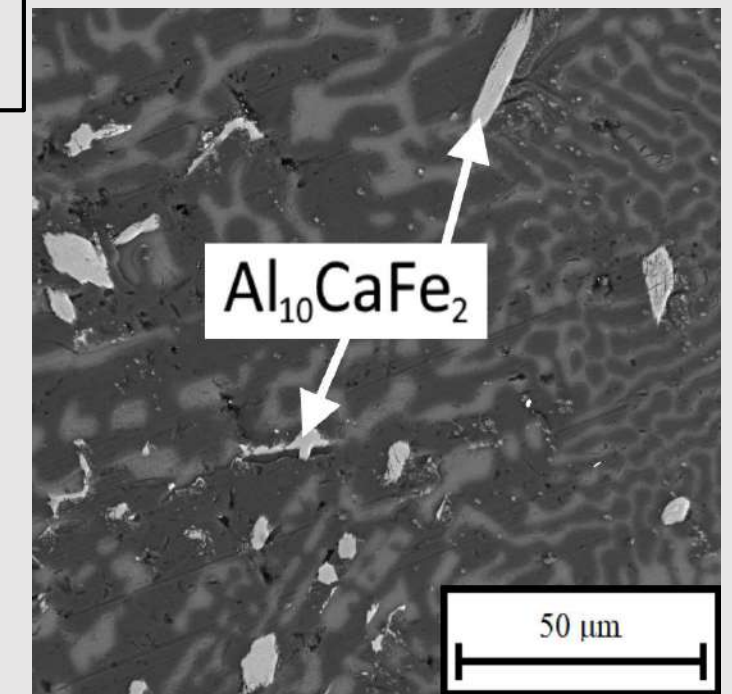
Precipitates of fine crystallized Fe-containing phases after slowly cooling in Al-13%Ca-0,5%Fe alloy.

(c)

Hot rolling at 400 °C with preliminary thermal treatment during 1 h.

SNOL

Rolling mill Duo for Hot Rolling

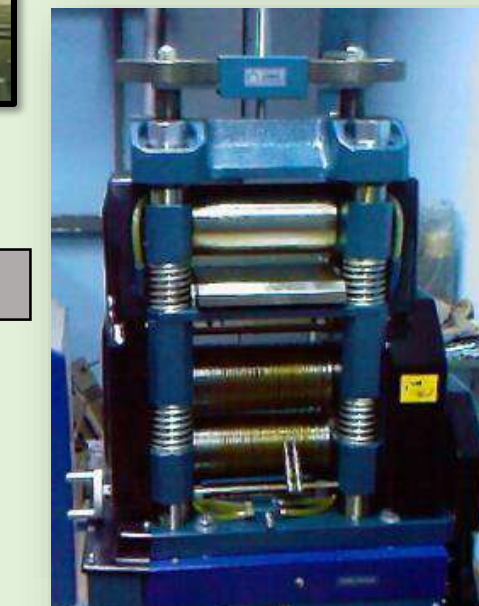Hot-rolled sheet 2 mm

Flat ingots 15x60x180 mm

Rolling mill for Cold Rolling

No heat treatment

SNOL

Annealing 350 °C during 3 h.

Cold-rolled sheet 0,5 mm

Mechanical properties (Zwick Z250)

The experimental alloy demonstrated a fairly high processability in hot and cold rolling. However, the ductility in the cold rolled state was found to be very low.

Alloy	UTS, Mpa	YS, Mpa	El., %	ρ, g/sm³
AMg2 (AA5051)[1]	165	-	18,0	2,69
AMg5 (AA5056)[1]	275	145	15,0	2,64
Al2.5Mg2.5Ca[2]	391±3	356±3	2,6±0,4	2,63
Al2.5Mg2.5Ca[3]	367±1	300±1	5,0±0,2	2,63
Al2.5Mg2.5Ca[4]	461±4	-	0,2	2,63

[1]sheet according to GOST 21631-76 (thickness 1-10 mm for AMg2, 0.6-4.5 mm for AMg5), annealed condition
[2]sheet (thickness 2 mm for Al2.5Mg2.5Ca), cold-worked condition
[3]sheet (thickness 2 mm for Al2.5Mg2.5Ca), annealed condition
[4]sheet (thickness 0,5 mm for Al2.5Mg2.5Ca), cold-worked condition

III International Conference and School
"Synthesis, Structure, and Properties of High-Entropy Materials"
October 11–15, 2021

№ 18

kruglova.natalie@gmail.com

MISIS
National University of
Science and Technology

STRUCTURE AND PROPERTIES OF ALUMINUM-CALCIUM CONDUCTIVE ALLOYS

Problem

The development strategy in energy industry is aimed at **increase in the proportion of aluminum as a conductive material**. This strategy also includes replacing copper wires with aluminum ones. This determines new requirements for aluminum conductive alloys, primarily in terms of their cable performance. One of the possible ways to increase the cable performance of an electrical line is to increase the cross-section of the conductive wire. However, this approach is laborious and requires re-equipment of an electrical line and reconstruction of a cable. In this connection, the most promising approach for **solving the indicated problem** is to **increase the heat resistant** of wire alloy.

As heat-resistant conductive aluminum alloys, a special place belongs to the **Al-7% REM (01417, TU 1-809-1038-96)** alloy. This alloy is intended for preparation using so-called granular technology, i.e., by rapidly solidification with subsequent treatment using powder metallurgy (RS/PM) methods. The **volume fraction of the second phases in this alloy reaches ~ 9 vol.%.**, which is represented by eutectic (Al) + $Al_{11}Ce_3$. The high content of rare-earth metals in the alloy and **the high cooling rate of ~ 1000 K / s** make it possible to achieve heat resistance on the wire up to 250 ° C inclusive.

Advantages of Al-7% REM (01417) alloy:
-high heat resistance (up to 250 ºC);
-high strength (UTS range: 80-230 MPa);
-high electrical conductivity (54-56% IACS).

Disadvantages of Al-7% REM (01417) alloy:
-difficult to execute production technology.

01417

Conclusions:
1. The need to create a new heat-resistant conductive material,
2. The need for a simpler production technology for a promising alloy
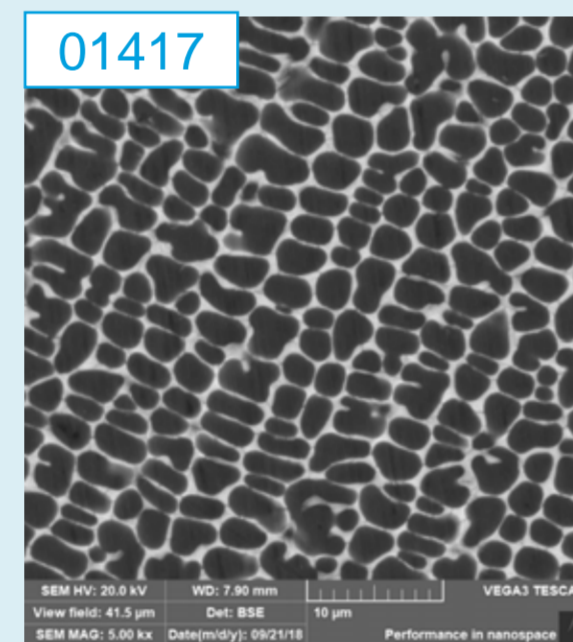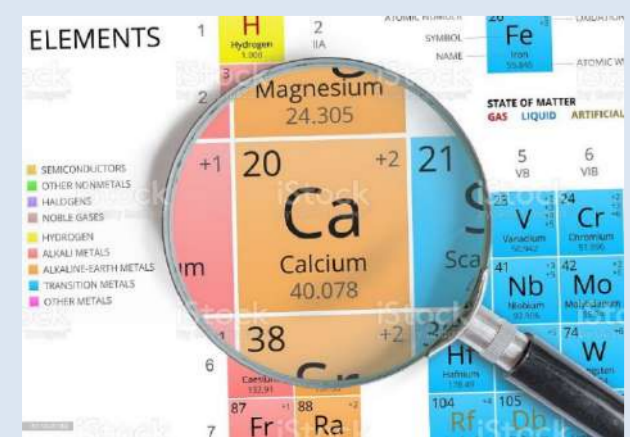
Solution concept

| no REM | no RS/PM technology | no V_c ~ 1000 K/s |

1. Search for an element that forms a dispersed eutectic, which is fundamentally similar in structural type to (Al) + $Al_{11}Ce_3$ eutectic (also designated as Al_4Ce).
   Purpose: increasing heat resistance and strength
2. Search for an element capable of binding Fe and Si impurities in phases of favorable (compact) morphology, which also ensures the absence of Si in solution (Al).
   **Purpose: to reduce electrical resistance**

Al4Ca1Fe0,6Si*

ELEMENTS
Magnesium 24.305
Ca Calcium 40.078
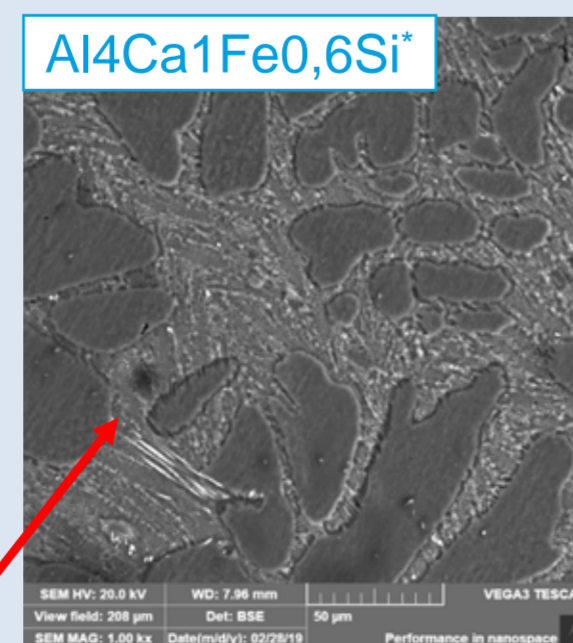
! **Dispersed eutectic** (Al) + Al_4Ca + Al_2CaSi_2 + $Al_{10}CaFe_2$, which binds Fe and Si into phases of compact morphology
! The absence of Si in the composition of the solid solution (Al) due to the formation the Al_2CaSi_2 phase
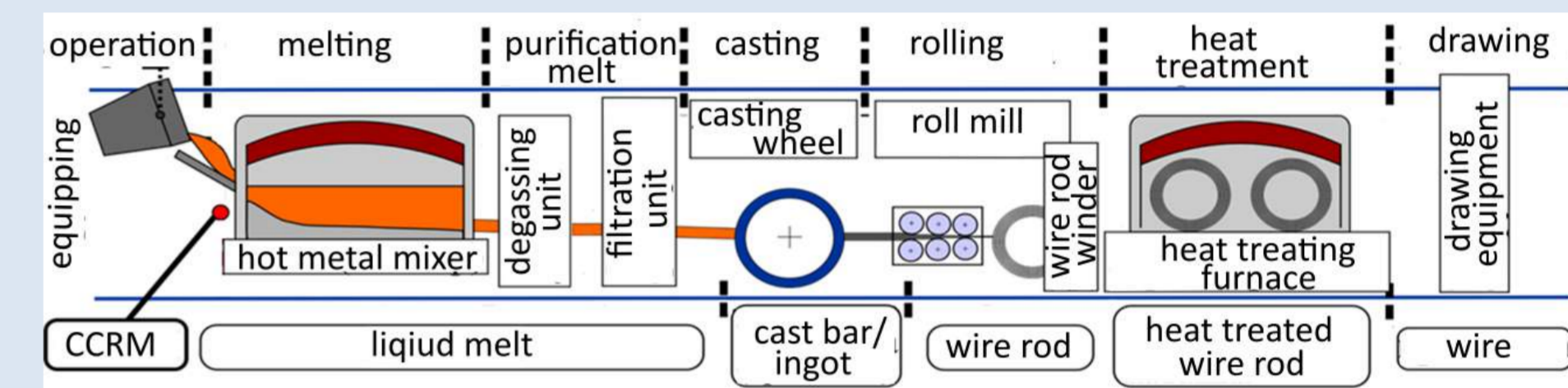
Solution concept

3. The choice of an alloying additive, which forms nanosized particles by the mechanism of precipitation hardening, which prevent recrystallization, and also does not form second phases with Ca, Fe and Si.
   Purpose: increasing the strength and heat resistance of an alloy
4. The possibility of using electrical aluminum scrap in the manufacture of alloy
5. Using Continuous Casting and Rolling Methods (CCRM) for the manufacture of conductive wire.
   Purpose: use of a simpler production technology

! CCRM technology provides ingot cooling rate of ~20 K/s. Laboratory technology for industrial process modeling ensures identical dendritic cell parameter in a cast billet

40
Zr
Zirconium
91.224
zone axis [0.0.1] Al
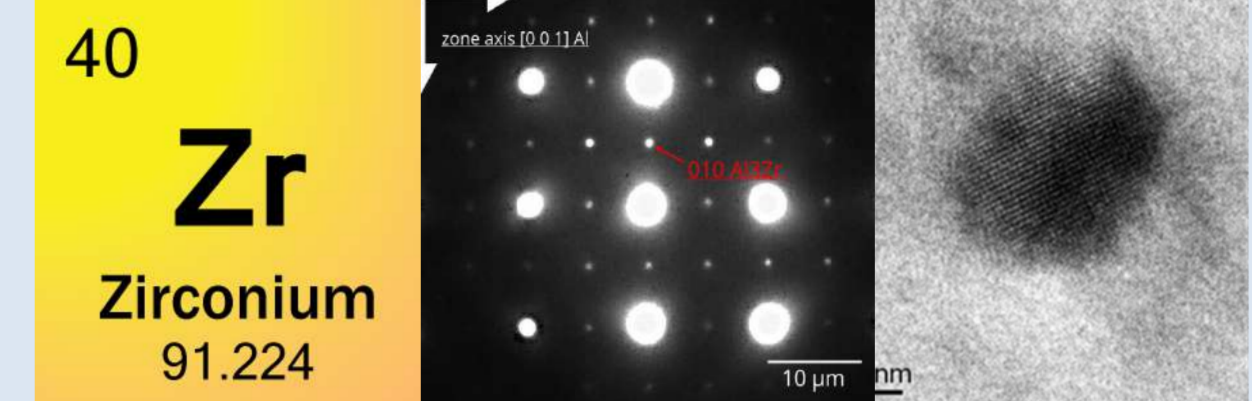
! **The atomic crystal lattice of the Al_3Zr (L12) phase (size ~ 10 nm) is coherent with the matrix phase - aluminum solid solution (Al)**

operation | melting | purification melt | casting | rolling | heat treatment | drawing

equipping — hot metal mixer — degassing unit — filtration unit — casting wheel — roll mill — wire rod winder — heat treating furnace — drawing equipment

CCRM | liqiud melt | cast bar/ingot | wire rod | heat treated wire rod | wire
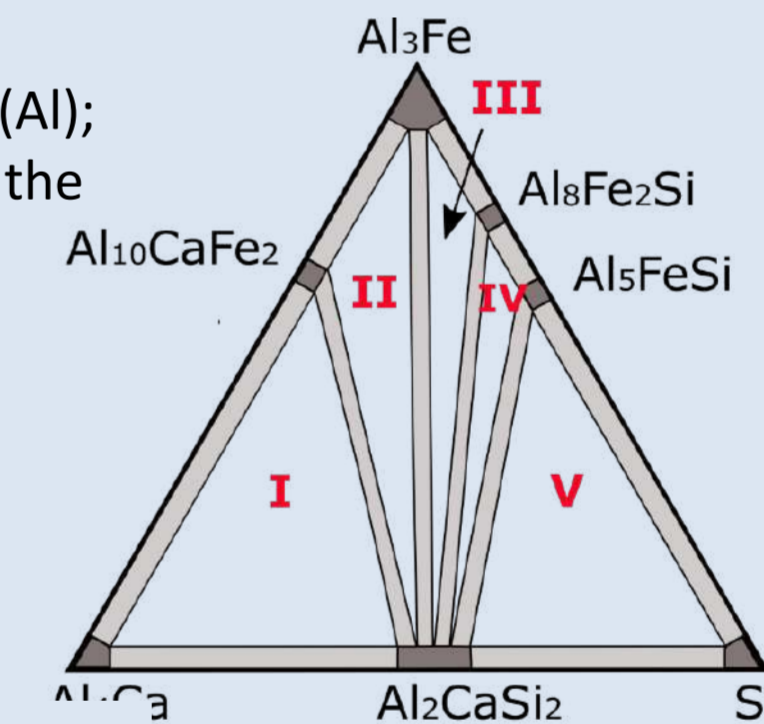
Solution of the problem

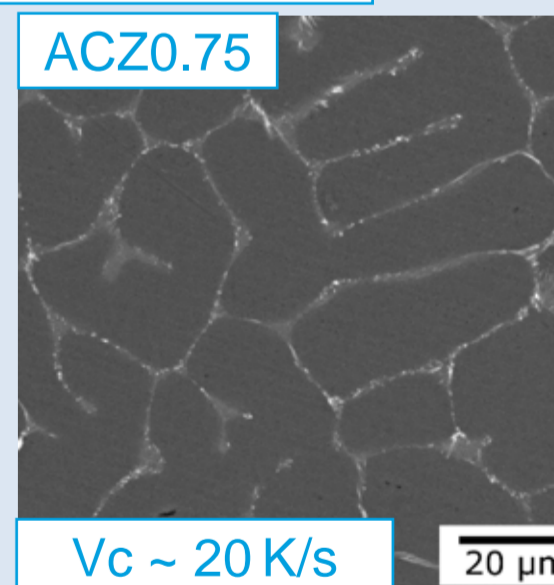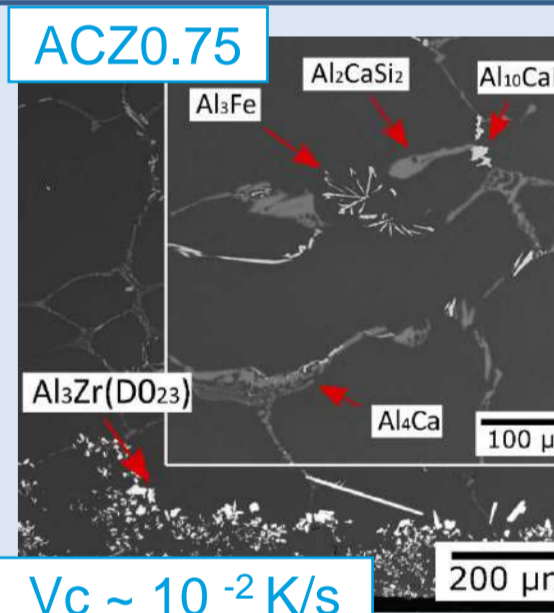1. **Selection of the alloys chemical composition**
Alloy requirements:
-**the volume fraction of the second phases is ~ 6 vol.% (01417 ~ 9 vol.%);**
-Si is bound in the Al_2CaSi_2 phase and is absent in aluminum solid solution (Al);
-the presence of the compact $Al_{10}CaFe_2$ particles in the eutectic instead of the Al_3Fe phase of acicular morphology;
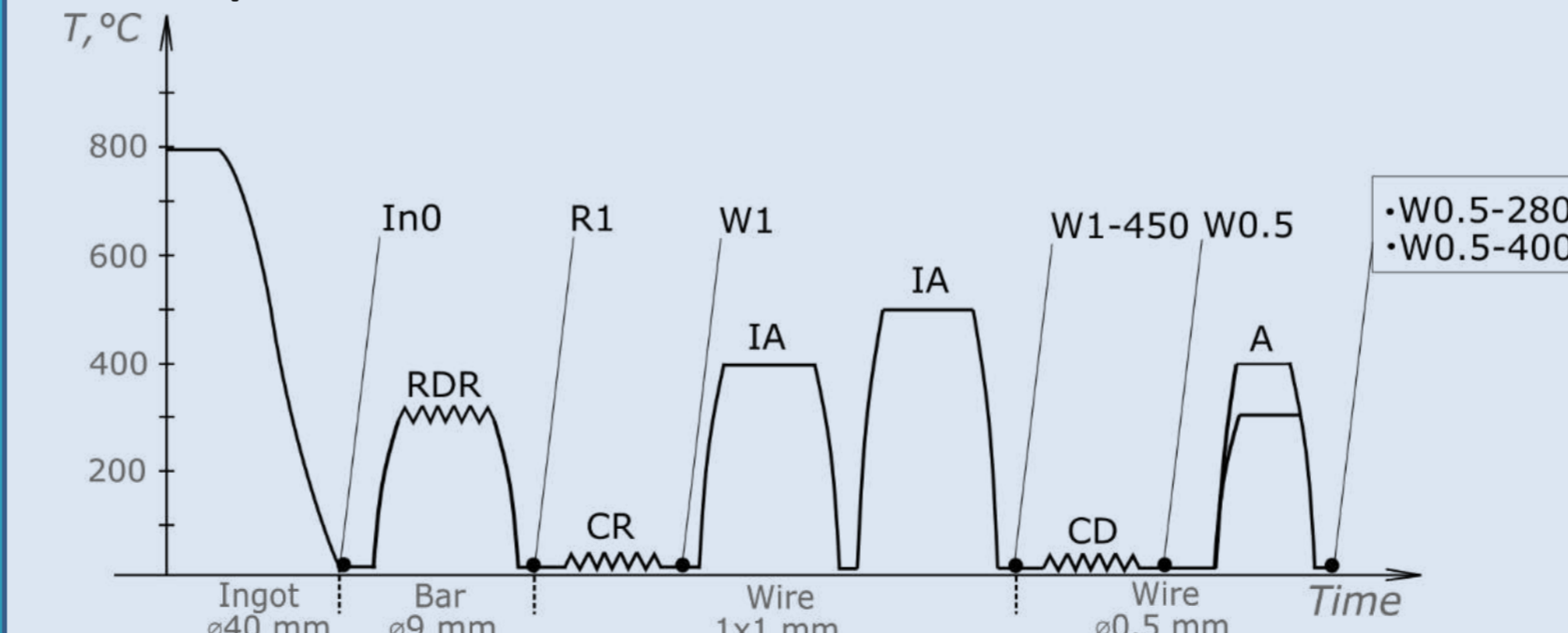- dispersed eutectic with the Al_4Ca phase.

Designation	Chemical composition of experimental alloys, wt.%				
	Ca	Fe	Si	Zr	Al
ACZ0.75	0,80	0,62	0,26	0,21	balance
ACZ0.5	0,51	0,66	0,67	0,25	

2. Wire production scheme

T, ºC

$In0$ — RDR — $R1$ — CR — $W1$ — IA — IA — W1-450 — W0.5 — CD — A
•W0.5-280
•W0.5-400

Ingot ⌀40 mm | Bar ⌀9 mm | Wire 1x1 mm | Wire ⌀0.5 mm | Time

Designation	Treatment mode
In0	Ingot diameter 40 mm
R1	Bar diameter 9 mm, radial-displacement rolling at 350 ºC
W1	Cold-rolled wire 1 mm from bar diameter 9 mm
W-450	Annealing of cold-rolled wire by two-stage regime: 400 ºC, 3h + 450 ºC, 3h
W0.5	Cold drawing of annealed wire to a diameter of 0.5 mm
W0.5-280	Annealing at 280 ºC for 1 hour of wire diameter 0.5 mm (**heat resistant test**)

Al_3Fe
III
Al_8Fe_2Si
$Al_{10}CaFe_2$ II IV Al_5FeSi
I V
Al_4Ca Al_2CaSi_2 Si

I - (Al)+Al_4Ca+$Al_{10}CaFe_2$+Al_2CaSi_2
II - (Al)+$Al_{10}CaFe_2$+Al_2CaSi_2+Al_3Fe
III - (Al)+Al_2CaSi_2+Al_3Fe+Al_8Fe_2Si
IV - (Al)+Al_2CaSi_2+Al_8Fe_2Si+Al_5FeSi
V - (Al)+Al_2CaSi_2+Al_5FeSi+(Si)

! **From the distribution in solid state of Al-Ca-Fe-Si-Zr system it follows that the Al_2CaSi_2 phase is present in all regions of this quaternary system. Considering the low solubility of Ca in (Al), this means that even at a small amount of calcium in Fe and Si containing alloys, the formation of this particular ternary compound is inevitable. Excess calcium should lead to the formation of the Al_4Ca and $Al_{10}CaFe_2$ phases**

ACZ0.75
Al_2CaSi_2 $Al_{10}CaFe_2$
Al_4Fe
$Al_3Zr(D0_{23})$ Al_4Ca
100 µm
V_c ~ 10^{-2} K/s
200 µm

ACZ0.75
V_c ~ 20 K/s
20 µm

Alloy	Designation	Electrical and mechanical properties		
		UTS, MPa	El, %	%, IACS
ACZ0.75	W1-450	-	-	54
	W0.5	190	3,2	-
ACZ0.5	W1-450	-	-	55
	W0.5	180	1,0	-
01417 (TU 1-809-1038-96)	cold-rolled	180-230	2.5-4.6	56-54

! Thermal resistance test (designation W0.5-280) showed less than 10% strength reduction

The obtained level of electro-mechanical properties allows considering alloys of the Al-Ca-Fe-Si-Zr system, obtained at cooling rates of a cast billet ~ 20 K / s, as an alternative to alloy 01417, in the production of which cooling rates of ~ 1000 K/s are used.

III International Conference and School
"Synthesis, Structure, and Properties of High-Entropy Materials"
October 11-15, 2021

№19

NEW LUMINESCENT CERAMIC MATERIAL BASED ON GLASS WITH CADMIUM SULFIDE NANOPARTICLES

Yu. V. Kuznetsova, I. D. Popov

Institute of Solid State Chemistry, Ural Branch of the Russian Academy of Sciences, Ekaterinburg, Russia

jukuznetsova@mail.ru

INTRODUCTION

In 2020, the global LED market share ranged from 52 to 69% of all light sources according to Grand View Research. This demonstrates the huge demand for light sources with energy efficiency in various fields, namely, art workshops, museums, printing, medicine, and light sources for vehicles. These areas have the highest requirements for LED devices: extreme working conditions, high luminous flux, high color rendering index, etc.

However, LEDs have some drawbacks: 1) a very large luminaire footprint in a high power (> 100,000 lumens) light sources; 2) limited directional illumination; 3) the unbalanced spectrum; 4) overheating of the phosphor and its destruction.

The promising concept to overcome these problems is laser-based light sources [1]. The use of a laser requires a new design of sources and stability of phosphors to convert large luminous flux. A ceramic-based phosphor meets the requirements of such materials. It provides less degradation, better control of light scattering and thermal conductivity.

The new ceramic luminescent material was synthesized using a silicate glass with cadmium sulfide quantum dots (CdS QD) and yttrium aluminum garnet (YAG).

MATERIALS & METHODS

The glass with CdS QD was synthesized as discussed in [2]. The commercial phosphors LE 525 and LE 570 based on YAG:Ce were used as second component of the ceramics. At the first stage, the initial components of ceramics were milled in a mortar. Then, milled glass and YAG were pressed into pills at different ratios, and further sintered at 610°C during 3 h at air. The effect of synthesis conditions (ratio of phosphor/matrix, pressure at compacting) on functional properties was studied. Reflectance, photoluminescence (PL) and photoluminescence quantum yield (QY) were measured by FS-5 spectrofluorometer (Edinburgh Instruments) at ambient temperature.

RESULTS & DISCUSSION

The choice of initial components was determined by the region of PL (Fig. 1a). The phosphors have PL between 470 and 700 nm. The heat treatment of the initial glass at 610°C during 3 h leads to the formation of CdS QDs with an average diameter of 4 nm which have a wide PL band between 550 and 900 nm with maximum intensity at 700 nm [2].

The change of phosphor/matrix ratio allows to modify the region of PL of the resulting ceramics (Fig. 1b). The optical absorption and excitation spectra show contributions both from matrix with CdS QDs and YAG:Ce (Fig. 2a). The study of PL excitation demonstrates the significant effect of excitation wavelength on the PL spectra due to partial overlapping of the absorption ranges (Fig. 2b).

The increase of glass content in the ceramics leads to a decrease of PL QY from 21.2 to 14.1% (Fig. 3a). Additionally, the increase of pressure while compacting the samples decreases the PL QY from 20 to 12.5% (Fig. 3b). We assume that high pressure might lead to oxidation of Ce^{3+} to Ce^{4+} due to better interaction between glass and YAG during heat treatment.

The increase of the content of the glass component directly affects the PL intensity in the red region and the change of spectral composition of PL.
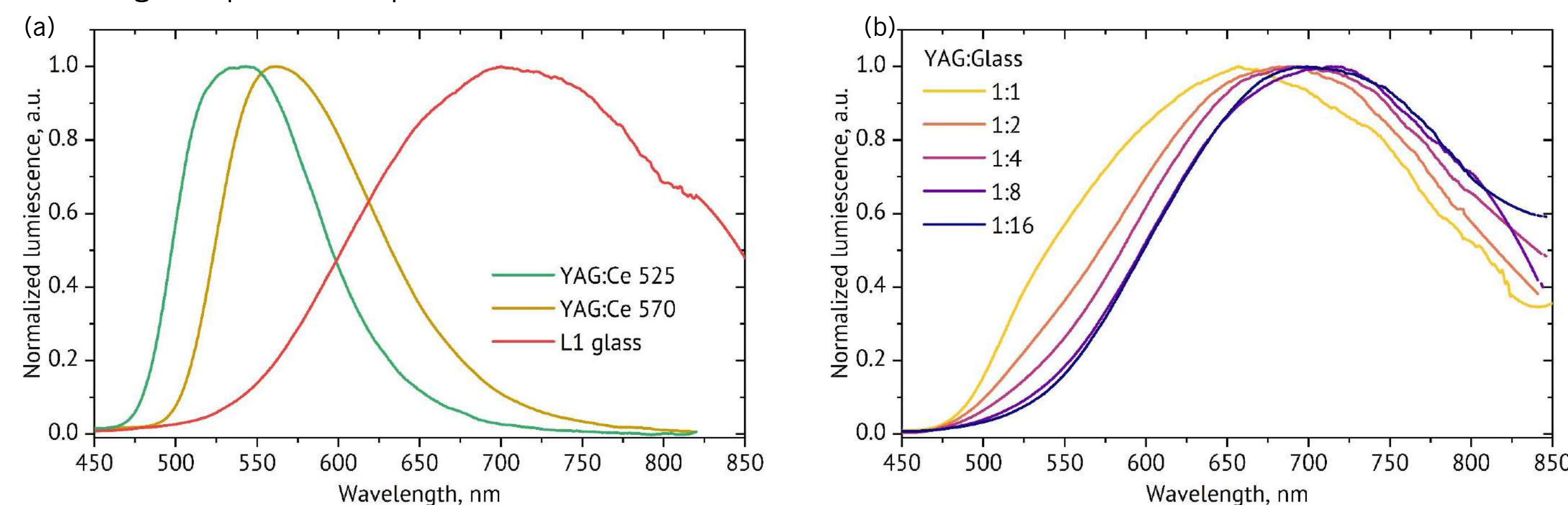

Fig. 1 (a) PL of initial components; (b) PL of YAG/CdS-glass ceramics depending on the YAG/glass mass ratio.
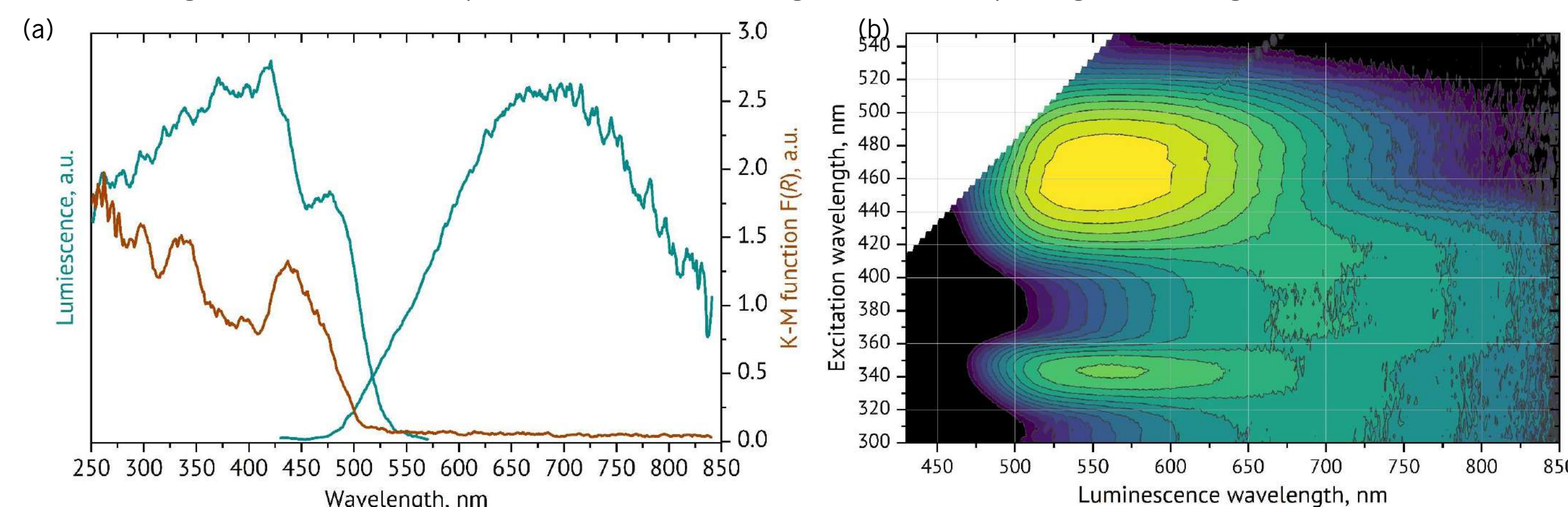

Fig. 2 (a) Optical absorption (brown), PL and PL excitation (green) of YAG/CdS-glass ceramics synthesized at glass/YAG mass ratio 2/1. The excitation wavelength was 405 nm. The PL excitation spectrum was recorded for emission at 700 nm; (b) The excitation wavelength map of YAG/CdS-glass ceramics synthesized at glass/YAG mass ratio 2/1.
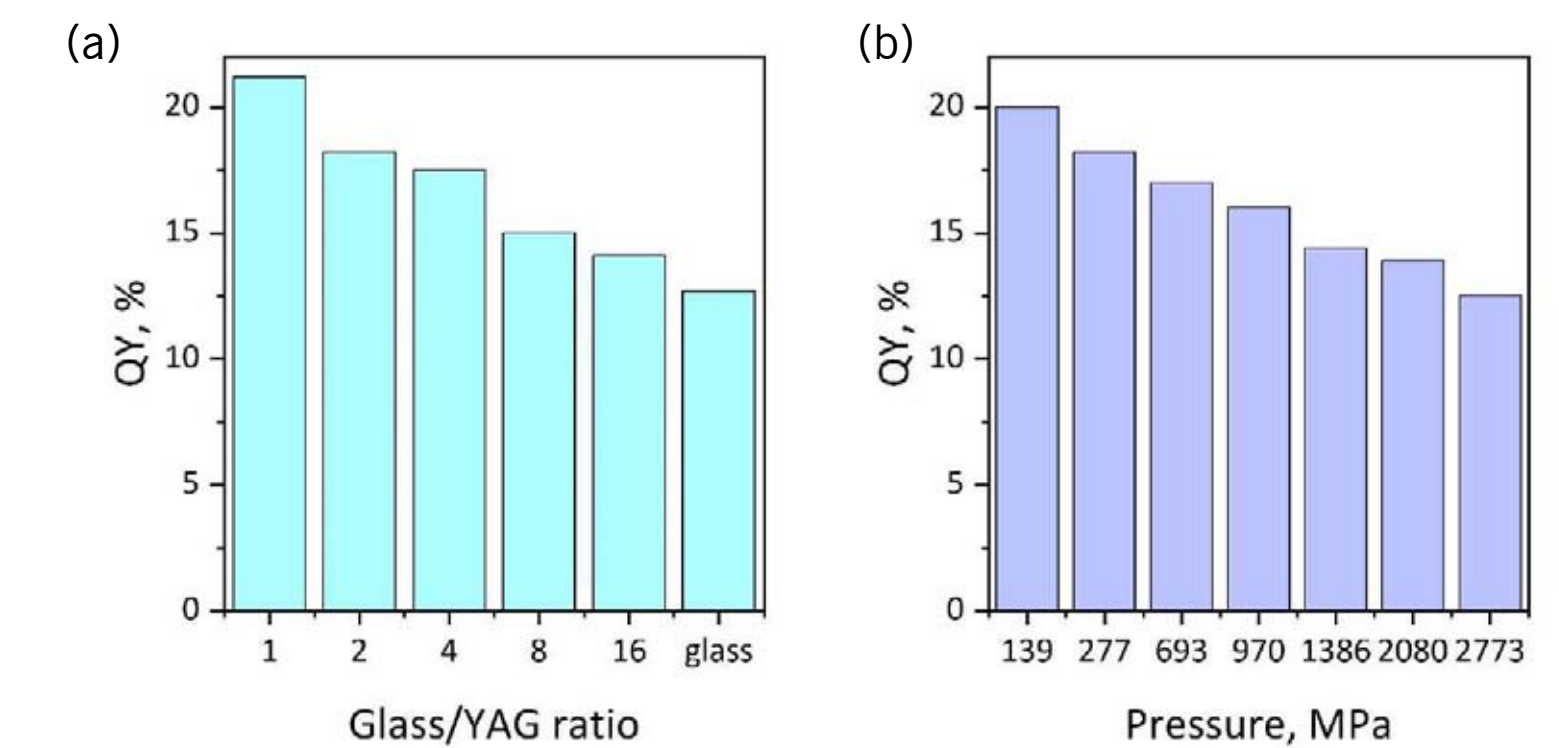

Fig. 3 Quantum yield of photoluminescence of YAG/CdS-glass ceramics depending on (a) the glass/YAG mass ratio and (b) pressure at compacting for sample glass/YAG mass ratio 2/1. The QY was measured in the range of 430-850 nm under the excitation of 405 nm.
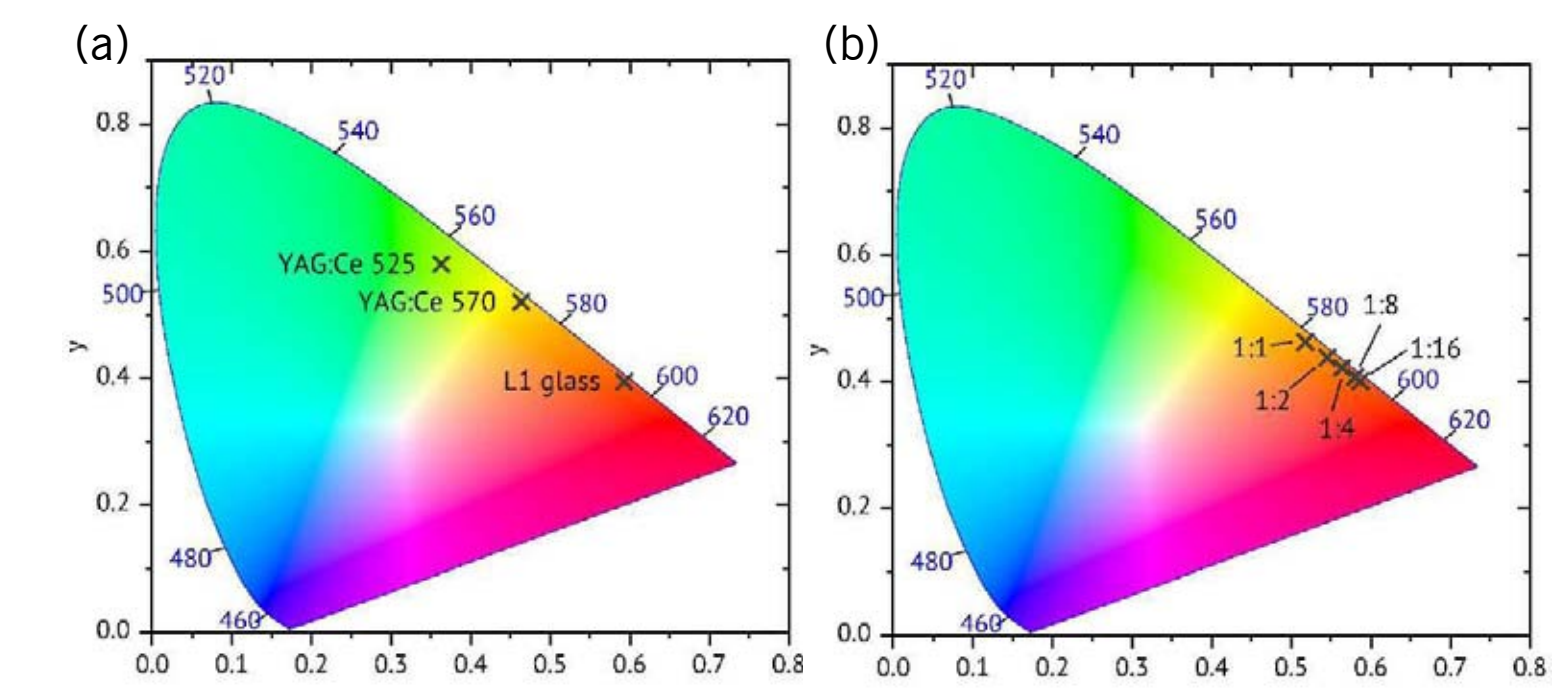

Fig. 4 Chromaticity coordinate diagram of (a) initial components and (b) YAG/CdS-glass ceramics depending on the YAG/glass mass ratio.

CONCLUSIONS

The technological aspects of the preparation of ceramics based on YAG:Ce and glass with CdS QDs and their influence on the spectral components of the material have been studied.
• At once, glass with CdS QDs performs the functions of both a matrix and a phosphor emitting in the yellow and red spectral regions.
• The use of glass with CdS QDs allows to compensate the unbalanced spectral composition of YAG.
• The more balanced and wide PL spectra are obtained at glass/YAG mass ratios 1/1 and 2/1.
• The high pressure at compacting decreases the PL QY.
• The variation of the excitation energy allows to switch ratio of the excited ceramic components that effects on the spectral composition of PL.

REFERENCES
1. J.A. Carey et al. LED professional. 2017. No 63. ISSN 1993-890X.
2. I.D Popov et al. J. Non-Cryst. Sol. 2020. V.529. P. 119781.
DOI: 10.1016/j.jnoncrysol.2019.119781

Scan QR-code to find more my publications

III International Conference and School
"Synthesis, Structure, and Properties of High-Entropy Materials"
October 11-15, 2021

№21

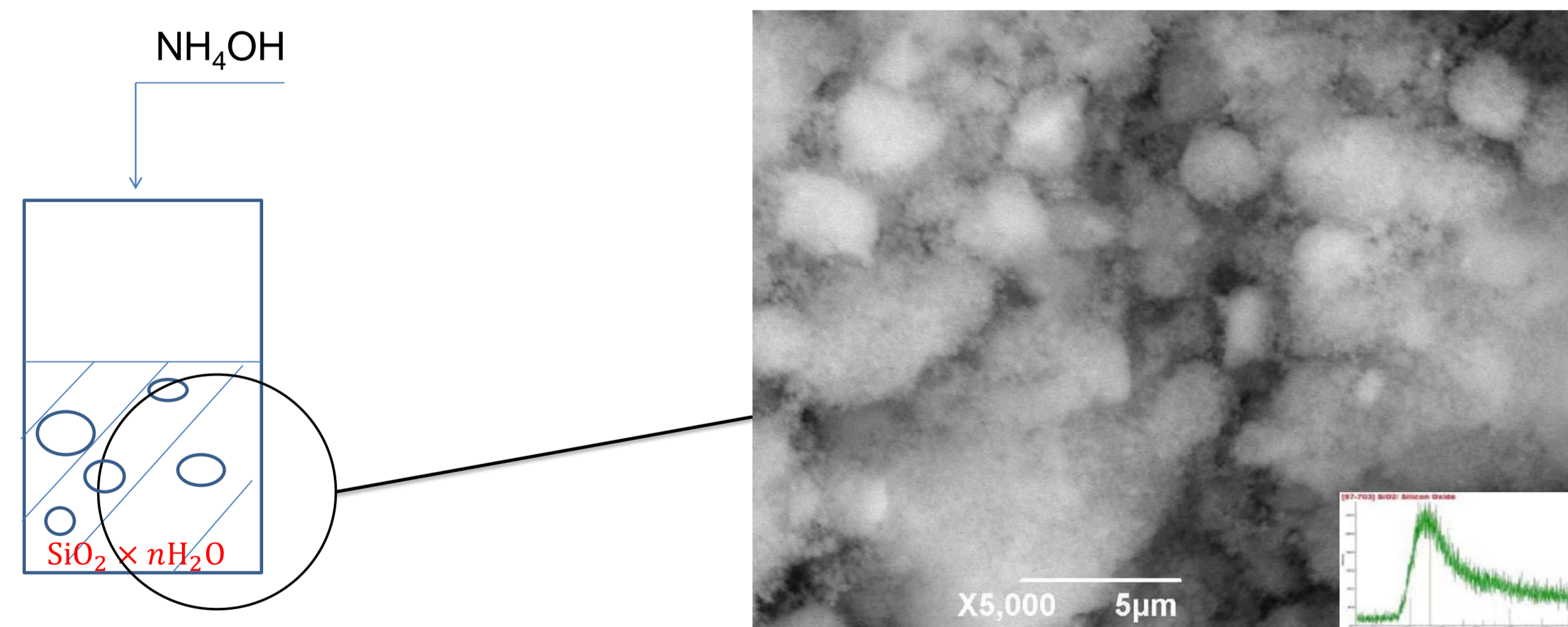# HYDROFLUORIDE TECHNOLOGY FOR PRODUCING NANOSIZED SILICON DIOXIDE FROM INDUSTRIAL WASTE

Medyankina I.S., Pasechnik L.A.
ISSC UB RAS, Ekaterinburg, Russia

lysira90@mail.ru

- The present work is related to the obtain SiO_2 from the fluoride solutions after hydrochemical processing of wet magnetic separation tailings of titanium magnetite ore beneficiation and RM.

In chemical terms, the technology is based on the ability of NH_4HF_2 to actively interact with all waste components – silica (about 20-50%), iron, titanium, calcium, magnesium, aluminum – to form simple and complex ammonium fluoromellates, such as

$$SiO_2 + 3NH_4HF_2 = (NH_4)_2SiF_6 + 2H_2O + NH_3$$

Fluorination was carried out with 1-30% NH_4HF_2 solution with stirring with holding at a temperature of up to 100°C for 1-6h.

NH_4OH

$SiO_2 \times nH_2O$

X5,000   5μm

The process is characterized by low rate constants and high activation energies. Compounds of Al, Fe, Ti, Ca, Mg are in the solid residue such the form of fluorometallates, simple fluorides and/or unreacted initial minerals. At pH 8-9 in the temperature range 25-50°C with constant stirring and slow neutralization with ammonia, a precipitate forms even at a concentration of less than 5 g/l Si by the reaction –

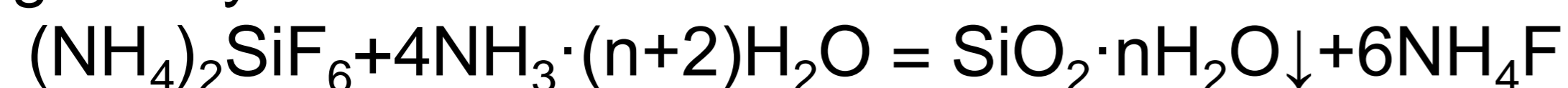$$(NH_4)_2SiF_6 + 4NH_3 \cdot (n+2)H_2O = SiO_2 \cdot nH_2O\downarrow + 6NH_4F$$

It was found that the content of SiO_2 in the final product is not less than 97% from tailings and 91% from RM. It was shown that the reduction of silicon content in waste less than 20% SiO_2 leads to a significant decrease in the concentration of silicon in solutions and an increase in impurity components. The XRD pattern of silica clearly indicated that no crystalline phases exist, as only a single broad peak between 15° and 30° (2θ) is observed. Specific surface area (BET method) reaches 360 m^2/g.
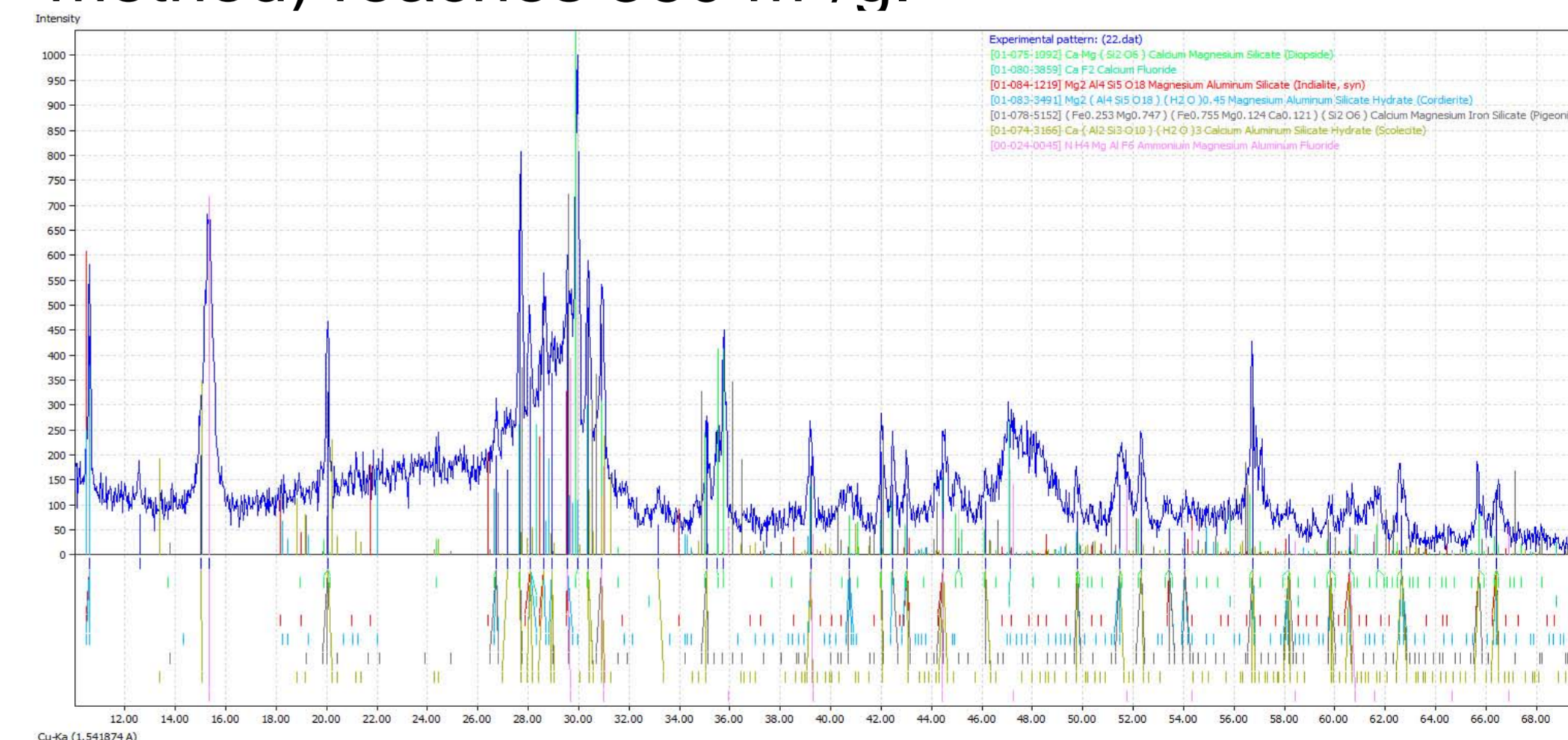
XRF of the residue after the hydrochemical process at a temperature 100 ºC

Chemical analysis of the residue after the hydrochemical process for tailings

Component	Content, at.%
Si	12-20
Fe	2-2,5
Ca	14-19
Mg	9-12
Al	6-7

III International Conference and School
"Synthesis, Structure, and Properties of High-Entropy Materials"
October 11-15, 2021

№ 26

E-mail   anton.nezhencev@gmail.com

ELECTRICAL PROPERTIES OF AMORPHOUS $(Cd_{0.9}Zn_{0.08}Mn_{0.02})_3As_2$ FILMS

Nezhencev A. V., Pilyuk E. A., Nikulicheva T. B., Borisenko A. V.

Belgorod National Research University, 85 Pobedy St, Belgorod 308015, Russia

Thin films $(Cd_{1-x-y}Zn_xMn_y)_3As_2$ (x + y = 0.1; y = 0.02) were obtained by high-frequency magnetron sputtering. The substrates were p-type silicon wafer (100) 0.4 mm thick coated with thermally grown SiO_2 oxide. The thickness of the films is 20 nm. Raman spectra of the obtained films $(Cd_{0.9}Zn_{0.08}Mn_{0.02})_3As_2$ shows that they have characteristic peaks at 38, 62, 100, 125, 191, 215, and 247 cm^{-1} (Fig. 1). The atomic force microscopy results show that all films are continuous with a granular surface structure with an average grain size of about 150 nm (Fig. 2). The scanning electron microscopy images show that the films are practically homogeneous. According to the distribution of the elements, the films within the measurement range had a homogeneous structure. The results of X-ray diffraction show diffraction patterns of films obtained on cold silicon substrates are typical for amorphous materials with broad "halo" peaks.
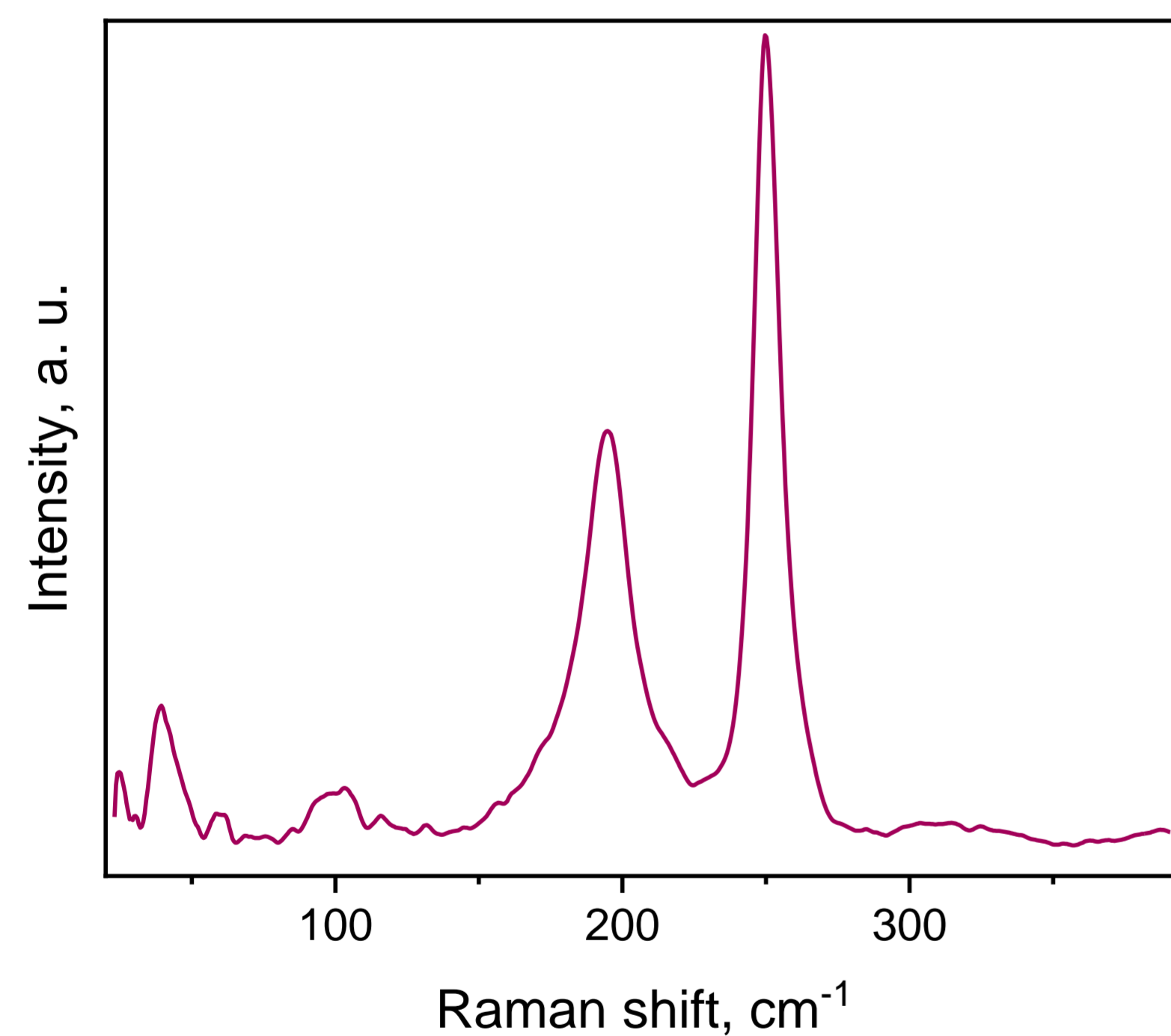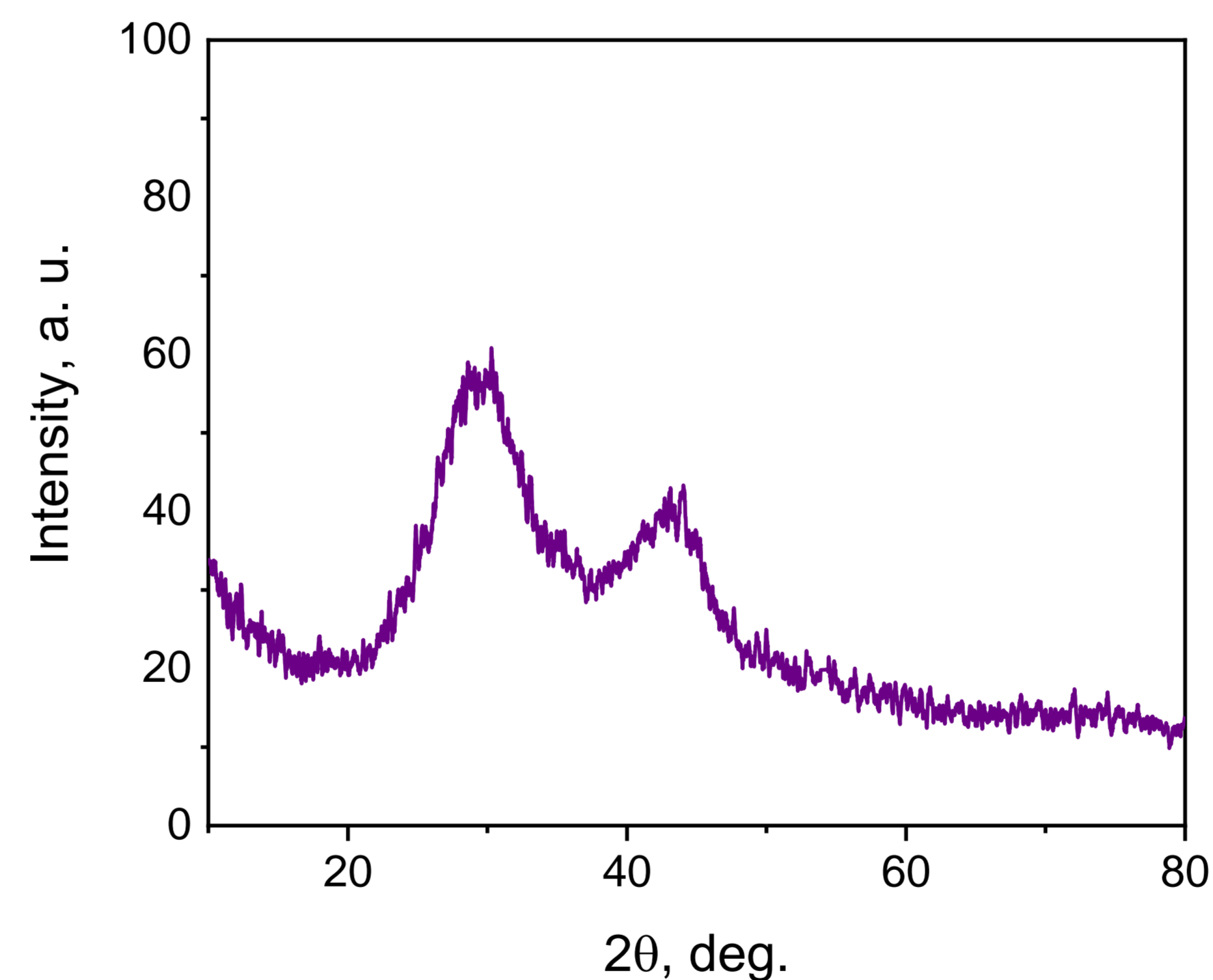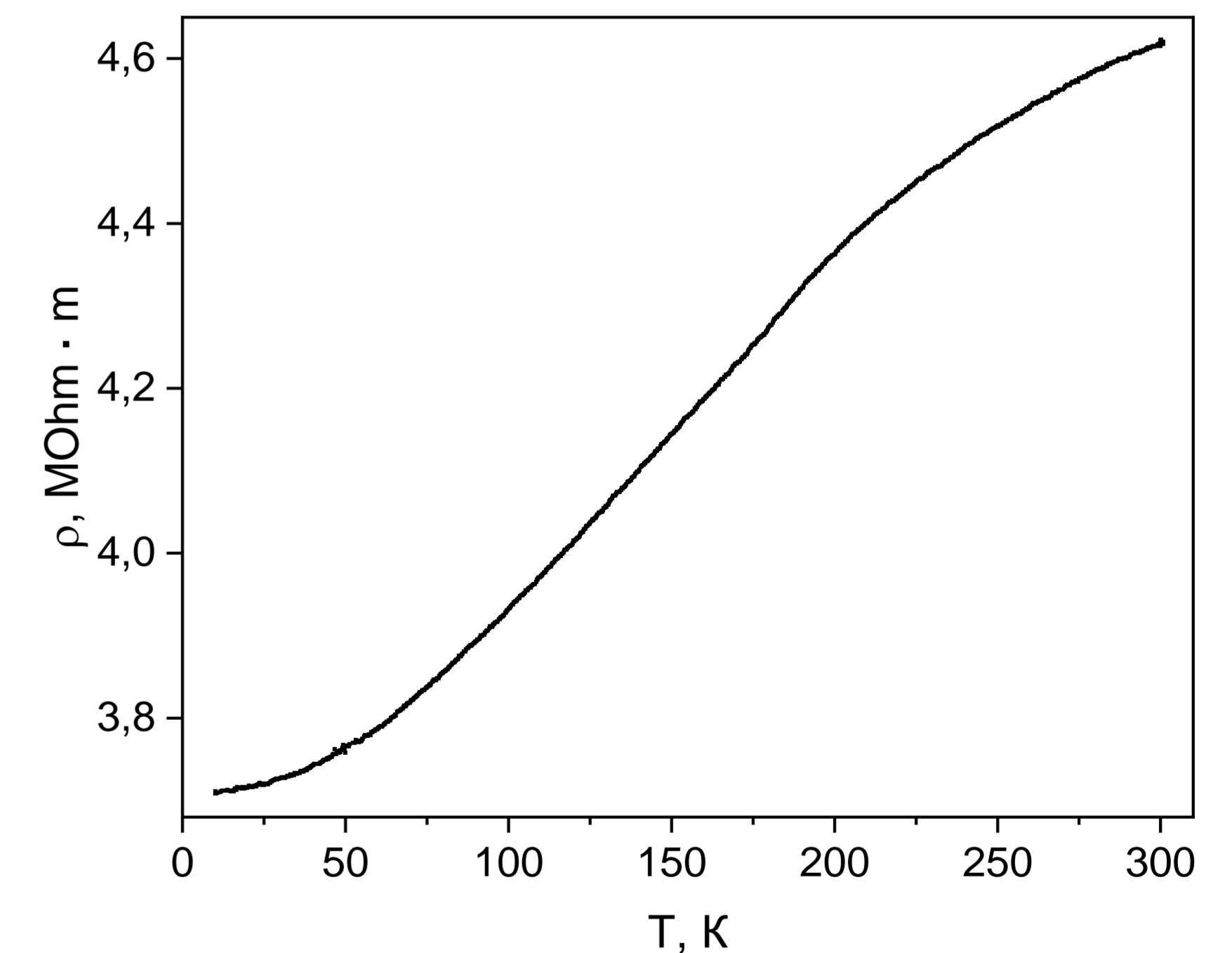

Fig 1. Raman spectra

Fig 2. Atomic force microscopy

Fig 3. Temperature dependence of the resistivity

Measurements of the electrical properties such as conductivity of $(Cd_{0.9}Zn_{0.08}Mn_{0.02})_3As_2$ thin films were taken according to the standard six-point scheme in the temperature range 10-300 K and magnetic fields up to 1 T. The results show that the resistivity of the film is increasing as well as temperature which corresponds to a metal type conductivity. The concentration and mobility of electrons, calculated using the results of measurements of the Hall constant, were 5.1×10^{20} cm^{-3} and 3.3×10^2 cm$^2 \cdot V^{-1} \cdot s^{-1}$ at 10 K and 6.6×10^{20} cm^{-3} and 2.1×10^2 cm$^2 \cdot V^{-1} \cdot s^{-1}$ at 300 K, respectively (Fig. 3). The concentration increases with increasing temperature and the mobility decreases with increasing temperature. The magnetoresistance is negative. It is mostly found in ferromagnetics, this can point out to the presence of the variable-range conductivity.

III International Conference and School "Synthesis, Structure, and Properties of High-Entropy Materials"
October 11-15, 2021

№27

sergeyneulybin@gmail.com

Neulybin S. D., Shchitsyn Yu. D., Ovchinnikov I. P.
Perm National Research Polytechnic University, Perm, Russia

APPLICATION OF PLASMA METALLIZATION TECHNOLOGY FOR RAPID PROTOTYPING OF PRODUCTS

Layer-by-layer plasma deposition of wire spraying products onto a base previously formed from an inexpensive material can be a promising method for forming blanks of large-sized items. Plasma metallization is seen as a promising method for obtaining prototypes of metal products, with wire spraying with a plasma arc of reverse polarity of the current.

Presents the results of spraying bronze of the chrome bronze brand with a productivity of 11 kg/h on a cylindrical steel base. The steel base is used exclusively as a backing material and is removed during subsequent machining.

Technology provides
- high productivity up to 15 kg / h;
- availability and wide selection of source material;
- possibility of forming products of complex shapes;
- minimization of thermal effects;
- reduction of the amount of residualstresses

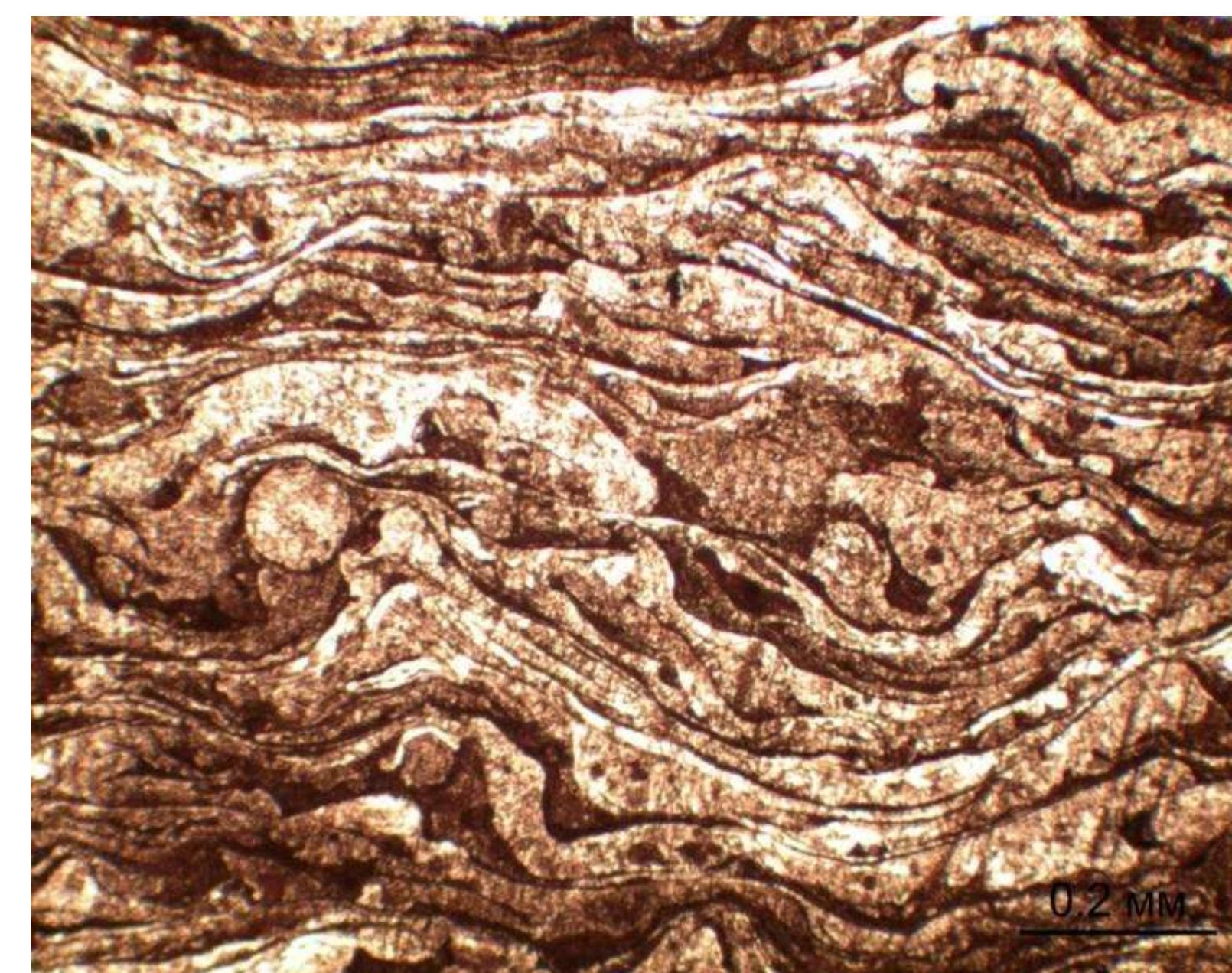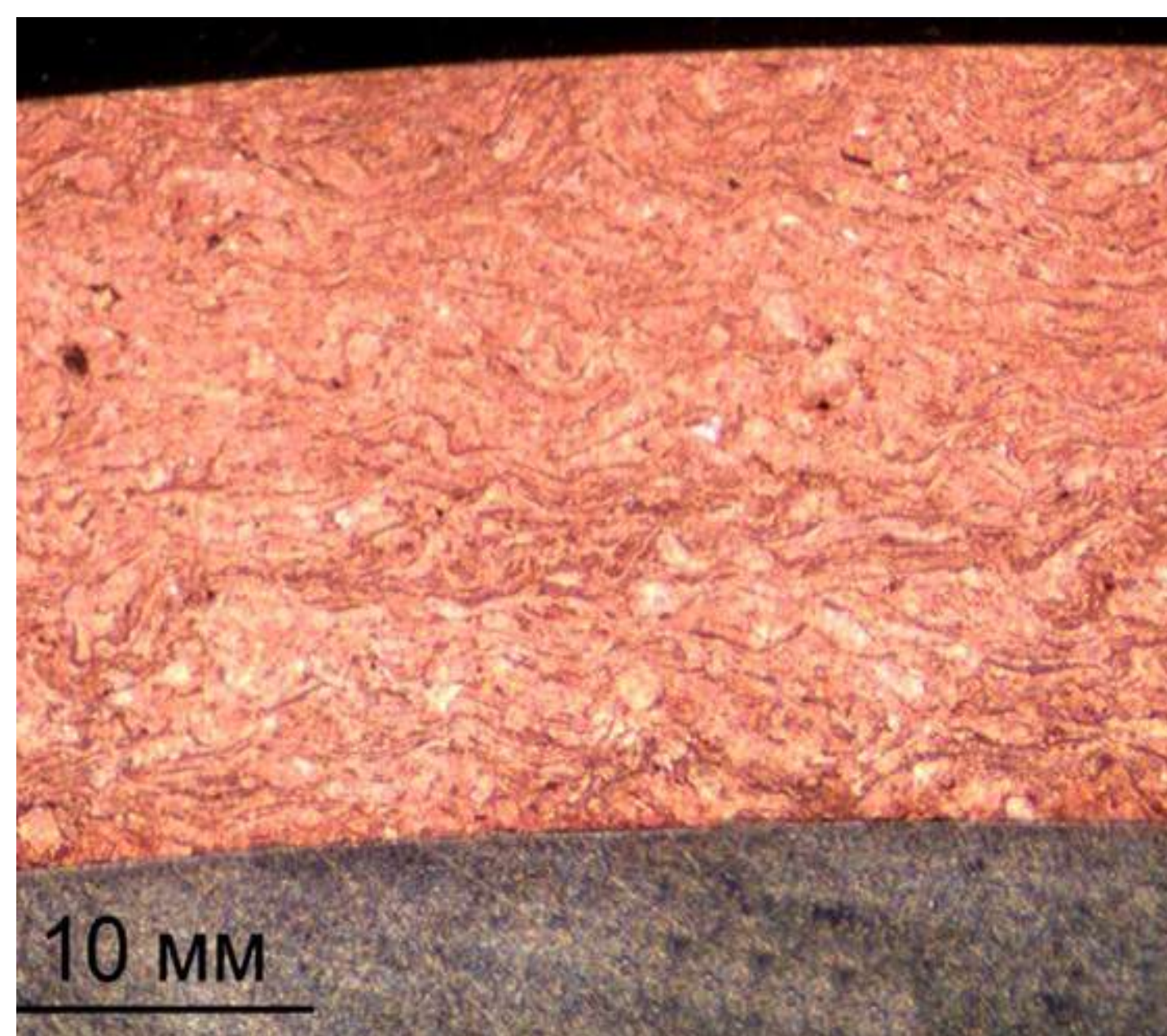Fig.1. An example of a bronze product formed by plasma metalization

Fig.2. Macro photography of formed bushing and microstructure

CONCLUSIONS

Layer-by-layer plasma deposition of wire spraying products on a base previously formed from an inexpensive material can be a promising method for the formation of blanks of large-sized products. Metallization provides high productivity (up to 15 kg / h), provides ample opportunities for regulating the chemical composition in the applied layers, in addition, the heating of the formed product is significantly reduced. It is planned to carry out a full range of studies of the structure, mechanical and physicochemical characteristics.